Finite Conductivity Fractures in Elliptical Coordinates

Michael Francis Riley

June 1991

FINITE CONDUCTIVITY FRACTURES
IN ELLIPTICAL COORDINATES

A DISSERTATION
SUBMITTED TO THE DEPARTMENT OF PETROLEUM ENGINEERING
AND THE COMMITTEE ON GRADUATE STUDIES
OF STANFORD UNIVERSITY
IN PARTIAL FULFILLMENT OF THE REQUIREMENTS
FOR THE DEGREE OF
DOCTOR OF PHILOSOPHY

By
Michael Francis Riley
June 1991

I certify that I have read this thesis and that in my opinion it is fully adequate, in scope and in quality, as a dissertation for the degree of Doctor of Philosophy.

_____
William E. Brigham
(Principal Adviser)

I certify that I have read this thesis and that in my opinion it is fully adequate, in scope and in quality, as a dissertation for the degree of Doctor of Philosophy.

_____
Roland N. Horne

I certify that I have read this thesis and that in my opinion it is fully adequate, in scope and in quality, as a dissertation for the degree of Doctor of Philosophy.

_____
Henry J. Ramey, Jr.

Approved for the University Committee on Graduate Studies:

_____
Dean of Graduate Studies

ii

ABSTRACT

Hydraulic fracturing is a widely used method of enhancing well performance. Indeed, a large number of wells, which could not otherwise be operated economically, are made highly profitable via hydraulic fracturing. The fracturing process is expensive, thus, it is important that means be available to evaluate fracture effectiveness. The most widely used tool in fracture evaluation is pressure transient analysis.

Many models have been proposed for analyzing pressure data from fractured wells. These models fall into two groups: numerical solutions of integral representations, which are used to compute pressures; and approximate models which illustrate qualitative pressure behavior but only give accurate pressures under restricted conditions.

The purpose of this study is to develop exact analytic solutions for the pressure response of a finite conductivity fracture. This model should be able to verify the existence of various flow regimes found in earlier studies. It is hoped that this solution could be modified to give simplified expressions for well pressures for all times and all fracture conductivity ranges.

The present work poses and solves the problem of a vertical finite conductivity fracture of elliptical cross section. The flow within the fracture is assumed to be incompressible and the reservoir is assumed to be infinite. The elliptical fracture geometry was chosen to facilitate the expression of fracture and reservoir pressures by eigenfunction expansions.

The solution is obtained by expressing the reservoir pressure as a series of Mathieu functions, and the fracture pressure as a series of cosines. The coefficients in these series satisfy an infinite set of linear relations, termed Fredholm sum equations. Exact solutions to these sum equations are obtained in forms which resemble continued

fractions of summations, or equivalently, which require iteration of rational forms.

Computation of the solution is not trivial, but is not overly computer intensive. For example, computation of well pressures for 150 values of dimensionless time between 10^{-3} and 10^{+3} requires less than five minutes of real tirne on an Apollo 10000 computer operating under moderate load. One of the findings of this study is that computation of Mathieu functions is not as computationally demanding as the literature suggests.

The exact solution becomes increasingly difficult to compute as time decreases. So, approximate solutions for well pressures are given for extremely low values of time. These solutions indicate that an elliptical fracture exhibits reservoir linear and bilinear flow. It had long been known that elliptical fractures would exhibit pseudoradial flow. So, the qualitative behavior of an elliptical fracture is essentially the same as that of a rectangular fracture. Indeed, the well pressures calculated in this work are quite close to those for a rectangular fracture.

The significance of the analytic nature of the solutions deserves emphasis. This problem requires the solution of the diffusivity equation for a composite system in nonradial geometry. Solutions to this type of problem are rarely, if ever, found. A great deal of effort has been expended to speed the calculation of the solutions, however, only partial success has been achieved. Generally applicable simplified well solutions have not been found.

This **work** is dedicated to the memory of my Father,

Matthew William Riley (**1923** - 1989)

*...et erat vir ille simples et rectus ac timens Deum et recendens **a** malo*

Job 1:1

ACKNOWLEDGMENT

Contents

List of Tables

List of Figures

Chapter 1

OVERVIEW

The present research has turned out to be much more involved than was first expected. Consequently, in this thesis, great pains have been taken to explain the problem and its solution in as clear and basic it manner as possible. However, we have not been wholly successful, so this chapter is intended to act as a roadmap through what is, at some points, rather treacherous terrain.

This chapter begins with a discussion of the motivation for this research and the research objectives. We then pose the problem and discuss its solution. The chapter ends with a discussion of the computational difficulties associated with evaluating the solution and the use of approximate solutions developed to overcome these difficulties.

1.1 La Raison d'Être

Hydraulic fracturing is a widely used method for increasing well productivity. Productivity increases occur because fracturing effectively increases the well surface area which makes flow to the well much more efficient.

The increase in surface area is achieved by injecting fluids into the formation at pressures above the formation parting pressure. Injecting a fluid at high pressure initiates the fracture and causes it to propagate. Subsequent injection of proppant allows the fracture to remain open after injection has ceased.

The flow of fluids to a propped fracture is much more efficient than flow to a

cylindrical wellbore. This is because the wellbore has a surface area of a few square feet while a fracture may have a surface area of a few *thousand* square feet. Therefore fracturing increases well production dramatically, often making unprofitable wells highly profitable.

While hydraulic fracturing is usually very effective, it is always very costly. Thus, it is essential that methods be available to evaluate the effectiveness of the fracturing process. The most widely used evaluation tool for hydraulic fractures is pressure transient testing or, equivalently, rate decline analysis.

Pressure transient analysis consists of two phases. The first phase consists of posing and solving the equations which govern flow in an idealized model. This model is assumed to reflect the mechanisms at work in the reservoir. The second phase consists of matching the rate and pressure measurements, taken in the field, to those from the assumed model. This work investigates only the first aspect of pressure transient testing of fractured wells—posing and solving the equations which govern flow in the model.

The prediction of the pressure response of fractured wells is not a new topic. Many models have been investigated which consider various aspects of the problem. However, these models either consider only a part of the problem, or they only allow approximate solution of the governing equations.

The most comprehensive model that has been investigated is the finite conductivity fracture model developed by Cinco and coauthors in a number of papers. The two most important of these are Cinco et al. (1978), where the model is proposed and the governing equations solved, and Cinco and Samaniego (1981), where the behavior of the solution is investigated.

The solution procedure used in the first of these papers is a numerical solution of an integral equation. This technique has come to be known as the boundary integral equation method, BIEM. The method is computationally intensive, and, since it is numerical, yields only approximate results. The pressures computed using this method appear to be accurate, although it is difficult to say just how accurate they are. (At this point the author must confess that he has not, implemented the BIEM technique, and so must be rather vague about its attributes.)

In Cinco and Samaniego (1981), the behavior of the well pressure is investigated. In this paper a simplified model was analyzed and used to identify the bilinear flow regime. The regimes of fracture linear flow and reservoir linear flow were also examined. The fracture linear flow regime results from expansion of fluid in the fracture. This regime is of too short a duration to be of practical use and so little is lost by assuming the fracture flow to be incompressible. A discussion of the BIEM technique for the case of incompressible fracture flow is given in Chapter **3.**

The intent of the present work is to present a model which depicts the flow of fluids into and through a finite conductivity vertical fracture. We **seek** an exact solution which can be used to find pressures anywhere in the fracture/reservoir system. The reason for pursuing an analytic solution is that it would be expected to be highly accurate and, if not computationally expedient, at least it would have the ability to be made computationally efficient. The ultimate goal is to provide solutions whose computation is sufficiently rapid to be of use in computer-aided well test interpretation.

Ideally, we would like to find an exact solution to Cinco's model. However, in order to find this solution, we have changed the fracture cross section from rectangular to elliptical. The reason for assuming an elliptical fracture is that it enables the use **of** elliptical coordinates. The purely steady-state form of the elliptical fracture problem was solved by Prats (1961) using the elliptical coordinate system. Our solution bears strong resemblance to Prats' solution.

1.2   The Problem and Solution

This section gives an overview of the model and the solution procedure employed in the present work. This is covered in some detail because the exposition of Chapters **4-7** is rather intricate.

This research poses the reservoir/fracture problem as a pair of coupled partial differential equations which are derived in Chapter 4. We seek exact solutions in terms of eigenfunction series expansions of the reservoir and fracture pressures. The series expansion for the reservoir pressure is derived in Chapter **5** which also discusses

Mathieu functions in detail. The series expansion for fracture pressure is given in Chapter 6.

Expressing pressures as series of eigenfunctions reduces the problem of determining pressures to the problem of determining the coefficients in the series. The difficulty in determining these coefficients is that the eigenfunctions of the reservoir pressure series, the Mathieu functions, ce_{2n}, are not orthogonal to the eigenfunctions in the fracture pressure series, the cosine functions, $\cos(2r\eta)$. Therefore, we must solve an infinite set of linear relations, termed Fredholm sum equations, to determine the values of the coefficients. The sum equations are developed in Chapter 6 and solved in Chapter 7.

The eigenfunction expansion of the reservoir pressure is obtained by applying the method of separation of variables to the two-dimensional cliffusivity equation. This requires the use of a coordinate system in which the diffusivity equation is separable. Because the reservoir sees the fracture as the line segment between $x_D = -1$ and $x_D = +1$ on the x_D-axis, the coordinate system must also express this line segment as a single value of one coordinate for all values of the second coordinate. The only coordinate system which satisfies these two requirements is the elliptical coordinate system.

The diffusivity equation, expressed in elliptical coordinates, and in Laplace space, is:

$$\frac{\partial^2 \bar{p}_R}{\partial \eta^2} + \frac{\partial^2 \bar{p}_R}{\partial \xi^2} = \frac{s}{2}[\cosh(2\xi) - \cos(2\eta)]\bar{p}_R \ . \tag{1.1}$$

In this equation, ξ plays a role similar to the radial coordinate and η plays a role similar to the angular coordinate. In Eq. 1.1, s is the parameter of Laplace transformation. A result of using elliptical coordinates is that the separated solutions of **Eq.** 1.1 are Mathieu functions. This is unfortunate because Mathieu functions are difficult to evaluate, although we have found that these difficulties have been exaggerated in the literature.

We require solutions of Eq. 1.1 which are even and π-periodic in η. These solutions must also vanish as ξ approaches infinity. The only combination of Mathieu functions which satisfies these requirements is the product, $ce_{2n}Fek_{2n}$. The functions, ce_{2n}, are the eigenfunctions of the reservoir solution. They are functions of the angular variable

and satisfy the periodicity requirements in η.

Because the product, $ce_{2n}Fek_{2n}$, forms a complete set when summed over n, we choose to represent the reservoir pressure by the series:

$$\bar{p}_R(\eta, \xi; s) = \sum_{n=0}^{\infty} \frac{(-1)^n \gamma_{2n} ce_{2n}(\eta; -s/4) Fek_{2n}(\xi; -s/4)}{Fek_{2n}(0; -s/4)} \tag{1.2}$$

This solution satisfies Eq. 1.1 for any values of γ_{2n}, because the separated solutions satisfy Eq. 1.1. The coefficients, γ_{2n}, must be specified so that the series satisfies the fracture equation at $\xi = 0$. The constants, $(-1)^n/Fek_{2n}(0; -s/4)$, have been included in the reservoir series to facilitate the equation of reservoir and fracture pressures at $\xi = 0$.

The fracture equation is found by considering a composite elliptical system producing at a constant rate and taking the limit as the inner ellipse collapses to a **line** segment. Taking this limit and assuming that the fracture flow is incompressible gives the equation governing flow in the fracture:

$$\frac{\partial^2 \bar{p}_f}{\partial \eta^2} - \frac{2}{F_E} \frac{\partial \bar{p}_R}{\partial \xi}\bigg|_{\xi=0} = \frac{-\pi}{s F_E} \delta(\eta - \pi/2). \tag{1.3}$$

In this equation F_E is the elliptical fracture conductivity. The Dirac delta function is used to account for well production. The delta function is used for convenience, since it simplifies series manipulation. The incompressible fracture flow assumption should be as valid for the elliptical case as it was for the rectangular case discussed in the previous section.

The solution of the fracture equation, Eq. 1.3, can be written as an eigenfunction expansion. In this case the eigenfunctions are cosines, so we choose to represent the fracture pressure as:

$$\bar{p}_f(\eta; s) = \sum_{r=0}^{\infty} (-1)^r \beta_{2r} \cos(2r\eta). \tag{1.4}$$

The two series, Eqs. 1.2 and 1.4, contain two sets of undietermined constants, γ_{2n} and β_{2r}. These two sets of unknowns must satisfy two constraints. One is that the reservoir pressure evaluated at $\xi = 0$ equal the fracture pressure for all values of η. Hence, Eq. 1.2 evaluated at $\xi = 0$ must equal Eq. 1.4. The second constraint is that the two series satisfy Eq. 1.3.

The equal pressure constraint and the orthogonality properties of the functions, $\cos(2r\eta)$, gives a relation between β_{2r} and γ_{2n}:

$$\beta_{2r} = \sum_{n=0}^{\infty} A_{2r}^{2n}\gamma_{2n} \ . \tag{1.5}$$

In this equation the terms, A_{2r}^{2n}, are Mathieu Fourier coefficients and are known functions of s.

Equation 1.5 gives an indication of the difficulty of using eigenfunction expansions to solve this problem. The difficulty arises because the eigenfunctions, ce_{2n}, are not orthogonal to the eigenfunctions, $\cos(2r\eta)$. This means that we cannot express the coefficients, β_{2r}, in terms of a finite number of the coefficients, γ_{2n}, and vice *versa*. This becomes more of a problem when we make use of the second constraint.

The second constraint is employed by inserting Eqs. 1.2 and 1.4 into Eq. 1.3. Subsequent use of Eq. 1.5 and the orthogonality properties of $\cos(2r\eta)$ removes the dependence of the fracture equation on η and γ_{2n}:

$$2F_E r^2 \beta_{2r} - \sum_{p=0}^{\infty} \epsilon_p \mho_{2p}^{2r}\beta_{2p} = \frac{2}{s\epsilon_r} \ . \tag{1.6}$$

Equation 1.6 is a Fredholm sum equation of the second kind. It consists of an infinite set of linear relations, each relation corresponding to a different value of r. The only unknowns in Eq. 1.6 are the coefficients, β_{2r} (or, equivalently, β_{2p}, the subscript, p, being a dummy index of summation). The kernel of the equation is $\mho_{2p}^{2r}$. The kernel is itself expressed as an infinite sum and is a known function of s. The quantity, $E_{,,}$ is also known.

The focal point of the entire solution procedure is to determine β_{2r} from Eq. 1.6. Once these coefficients have been found, the fracture pressure is determined by summing Eq. 1.4. The coefficients, γ_{2n}, are found by evaluating a series analogous Eq. 1.5. The reservoir pressure is then found by evaluating Eq. 1.2.

The solution to the sum equation, Eq. 1.6, was found quite by accident. In attempting to find an approximating form valid for late times, we used the simple rearrangement of Eq. 1.6:

$$\beta_{2r} = \frac{2}{s\epsilon_r \left(2F_E r^2 - \sum_{p=0}^{\infty} \epsilon_p \mho_{2p}^{2r}\beta_{2p}/\beta_{2r}\right)} \ . \tag{1.7}$$

This form gives the correct expression for β_{2r} as s approaches zero (or equivalently as time becomes infinite) for any values of β_{2r} used in the right hand side. **As** this form was used, it became apparent that any reasonable guess for β_{2r} put in the right hand side of Eq. 1.7 resulted in a better approximation. Using this approximation as the new guess resulted in an iterative technique which seems always to converge.

Theoretically, Eq. 1.7 gives an iterative procedure which converges for all values of F_E. Computationally, however, this procedure works efficiently only for large values of fracture conductivity. There is a second sum equation in terms of β_{2r} which is amenable to iterative solution in exactly the same way as Eq. 1.7. This second solution converges rapidly for small values of F_E.

Thus, we have two iterative solutions which have favorable convergence properties depending on whether F_E is large or small. The reason we are confident that these two procedures yield exact results is that, computationally speaking, they are quite independent and both converge to the same result.

The procedure outlined above works well as long as s is small. **As** s increases the process becomes tedious because it requires the computation of a large number of terms. For this reason an alternate procedure was chosen to evaluate well pressures for t_{Dx_f} less than 10^{-3}.

1.3   Well Pressures at Early Times

Because the exact solutions become difficult to evaluate **as** the Laplace transform parameter, s, increases, approximate solutions are developed in Chapter 8 which give accurate well pressures at early times. These solutions combine the solutions to three simplified problems. The first problem assumes that the fracture is infinitely long and has a rectangular cross section. The second problem assumes that the fracture is elliptical, but that flow in the reservoir is one-dimensional. The third model assumes that the fracture conductivity is infinite.

The first model uses the solution of Wilkinson (1989) for an infinitely long fracture of rectangular cross section. This solution gives accurate well pressures for very low conductivity fractures because, if the conductivity is low, the fracture length has little

effect on the well pressure. Wilkinson's solution can be used for the elliptical fracture because, near its minor axis, an ellipse is closely approximated by a rectangle.

The second model assumes that the reservoir pressure can be approximated by $\bar{p}_R \simeq \bar{p}_f \exp(-\sqrt{s}y_D)$, i.e., that flow in the reservoir is essentially one-dimensional. Using this expression to give the reservoir influx term in Eq. **1.3** results in a ordinary differential equation for fracture pressure. This differential equation is solved by a perturbation procedure which gives pressures at the well only. These well pressures are valid for all values of fracture conductivity for extremely small values of time. This solution shows that the flow regimes of bilinear and reservoir linear flow exist for the elliptical fracture.

The third approximate problem assumes that the fracture conductivity is infinite. Because we desire a solution that is valid for large s only, we use an approximate solution that is computationally expedient for small values of time.

With these three approximate solutions in hand, we give composite solutions which are valid for all fracture conductivities for t_{Dx_f} less than 10^{-3}.

The use of the composite solution for short times together with the exact solution for long times, yields a solution which gives accurate well pressures for all fracture conductivities and all times. This solution shows that the pressures from the elliptical fracture model do not vary markedly from those of the rectangular fracture model.

Chapter 2

REVIEW OF LITERATURE

In this chapter we discuss the literature on pressure transient methods applied to hydraulic fractures and the literature on Mathieu functions. The hydraulic fracture section will discuss only those references which bear directly on this research. The section on Mathieu functions discusses those references which pertain to the behavior of these functions and their computation.

2.1 Hydraulic Fractures

The literature on vertical fractures goes back to Muskat (1937), and maybe even further. We do not intend to give an exhaustive account of the literature back to 1937, but only to highlight those works which have a direct bearing on the present work: those using Green's function techniques, approximate solutions, and elliptical geometries. An extensive review of the subject of pressure transients in hydraulically fractured reservoirs, through 1982, is given by Cinco (1982).

The first work on pressure transients in fractured wells using the Green's function technique is that of Gringarten et al. (1974). These authors posed the problem of an infinite conductivity fracture producing at a constant rate as an integral equation. In this integral equation, the flux distribution was the unknown and the free space Green's function was the kernel. The solution procedure consisted of discretizing the equation in time and space and obtaining the flux distribution numerically. This

type of procedure has been used in many different fields and has become known as the boundary integral equation method, BIEM.

Gringarten et al. (1974) gave the flux distribution for various times, but apparently did not use it to calculate pressures. Instead, they investigated the discretized equations and showed that a uniform flux fracture evaluated at a certain point along the fracture (they gave $x = 0.732x_f$) has the same value at early and late times as the infinite conductivity fracture. There has been some debate as to whether this use of the uniform flux fracture gave the correct values of pressures at intermediate times. Kuchuk et al. (1988) indicated that this "pressure point method" will not capture the character of the infinite conductivity fracture at intermediate times. Papatzacos (1987) states that the differences between the exact solution and the uniform flux approximation are as large as four percent.

Cinco et al. (1978) used a version of the BIEM to evaluate the pressure response of a finite conductivity fracture of rectangular cross section. The finite conductivity model accounts for pressure drops along the fracture. The procedure used the integral of Gringarten et al. (1974) to represent reservoir pressure and a second integral to represent fracture pressure. Equating these two integrals at the fracture face resulted in an integral equation which was discretized and solved numerically. The use of this BIEM technique gives more accurate pressures than the finite difference method used by Agarwal et al. (1979) or the finite element treatment of Barker and Ramey (1978).

Cinco and coauthors extended the BIEM to investigate less ideal cases. The effects of wellbore storage and skin were investigated by Cinco and Samaniego (1977). The inclusion of wellbore storage was a significant accomplishment since the integral relations were expressed in real space (as opposed to Laplace space).

All of the BIEM treatments described above were performed without the use of the Laplace transformation. This means that they all involved a double integral over time and space. The use of the Laplace transformation eliminates the time integral leaving only an integral in space. The Laplace transform has been used in vertical fracture problems only recently; in fact, the first evaluation of the uniform flux solution in Laplace space was given by Kuchuk (1987). The BIEM solution of the finite conductivity problem in Laplace space, for the case of double porosity reservoirs,

was obtained by van Kruysdijk (1988) and Cinco and Meng (1988).

As alluded to above, the BIEM is essentially a numerical technique — an accurate numerical technique, but a numerical technique nonetheless. One drawback of not having analytic expressions for the solutions is the lack of approximate solutions for various time and parameter ranges. To overcome this difficulty, several models have been proposed to give accurate solutions for certain time and conductivity ranges. First among these was the bilinear flow model of Cinco and Samaniego (1981). These authors considered an infinitely long fracture producing from a reservoir that exhibited linear flow perpendicular to the fracture. Using this model, the authors were able to demonstrate the existence of a bilinear flow regime which exhibited a one-quarter slope line on a log-log graph of pressure versus time. They also showed that the fracture linear flow regime, which results from decompression of fluids in the fracture, ends at times too early to be of practical use. So, little is lost by assuming that flow within the fracture is incompressible.

The drawback of assuming linear flow in the reservoir is that it does not allow the radial flow regime to develop. In a later paper, Cinco et al. (1987), allowed two-dimensional flow in the reservoir and showed that the solution exhibited radial flow and was a good approximation for fractures of very low conductivity. The authors did not give closed form expressions for the solution. The closed formed expressions were given by Wilkinson (1989).

Lee and Brockenbrough (1986) developed a model that exhibited both bilinear and reservoir linear flow — the trilinear model. The important feature of this model was the assumption of one-dimensional flow to a fracture of finite length. The third region in the model, which exhibited one-dimensional flow in the far field parallel to the fracture, had little effect on the solution. Since the trilinear model is a combination of linear flow regions, it does not exhibit radial flow. However, it does exhibit all of the regimes before the onset of radial flow including the effects of wellbore storage and fracture face skin.

The most accurate approximate model to date is that of Wilkinson (1989). This model neglects all of the flow in the reservoir that is not adjacent to the fracture; so that the reservoir becomes an infinitely long, finite width strip. In this strip

two-dimensional flow is allowed, but the sides of the strip are closed to flow. The solution was presented in terms of a Fourier cosine series. 'Wilkinson then combined this solution with the infinite conductivity solution to obtain an approximate well solution. This solution was found to work well for high conductivity fractures, but for low conductivity fractures a correction term was required.

The works cited above do not give exact solutions to either the infinite or finite conductivity fracture problems. The only exact solutions to these problems have been found by considering the fracture to be a degenerate ellipse. Exact solutions have been found for the infinite conductivity case and for the steady-state finite conductivity case by expressing the problem in elliptical coordinates.

Prats (1962) solved the problem of an infinite conductivity fracture producing from a reservoir which had an elliptical outer boundary. The Laplace space solution was expressed as a series of Mathieu functions. Mathieu functions always arise when solving unsteady problems in elliptical geometries.

Kucuk and Brigham (1979) used the solution given by Tranter (1951) to express the solution of an elliptical wellbore producing at a constant rate from an infinite system. The infinite conductivity fracture is a limiting case of Kucuk and Brigham's elliptical well. These authors gave the reservoir pressure for the fracture producing at constant pressure, but gave only the wellbore pressure for the constant rate case.

Papatzacos (1987) gave the solution for reservoir pressure for an infinite conductivity fracture producing at constant rate. He approached the problem through the integral formulation of Gringarten et al. (1974). The exact solution was derived by means of a Mathieu function expansion of the kernel of the integral.

Prats (1961) gave the only analytic treatment of a finite conductivity fracture. Prats considered an elliptical fracture producing from an elliptical reservoir. The flow in both regions was assumed to be incompressible. Prats gave closed form solutions, and, since the problem was steady state, the solutions did not involve Mathieu functions.

A problem closely related to the one considered in this work, is that of a composite elliptical system. Obut and Ertekin (1987) investigated the problem of waterflooding a hydraulically fractured reservoir by considering a composite elliptical system. They

gave closed form solutions in terms of Mathieu functions, but unfortunately, they made an error when considering the matching conditions at the interface. Obut and Ertekin apparently did not realize that Mathieu functions of different parameters were not orthogonal to each other. In a discussion of Obut and Ertekin's work, Riley (1990) showed the difficulties associated with solving composite elliptical problems. In this discussion, Riley used the method of Yeh (1963) to show that the application of separation of variables to the composite elliptical problem results in a pair of sum equations rather than an explicit solution.

In the present research we model the fracture/reservoir system as a composite problem in elliptical geometry and consider the unsteady case. The problem can be viewed as a combination of those considered by Prats (1961) and Obut and Ertekin (1987).

2.2   Mathieu Functions

This section gives a review of the literature on Mathieu functions. The aim is to show only those references which were found to be useful for the purposes of the present research.

There is only one text devoted solely to the subject of Mathieu functions. This book, McLachlan (1947), gives a good explanation of the properties of Mathieu functions and is written on a level comprehensible to the engineer.

Another useful source is Chapter 2 of the second volume of Erdelyi et al. (1955). The exposition is clear and readily understandable and shows how Mathieu functions relate to the other higher transcendental functions. The drawback of this treatment is its brevity.

Another important reference is the book on Mathieu functions and Spheroidal Wave functions by Meixner and Schafke (1954). This book appears to give some information that is missing in the previously cited references. The drawback of this reference is that it is written on a more technical level and is written in German. There may well be some important information in this reference that was overlooked by the present author.

Mathieu functions are discussed by Morse and Feshbach (1953) in their two volume work on mathematical physics. The treatment of these functions is scattered throughout the two volumes and is primarily concerned with solving problems in elliptical geometries.

The standard reference on higher transcendental functions is the Handbook of Mathematical Functions (Abramowitz and Stegun (1972)). The section on Mathieu functions contains some useful formulae, but most of them can be found in McLachlan (1947).

The first concern when dealing with Mathieu functions is to determine their eigenvalues. To determine these eigenvalues, it is useful to have power series and asymptotic representations. Rubin (1964) gave recursive formulae for the coefficients in power series expansions of Mathieu eigenvalues. The power series are useful for small values of the Laplace parameter, s. Meixner et al. (1980) gave the corresponding recursive formulae for the asymptotic series, which is useful for large values of s.

The power series and asymptotic series will give approximations to the eigenvalues only. The final determination of the eigenvalues is made through the evaluation of a continued fraction. This continued fraction is also used to determine the Mathieu Fourier coefficients, A_{2r}^{2n}. The use of the continued fraction is detailed by Blanch (1966).

The author wishes to emphasize the importance of McLachlan (1947) and Blanch (1966) to the present study. Without these two works, this research would not have been possible.

Chapter 3

THE RECTANGULAR
FRACTURE MODEL

In this chapter we discuss the rectangular fracture problem in some detail. The methods discussed in this chapter represent the current stake of the art in finite conductivity fractures. The focus of this chapter is a boundary integral element method (BIEM) similar to that used by Cinco et al. (1978). However, we make two important digressions. The first discusses the difficulties associated with solving the finite conductivity fracture problem in rectangular coordinates. The second digression investigates an approximate model which gives well pressure behavior at early times.

Before we can discuss solution techniques, we need to present the governing equations. These governing equations are developed in the first section.

3.1 The Governing Differential Equations

This section is concerned with the equations which govern the pressure response of **a** rectangular finite conductivity fracture. To fully specify the problem we consider two domains. The first domain represents the reservoir and the second represents the fracture. Flow in each domain is governed by a differential equation and associated boundary conditions.

3.1.1 The Reservoir Equation

In this subsection we present the diffusivity equation and boundary conditions which govern flow in the reservoir. At the end of the subsection we discuss mixed boundary value problems. We do this to illustrate the difficulties associated with solving this type of problem analytically.

Throughout this work, we assume that the reservoir is infinite, homogeneous and isotropic. The reservoir will "see" the fracture as a zero thickness strip occupying the x-axis from $-x_f$ to $+x_f$. Thus, the reservoir equation and boundary conditions will be the same for the rectangular fracture and the elliptical fracture. The fracture is assumed to be homogeneous, isotropic, to produce from its axis at a constant rate per unit height, and to have height equal to that of the reservoir.

Because of the simplicity of the model, the flow in the reservoir is governed by the two-dimensional diffusivity equation:

$$\frac{\partial^2 p_{RD}}{\partial x_D^2} + \frac{\partial^2 p_{RD}}{\partial y_D^2} = \frac{\partial p_{RD}}{\partial t_{Dx_f}} \ . \tag{3.1}$$

We will not discuss the derivation of this equation. A complete explanation of the derivation is given in the second chapter of Matthews and Russell (1967). The dimensionless quantities in Eq. **3.1** are defined in the usual way, except that the length scale is the fracture half-length, x_f:

$$p_{RD} = \frac{2\pi k_R h (p_i - p_R)}{q\mu} \ , \quad t_{Dx_f} = \frac{k_R t}{\phi_R \mu c_{Rt} x_f^2} \ , \quad x_D = \frac{x}{x_f} \ , \quad y_D = \frac{y}{x_f} \ . \tag{3.2}$$

The reservoir initial condition is $p_{RD}(t_{Dx_f} = 0) = 0$, i.e. the reservoir is initially at a constant pressure, p;. Therefore, Laplace transformation of the diffusivity equation, with respect to t_{Dx_f}, gives:

$$\frac{\partial^2 \bar{p}_R}{\text{ax;}} + \frac{\partial^2 \bar{p}_R}{\partial y_D^2} = s\bar{p}_R \ . \tag{3.3}$$

In this equation, s, is the parameter of Laplace transformation, and $\bar{p}_R$ is the Laplace transform of p_{RD}. Throughout this work, a "bar" denotes a transformed quantity. Equation **3.3** is usually referred to as the two-dimensional Helmholtz equation, but we shall refer to it as the diffusivity equation.

To fully constrain the reservoir problem, boundary conditions are required. The first condition is that the dimensionless pressure approach zero as distance from the fracture approaches infinity. There are also symmetry conditions which arise because the fracture produces from its midpoint. The first symmetry condition is that no fluid crosses the y-axis. Therefore, the x-derivative of reservoir pressure must be zero along the y-axis.

The remaining conditions are specified on the x-axis. It is these conditions which make solution of the rectangular fracture problem intractable. The symmetry of the fracture placement implies that no fluid crosses the x-axis to the left or right of the fracture. This requires that the y-derivative of reservoir pressure be zero on the x-axis, *but* only *for* $x_D < -1$ *and* $x_D > +1$. The boundary condition on the fracture itself is that the reservoir pressure equals the fracture pressure. Explicitly stated, these x-axis conditions are:

$$\left.\frac{\partial \bar{p}_R}{\partial y_D}\right|_{y_D=0} = 0 \ , \quad x_D > +1 \ ; \qquad \left.\frac{\partial \bar{p}_R}{\partial y_D}\right|_{y_D=0} = 0 \ , \quad x_D < -1 \ ; \tag{3.4}$$

$$\bar{p}_R(y_D = 0, x_D; s) = \bar{p}_f(x_D; s) \ , \quad -1 \leq x_D \leq +1 \ . \tag{3.5}$$

This set of conditions is indicative of a *mixed* boundary value problem. The term, mixed boundary value problem, refers to the fact that the dependent variable is specified over one segment of the boundary and its derivative is specified over the remainder. Problems of mixed type are notoriously difficult to solve. So, we end this subsection with a discussion of mixed boundary value problems.

Mixed Boundary Value Problems

As an illustration of the difficulty of solving mixed problems, we consider two cases. The first is the uniform flux fracture and the second is the infinite conductivity fracture.

The first problem, the uniform flux fracture, is one of unmixed type. In the uniform flux case we specify the y-derivative on the fracture face. Aside from this, the uniform flux problem is identical to that outlined earlier: the reservoir pressure

must satisfy the diffusivity equation, and all of the boundary and symmetry conditions outlined earlier apply, except for Eq. **3.5.** The boundary coindition on the fracture is:

$$\frac{\partial \bar{p}_R}{\partial y_D}\bigg|_{y_D=0+} = -\frac{\pi}{2s} , \qquad -1 \le x_D \le +1 . \tag{3.6}$$

The distinguishing feature of the uniform flux problem is that the boundary conditions on the x-axis all specify the value of the y-derivative. This makes the uniform flux case an unmixed boundary value problem.

The uniform flux problem can be solved in many ways. The conventional approach is to apply a cosine transformation, with respect to y_D, to Eq. **3.3.** This results in a readily solvable ordinary differential equation because the cosine transform utilizes the derivative condition at $y_D = 0$. An alternative method is to integrate the free space Green's function directly in the manner of Gringarten et al. **(1974).** These methods are directly applicable because the y-derivative is given along the entire x-axis.

If instead, we seek the solution for an infinite conductivity fracture producing at constant pressure, the fracture boundary condition becomes:

$$\bar{p}_R(y_D = 0, x_D; s) = \frac{1}{s} , \qquad -1 \le x_D \le +1 . \tag{3.7}$$

The diffusivity equation and the remaining boundary conditions are unchanged.

We now have a mixed boundary value problem. The only change is that the pressure, rather than the derivative of pressure, is specified on the fracture. This does not seem as if it changes the problem significantly, but it does. The problem can no longer be solved using the cosine transform because we are given gradient conditions only on portions of the x-axis. Similarly, the Green's function approach changes the problem into an integral equation, but does not give its explicit solution.

It would be instructive to give the fundamental principle which underlies the difficulty of solving mixed boundary value problems. However, this principle is unknown to the present author. We can only state that if the unknown function, its derivatives *or* the sum of the two are given along each bounding surface, then there is hope **of** finding the solution using ordinary means. If one type of boundary condition is given over part of the boundary and another over the remainder, the solution can only be

found using extraordinary means. For the case of the infinite conductivity fracture these extraordinary means consist of the use of elliptical coordinates and Mathieu functions.

We have made this digression to explain the difficulties associated with solving a mixed boundary value problem. The case of a finite conductivity fracture is more complicated yet. This is because we have specified that the reservoir pressure equals the fracture pressure at the fracture face, and the fracture pressure itself satisfies a differential equation. The fracture differential equation is the subject of the next subsection.

3.1.2 The Fracture Equation

In this subsection we describe the differential equation that governs flow within a rectangular finite conductivity fracture. We will not give the derivation here. The equation can be derived in a way analogous to that for the elliptical fracture given in Chapter **4.**

The rectangular finite conductivity fracture is assumed to have constant, although infinitesimal, width. The fluid flow into the fracture is accounted for by the derivative of the reservoir pressure at the fracture face and the flow within the fracture is assumed to be one-dimensional. Incorporating these assumptions into a material balance, eliminating the density in favor of the pressure and assuming the pressure gradients are small gives:

$$\frac{\partial^2 p_{fD}}{\partial x_D^2} + \frac{2}{F_D}\frac{\partial p_{RD}}{\partial y_D}\bigg|_{y_D=0+} = \kappa_D\frac{\partial p_{fD}}{\partial t_{Dx_f}} , \tag{3.8}$$

The fracture conductivity, F_D, is equal to $k_f w/k_R x_f$, and the diffusivity ratio, κ_D, is equal to $k_R\phi_f c_{tf}/k_f\phi_R c_{tR}$.

The diffusivity ratio, κ_D, in Eq. **3.8** is normally on the order of 10^{-7} and has been found by Cinco and Samaniego (**1981**) to have an effect on well pressure only for extremely small values of time. Hence, we will ignore the right hand side of Eq. **3.8** without any significant loss of applicability. To simplify the problem further, we will transform it into Laplace space. In Laplace space the fracture equation then

becomes:

$$\frac{\partial^2 \bar{p}_f}{\partial x_D^2} + \frac{2}{F_D} \left.\frac{\partial \bar{p}_R}{\partial y_D}\right|_{y_D=0+} = 0 \ . \tag{3.9}$$

Since, the initial condition for the fracture pressure is $p_{fD}(t_{Dx_f} = 0) = 0$, no initial condition appears in this equation.

Equation **3.9** requires two boundary conditions:

$$\left.\frac{\partial \bar{p}_f}{\partial x_D}\right|_{x_D=0+} = -\frac{\pi}{sF_D} \ , \qquad \left.\frac{\partial \bar{p}_f}{\partial x_D}\right|_{x_D=+1} = 0 \ . \tag{3.10}$$

Here we have restricted consideration to the right wing of the fracture. An equivalent set of conditions holds for negative x_D. The first boundary condition specifies that the fracture produces at a constant rate. The second condition specifies that no fluid enters the fracture at its tips.

This concludes the discussion of the fracture problem. The remainder of this chapter will discuss the solution techniques for the pair of differential equations, Eqs. **3.3** and **3.9.**

3.2   The Integral Equation Formulation

In this section we discuss a variant of the solution procedure employed by Cinco et al. **(1978)** for the rectangular fracture. The procedure involves recasting the differential equations and boundary conditions of the previous section into integral form. The resulting integral equation is then solved numerically. This method is essentially that presented in Cinco and Meng **(1988).** The integral formulation requires two integral representations: one each for the fracture and the reservoir.

3.2.1   The Reservoir Integral

This subsection discusses the formulation of an integral expression for the reservoir pressure. The formulation uses the fundamental solution, K_0, and the flux distribution, q', to express the pressure in the reservoir. This converts the problem of determining reservoir pressure to one of determining the flux distribution at the fracture face.

As discussed in the previous section, the pressure in the reservoir is governed by the transformed two-dimensional diffusivity equation:

$$\frac{\partial^2 \bar{p}_R}{\partial x_D^2} + \frac{\partial^2 \bar{p}_R}{\partial y_D^2} = s\bar{p}_R \; . \tag{3.11}$$

We now construct a fairly general solution to the diffusivity equation using the notion of the fundamental solution. This form can be found through the use of Green's functions. For simplicity, however, we choose to develop the integral representation by superposing line source wells.

The fundamental solution of the two-dimensional diffusivity equation is essentially that of a line source well producing at a rate, $\bar{q}(s)$, from an infinite medium. The solution to this problem is well known and is given by the modified Bessel function, K_0:

$$\bar{p}_R(r_D; s) = \bar{q}(s) \, K_0(r_D\sqrt{s}) \; , \tag{3.12}$$

where r_D is the distance from the well to any point in the reservoir.

If more than one line source well produces from the reservoir, the pressure response is given by the sum of the contributions of the individual wells. In the case of a fracture, the only outflow from the reservoir is at the fracture face. So, we approximate the fracture outflow by a number of line source wells along the x-axis at positions x_i:

$$\bar{p}_R(y_D, x_D; s) = \sum_{i=1}^{n_{wells}} \bar{q}_i(s) \, K_0(r_{Di}\sqrt{s}) \; . \tag{3.13}$$

In this equation r_{Di} is $\sqrt{(x_D - x_i)^2 + y_D^2}$.

At this point we need to discuss the approximate solution, Eq. **3.13,** *vis a vis,* the diffusivity equation, Eq. **3.11.** Equation **3.13** is a solution to the diffusivity equation because each term in the sum is a solution. Also, the approximate solution automatically satisfies the symmetry constraint that no fluid cross the x-axis because the only outflow points are on the x-axis. The final symmetry condition, that no fluid crosses the y-axis, will be satisfied if wells of equal rate are placed symmetrically about the y-axis.

The only condition that Eq. **3.13** does not fulfill is that reservoir pressure equals fracture pressure at the fracture face. We cannot hope that a finite sum of line source

wells will satisfy this condition, since each well location has a logarithmic singularity associated with it. This will always be the case if the individual flowrates, $\bar{q}_i$, are finite. To overcome this difficulty we take the limit as the number of wells becomes infinite. If we assume, that as the number of wells becomes infinite, they are evenly distributed along the fracture, an integral results:

$$\bar{p}_R(y_D, x_D; s) = \int_{-1}^{+1} \bar{q}'(x') \, K_0 \left(\sqrt{s} \sqrt{(x' - x_D)^2 + y_D^2} \right) dx' \, . \qquad (3.14)$$

The term, $\bar{q}'$, is the flux density, or flux distribution, at any point on the fracture. The prime is used in the notation for flux distribution because it is not the flowrate but the flowrate per unit length along the fracture.

The flux density is proportional to the Darcy velocity and can be written in terms of the y-derivative of reservoir pressure:

$$\bar{q}'(x') = -\frac{1}{\pi} \left. \frac{\partial \bar{p}_R}{\partial y_D} \right|_{y_D = 0^+} \, . \qquad (3.15)$$

Note that the integral of the flux distribution along the fracture must equal $1/s$ because the fracture flow is incompressible.

Equation **3.14** is the final representation for the reservoir pressure. It satisfies the diffusivity equation and all of the boundary/symmetry conditions as long as $\bar{q}'$ is symmetric about the y-axis. To satisfy the equality of fracture and reservoir pressures at the fracture face, we restrict Eq. **3.14** to the fracture face and assign it to be equal to the fracture pressure:

$$\bar{p}_f(x_D; s) = \int_{-1}^{+1} \bar{q}'(x') \, K_0(\sqrt{s}|x' - x_D|) dx' \, . \qquad (3.16)$$

Equation **3.16** is half of the final integral equation. The complete integral formulation requires an integral representation of the fracture equation.

3.2.2   The Fracture Integral

In this subsection we derive an integral representation of the fracture differential equation. This will be accomplished by means of a double integration.

The differential equation governing fracture flow is given by Eq. **3.9.** If we use Eq. **3.15** to represent the first derivative of the reservoir pressure, Eq. **3.9** becomes:

$$\frac{\partial^2 \bar{p}_f}{\partial x_D^2} = \frac{2\pi}{F_D}\, \bar{q}'(x_D) \; . \tag{3.17}$$

The boundary conditions associated with this equation are given by Eq **3.10.**

The method of transforming Eq. **3.17** into an integral form is double integration. If we integrate Eq. **3.17** with respect to x_D, twice, from zero to x_D, and use Eq. **3.10,** the result is:

$$\bar{p}_f(x_D; s) = \bar{p}_w(s) - \frac{\pi x_D}{s F_D} + \frac{2\pi}{F_D} \int_0^{x_D} \int_0^{x'} \bar{q}'(x'') dx'' dx' \; , \tag{3.18}$$

where $\bar{p}_w$ is the well pressure.

Equation 3.18 does not appear in the usual form of integral equation. We can convert it to a more recognizable form by expressing the double integral as a single integral:

$$\int_0^{x_D} \int_0^{x'} \bar{q}(x'') dx'' dx' = \int_0^{x_D} (x_D - x')\, \bar{q}'(x') dx'. \tag{3.19}$$

This last form is the result of changing the order of integration in the double integral.

3.2.3   The Final Integral Formulation

In this subsection **we** give the final integral formulation for the rectangular fracture. We then briefly discuss the numerical approach used for its solution.

If we equate the two integral formulations for fracture pressure, Eqs. **3.16** and **3.18,** and use Eq. **3.19,** an integral equation for $\bar{q}'$ results:

$$\bar{p}_w(s) - \frac{\pi x_D}{s F_D} = \int_{-1}^{+1} \bar{q}'(x')\, K_0(\sqrt{s}|x' - x_D|) dx' - \frac{2\pi}{F_D} \int_0^{x_D} (x_D - x')\, \bar{q}'(x') dx' \; . \tag{3.20}$$

In this equation the unknowns are the flux distribution, $\bar{q}'$, and the well pressure, $\bar{p}_w$.

Equation **3.20** is the final integral form and is equivalent to that given by Cinco and Meng (1988). The oddity in Eq. **3.20** is that the well pressure is present. It would appear that Eq. **3.20** does not fully constrain $\bar{q}'$, because the well pressure is

not known a *priori*. This is true. To fully constrain the problem we need the material balance condition that fracture influx equals well production:

$$\int_{-1}^{+1} \bar{q}'(x')dx' = \frac{1}{s} . \tag{3.21}$$

Thus, it appears that the occurrence of well pressure in the integral equation is a result of the incompressible fracture flow assumption.

Exact solution of Eq. **3.20** does not appear to be feasible. The commonly used solution procedures: transform methods, eigenfunction expansion, complex analysis techniques and generating function methods, are not useful in this case. The reason these techniques are not useful is that the kernels of the integrals in Eq. **3.20** have characters that differ greatly.

Since an exact solution technique is unavailable, numerical means have been used. The numerical solutions of Eq. **3.20** convert the integral form to an approximate algebraic form. The algebraic form arises from the approximation of the integrals by Riemann sums. We will not detail the numerics involved. Suffice it to say that the method divides the fracture into n segments. The flux in each of these segments is assumed to be constant. This gives a set of n equations with $n + 1$ unknowns. The remaining constraint is provided by discretizing Eq. **3.21.**

The solution of the set of $n + 1$ equations, gives the well pressure and the flux distribution. Once the flux distribution is determined, reservoir pressures may be calculated from Eq. **3.14.**

It would be useful to have some appraisal of the efficiency of the BIEM just described: an appraisal both of the speed and the accuracy of the method. Unfortunately, no appraisal has been given in the literature, nor has the present author implemented this procedure.

This ends the discussion of the BIEM applied to the rectangular fracture problem. This method appears to give accurate pressures, however determining qualitative pressure behavior using this method is difficult.

The most widely used means of identifying qualitative behavior is to examine the solutions of simplified problems. Many simplified models have been presented in the literature. The next section examines a representative model.

3.3 An Approximate Model

In this section we investigate the early time behavior of the wellbore pressure by means of a simplified model. We pursue this model because it can be used to identify the bilinear and reservoir linear flow regimes and is similar to a model we investigate in Chapter 8 for the elliptical fracture.

The distinguishing feature of this model is that it assumes reservoir fluids flow in the y-direction only. Using this assumption, the diffusivity equation, Eq. **3.3,** becomes:

$$\frac{\partial^2 \bar{p}_R}{\partial y_D^2} - s \bar{p}_R = 0 \ . \tag{3.22}$$

This equation is an ordinary differential equation with constant coefficients and possesses exponential solutions. The solution to Eq. **3.22,** which is bounded at infinity and is equal to the fracture pressure at $y_D = 0$, is:

$$\bar{p}_R(x_D, y_D; s) = \bar{p}_f(x_D; s) \, e^{-\sqrt{s} y_D} \ . \tag{3.23}$$

Note that we have not employed the boundary conditions specified on the x-axis outside of the fracture. The effect of ignoring these conditions is that the solution becomes increasingly unreliable away from the well.

The importance of Eq. **3.23** is that it transforms the fracture equation, Eq. **3.9,** into an ordinary differential equation. When Eq. **3.23** is used to give the reservoir influx term in Eq. **3.9,** the fracture equation becomes:

$$\frac{\partial^2 \bar{p}_f}{\partial x_D^2} - \frac{2\sqrt{s}}{F_D} \, \bar{p}_f = 0 \ . \tag{3.24}$$

The boundary conditions are unchanged:

$$\left. \frac{\partial \bar{p}_f}{\partial x_D} \right|_{x_D=0+} = -\frac{\pi}{s F_D} \ , \qquad \left. \frac{\partial \bar{p}_f}{\partial x_D} \right|_{x_D=+1} = 0 \ . \tag{3.25}$$

The solutions to Eq. **3.24** are exponentials or, equivalently, hyperbolic sines and cosines. Thus, the solution is easily obtained. Evaluated at the wellbore, the solution is:

$$\bar{p}_w = \bar{p}_f(x_D = 0; s) = \frac{\pi \coth\left(\sqrt{2\sqrt{s}/F_D}\right)}{s^{5/4}\sqrt{2F_D}} \ . \tag{3.26}$$

This expression is a limiting form of the trilinear solution of Lee and Brockenbrough (**1986**). The importance of **Eq. 3.26** is that it represents bilinear flow, linear flow, the transition between these two regimes and nothing else. This expression does not exhibit pseudoradial flow because we have neglected reservoir flow in the z-direction. However, it does give a limiting curve to which all well pressure curves must merge at early times.

The optimum way to represent this early time limiting curve can be seen by examining **Eq. 3.26** in relation to the change of scale property of the Laplace transformation:

$$\frac{\bar{\bar{\Phi}}(s/c)}{c} = \mathcal{L}\{(a(ct)\}. \tag{3.27}$$

The application of the change of scale property shows that **Eq. 3.26** represents a single curve when $p_{Dw}F_D$ is graphed versus $t_{Dx_f}F_D^2$.

The short time and long time behaviors of this limiting curve are found by evaluating **Eq. 3.26** as s approaches infinity and as s approaches zero, respectively. These two limiting forms are:

$$\bar{p}_w(s \to \infty) = \frac{\pi}{s^{5/4}\sqrt{2F_D}} = \mathcal{L}\left\{\frac{\pi t_{Dx_f}^{1/4}}{\Gamma(5/4)\sqrt{2F_D}}\right\}, \quad \Gamma(5/4) \simeq 0.9064 , \tag{3.28}$$

and

$$\bar{p}_w(s \to 0) = \frac{\pi}{2s\sqrt{s}} + \frac{\pi}{3sF_D} = \mathcal{L}\left\{\sqrt{\pi t_{Dx_f}} + \frac{\pi}{3F_D}\right\} . \tag{3.29}$$

The first limiting form, **Eq. 3.28,** was first found by Cinco and Samaniego (**1981**) and gives well pressure during the bilinear flow regime. The characteristic feature of this regime is that it plots as a one-quarter slope line on a log-log graph of pressure drop versus time.

The second limiting form, **Eq. 3.29,** was given by Cinco et al. (**1984**) and gives the well pressure during the reservoir linear flow regime. The characteristic feature of this regime is that it approaches a one-half slope line on a log-log graph. The reservoir linear flow regime occurs for fractures of high concluctivity only.

Figure **3.1** shows a graph of well pressures, given by Cinco et al. (1978), plotted on a log-log graph of $p_{Dw}F_D$ versus $t_{Dx_f}F_D^2$. The bold curve is a graph of **Eq. 3.26.** Figure **3.1** is one of the most useful sets of curves currently available for the analysis
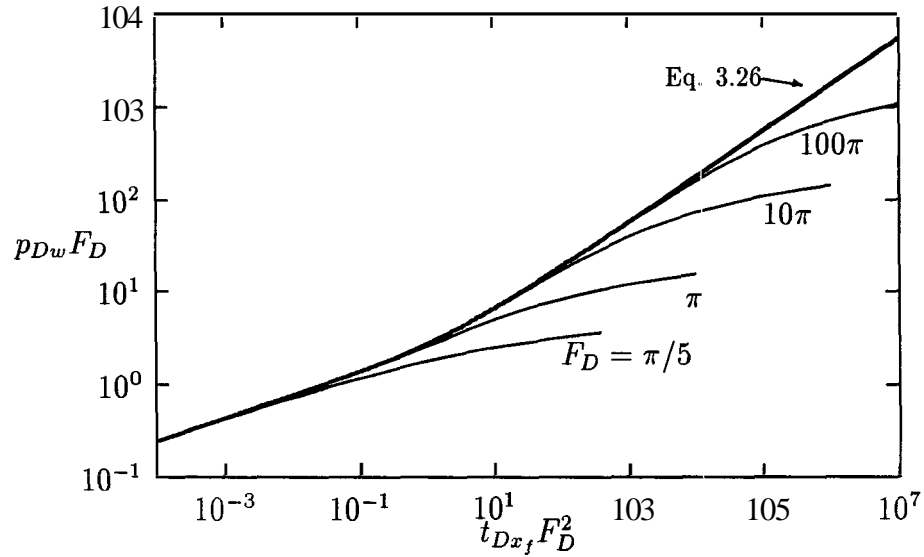
Figure 3.1: Cinco and Samaniego's Type Curves

of well test data from hydraulically fractured wells. This method of presentation is due to Cinco and Samaniego (1981).

This concludes the discussion of the rectangular fracture model. This chapter was meant as a review of the current state of the art of the solution methods for rectangular finite conductivity fractures. We also intended this chapter to show that it is infeasible to solve the rectangular fracture problem analytically and that approximate models are useful. The remainder of this work will be devoted to the problem of an elliptical fracture. We choose the cross section to be elliptical because it results in a problem which is amenable to analytic solution.

Chapter 4

GOVERNING EQUATIONS FOR ELLIPTICAL FRACTURE

In this chapter we present the pair of differential equations which govern the elliptical finite conductivity fracture case. This pair of equations is analogous to Eqs. **3.3** and 3.8 of Chapter **3.** We change the geometry from rectangular to elliptical to facilitate analytic solution of the problem. This necessitates expressing the reservoir equation in elliptical coordinates and representing the fracture as a degenerate ellipse.

4.1   The Reservoir Equation

The purpose of this section is to present the two-dimensional diffusivity equation in elliptical coordinates. This will require a discussion of the elliptical coordinate system.

The reservoir flow to the elliptical fracture is governed by the same equation as for the rectangular fracture case: the two-dimensional diffusivity equation, Eq. **3.3.** This is because both cases represent the fracture as a zero-width strip. Thus, reservoir pressure in the elliptical fracture case satisfies:

$$\frac{\partial^2 \bar{p}_R}{\partial x_D{}^2} + \frac{\partial^2 \bar{p}_R}{\partial y_D{}^2} = s\bar{p}_R \ . \tag{4.1}$$

In this work we pursue solutions in the form of eigenfunction expansions. The

reservoir expansion is found by applying the method of sepatration of variables to the diffusivity equation. To use separation of variables, we require a coordinate system in which the two-dimensional diffusivity equation separates. Only four coordinate systems satisfy this separability requirement: Cartesian, cylindrical, parabolic, and elliptical coordinates. An additional requirement is that the strip, which represents the fracture, be expressible by one coordinate for all other values of the second coordinate. Of the four coordinate systems mentioned, only the elliptical system satisfies this requirement.

4.1.1 Elliptical Coordinates

The elliptical coordinate system, shown in Fig. **4.1,** is constructed from the relations:

$$x_D = x/x_f = \cos(\eta)\cosh(\xi) , \tag{4.2}$$

$$y_D = y/x_f = \sin(\eta)\sinh(\xi) . \tag{4.3}$$

The elliptical coordinate system consists of a family of ellipses and a family of hyperbolas; each with foci at \$1 and -1 on the x_D-axis. The hyperbolas are labeled for various values of η from 0 to 2π. In this system η plays a role similar to the angular coordinate. The ellipses are labeled for various values of ξ starting from 0. In this system ξ plays a role similar to the radial coordinate. As ξ increases, the ellipses resemble circles and the hyperbolas become radii of these circles.

The significant feature of this coordinate system is that the degenerate ellipse, $\xi = 0$, is the line segment joining the two foci. From the viewpoint of the reservoir this degenerate ellipse represents the fracture. This is an improvement over the Cartesian coordinate system, in which the fracture is represented as $y_D = 0$ for some values of x_D but not for others.

Aside from the basic geometry of the system, we are concerned with the transformation of differential quantities: primarily the arc-length and the Laplacian. The required transformations can be found using conventional methods of coordinate transformation which employ the scale factors, h_η and h_ξ. The scale factors measure the ratio of the infinitesimal element of arc-length in the new coordinate system
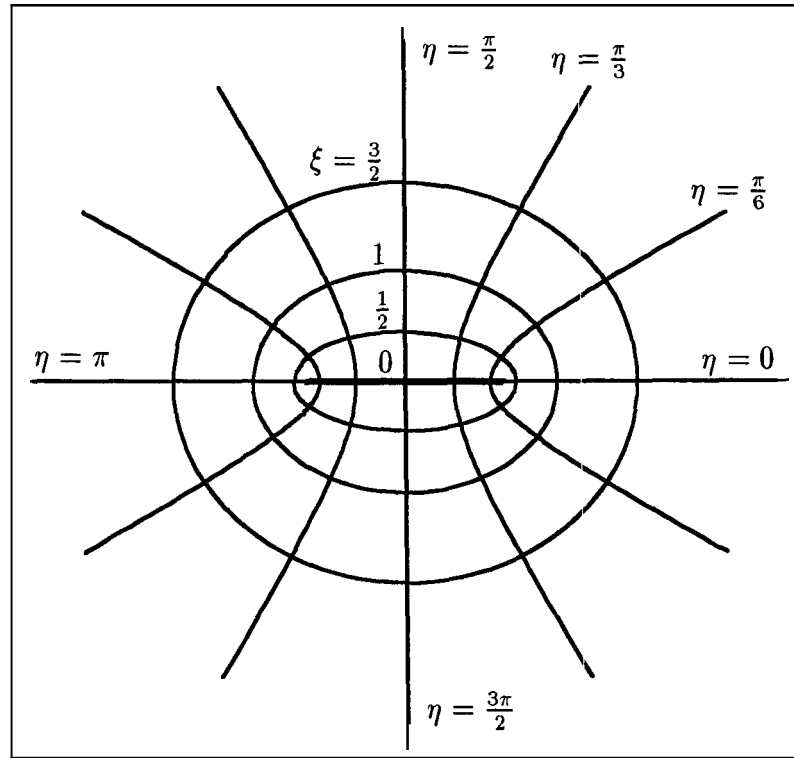
Figure **4.1:** Elliptical Coordinates

to that in the Cartesian system. In elliptical coordinates the two scale factors are equal and are given by:

$$h_\eta = h_\xi = \sqrt{\frac{1}{2}(\cosh(2\xi) - \cos(2\eta))} \tag{4.4}$$

Using the scale factors, we can immediately transform the Laplacian and arc-length from Cartesian to elliptical coordinates.

The two-dimensional Laplacian of a quantity, Φ, is given by the expression:

$$\frac{\partial^2 \Phi}{\partial x_D{}^2} + \frac{\partial^2 \Phi}{\partial y_D{}^2} = \frac{1}{h_\xi h_\eta}\left(\frac{\partial^2 \Phi}{\partial \xi^2} + \frac{\partial^2 \Phi}{\partial \eta^2}\right) = \frac{2}{\cosh(2\xi) - \cos(2\eta)}\left(\frac{\partial^2 \Phi}{\partial \xi^2} + \frac{\partial^2 \Phi}{\partial \eta^2}\right) . \tag{4.5}$$

If we consider arc-length to be a vector, its differential element is given by:

$$d\vec{s} = dx_D \; \hat{x}_D + dy_D \; \hat{y}_D = h_\xi d\xi \; \hat{\xi} + h_\eta d\eta \; \hat{\eta} = \sqrt{\frac{\cosh(2\xi) - \cos(2\eta)}{2}} \left(d\xi \; \hat{\xi} + d\eta \; \hat{\eta} \right).$$
$$(4.6)$$

In this equation the "hats" denote unit vectors in the direction of the quantities they overlay.

It is now a simple matter to transform Eq. **4.1** into elliptical coordinates. We need only replace the left-hand side of Eq. 4.1 by the final form in Eq. **4.5,** and rearrange:

$$\frac{\partial^2 \bar{p}_R}{\partial \xi^2} + \frac{\partial^2 \bar{p}_R}{\partial \eta^2} = \frac{s}{2}[\cosh(2\xi) - \cos(2\eta)] \; \bar{p}_R \; . \tag{4.7}$$

Equation 4.7 is the diffusivity equation expressed in elliptical coordinates. This new form is completely equivalent to Eq. **4.1.** Equation **4.7** is preferred because it allows us to express the fracture at a single value of ξ, $\xi = 0$.

The boundary conditions associated with Eq. **4.7** are the same as in the rectangular fracture formulation of Chapter **3** but must be expressed in elliptical coordinates. The condition that no fluid crosses the x or y-axis is equivalent to specifying that the derivative of reservoir pressure, with respect to η, is zero at $\eta = 0$, $\pi/2$, π, and $3\pi/2$. The boundedness condition in the far field is equivalent to specifying that $\bar{p}_R$ approaches zero as ξ approaches infinity. The inner boundary condition is that $\bar{p}_R$ equals $\bar{p}_f$ at $\xi = 0$.

4.2   The Fracture Equation

In this section we derive the differential equation which governs fracture flow and discuss its boundary conditions. The fracture equation is derived by applying a material balance to a long thin ellipse and taking the limit as the minor axis of the ellipse vanishes. The boundary conditions will be homogeneous because we choose to account for well production by means of the Dirac delta function.

We start with a control volume (CV) that is part of a thin ellipse of width ξ_0, as shown in Fig. 4.2, and assume that flow within the CV takes place only in the 17-direction. Flow in the ξ-direction is represented by a source term, a first derivative
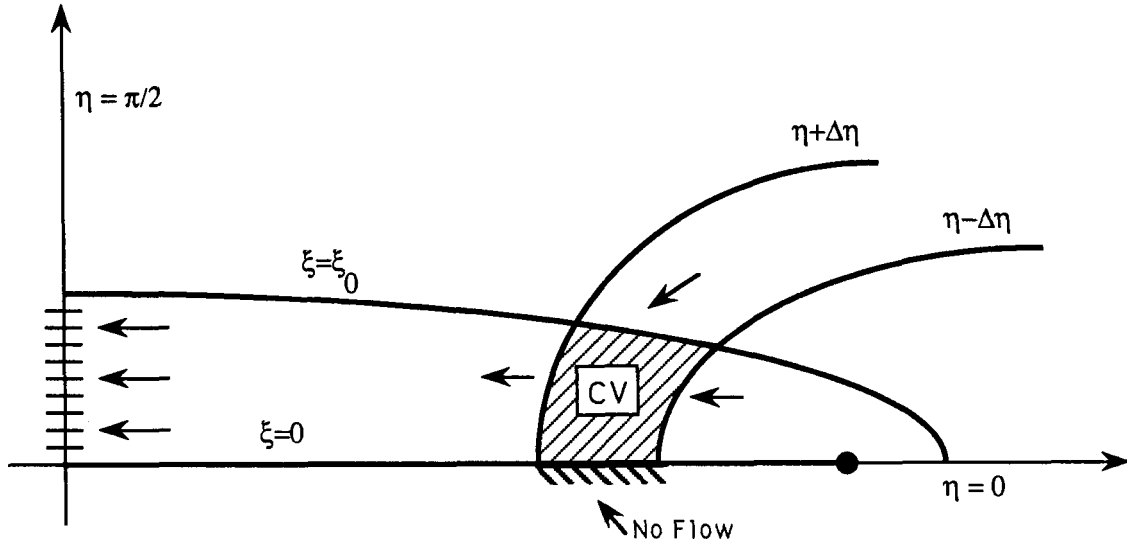
Figure *4.2:* The Elliptical Fracture

at $\xi = \xi_0$. The symmetry of the problem allows us to restrict our attention to the first quadrant as long as we ensure that no fluid crosses the x-axis.

In Fig. *4.2* the CV has width $2\Delta\eta$ and is centered at an arbitrary position η. The conservation of mass applied to the CV is:

$$\rho v A|_{\eta+\Delta\eta} - \rho v A|_{\eta-\Delta\eta} + \rho v A|_{\xi_0} = (\rho\phi V|_{t+\Delta t} - \rho\phi V|_t)/\Delta t. \qquad (4.8)$$

In this equation: v is the volume flux, A is the cross-sectional area and V is the volume element. The other nomenclature should be self explanatory. We can write the velocities, cross-sectional areas and volume element in terms of derivatives and scale factors:

$$\rho \frac{k_f}{\mu} \frac{1}{h_\eta} \frac{\partial p_f}{\partial \eta} \; hh_\xi \xi_0 \bigg|_{\eta+\Delta\eta} - \rho \frac{k_f}{\mu} \frac{1}{h_\eta} \frac{\partial p_f}{\partial \eta} \; hh_\xi \xi_0 \bigg|_{\eta-\Delta\eta} + \rho \frac{k_R}{\mu} \frac{1}{h_\xi} \frac{\partial p_R}{\partial \xi} \; hh_\eta 2\Delta\eta \bigg|_{\xi_0}$$

$$- \frac{\rho\phi \; hh_\xi \xi_0 \; h_\eta 2\Delta\eta|_{t+\Delta t} - \rho\phi \; hh_\xi \xi_0 \; h_\eta 2\Delta\eta|_t}{At} \cdot \qquad (4.9)$$

In this equation, h is the reservoir thickness, while h_ξ and h, are the scale factors defined by Eq. **4.4.** Recalling that $h, = h_\xi$ allows us to simplify the expression

considerably:

$$\frac{\Delta(\frac{\rho k_f}{\mu} \frac{\partial p_f}{\partial \eta})}{\Delta \eta} + \frac{\rho k_R}{\xi_0 \mu} \frac{\partial p_R}{\partial \xi}\bigg|_{\xi_0} = \frac{\Delta(\rho \phi h_\xi h_\eta)}{\Delta t} . \qquad (4.10)$$

To put this equation into differential form: we take the limit as $\Delta \eta$ and At approach zero, assume ϕ and μ are pressure independent, assume the fluid compressibility is small and constant, and assume that the pressure gradients are small. We also assume that as ξ_0 approaches zero, k_f approaches infinity, such that, the product, $k_f \xi_0$, is nonzero and finite. To keep the diffusivity ratio from vanishing, we assume that fracture compressibility becomes infinite as fracture permeability becomes infinite. The result of performing these operations is:

$$\frac{\partial^2 p_{fD}}{\partial \eta^2} + \frac{2}{F_E} \frac{\partial p_{RD}}{\partial \xi}\bigg|_{\xi=0} = \frac{\kappa_D}{2}[1 - \cos(2\eta)] \frac{\partial p_{fD}}{\partial t_{Dx_f}} . \qquad (4.11)$$

All of the dimensionless terms are defined using reservoir properties, as in Chapter **3,** and κ_D is the diffusivity ratio, $\phi_f c_{tf} k_R / \phi_R c_{tR} k_f$. The elliptical fracture conductivity, F_E, is defined as $2k_f \xi_0 / k_R$. Fracture conductivity is defined in this way so that F_E and the rectangular fracture conductivity, F_D, represent the same quantity *ut the* **well.** This is important because the width of the elliptical fracture, and hence its flow capacity, decreases toward the fracture ends, while the width of a rectangular fracture is constant. Thus, F_E and F_D represent different quantities. We have chosen to match their definitions at the well to facilitate comparison of pressures in Chapter **9.**

The initial condition for the fracture is $p_{fD}(t_{Dx_f} = 0) = 0$. So, Laplace transformation of Eq. 4.11 yields:

$$\frac{\partial^2 \bar{p}_f}{\partial \eta^2} + \frac{2}{F_E} \frac{\partial \bar{p}_R}{\partial \xi}\bigg|_{\xi=0} = \frac{s\kappa_D}{2}[1 - \cos(2\eta)] \, \bar{p}_f . \qquad \textbf{(4.12)}$$

Equation 4.12 requires two boundary conditions. If we assume that the well produces at a constant rate and use Darcy's law to model flow at the well, the constant rate inner boundary condition is:

$$\frac{\partial \bar{p}_f}{\partial \eta}\bigg|_{\eta=\pi/2^-} = \frac{\pi}{sF_E} . \qquad (4.13)$$

The outer boundary condition, at $\eta = 0$, specifies that no fluid crosses the z-axis. Thus, the outer boundary condition for the fracture is the homogeneous condition:

$$\frac{\partial \bar{p}_f}{\partial \eta}\bigg|_{\eta=0} = 0 . \tag{4.14}$$

The fracture problem is difficult to solve with this pair of boundary conditions because they complicate the use of Fourier representations for the fracture pressure. The reason is that termwise differentiation of Fourier series is allowed only under certain conditions. We can avoid this difficulty by accountiing for well production by means of the Dirac delta function. Using the delta function we can account for well production in Eq. **4.12,** itself

$$\frac{\partial^2 \bar{p}_f}{\partial \eta^2} + \frac{2}{F_E}\frac{\partial \bar{p}_R}{\partial \xi}\bigg|_{\xi=0} - \frac{s\kappa_D}{2}[1 - \cos(2\eta)]\,\bar{p}_f = \frac{-\pi}{sF_E}\delta(\eta - \pi/2) . \tag{4.15}$$

Since we have taken well production into account in the differential equation, we now require both the inner and outer boundary conditions to be homogeneous:

$$\frac{\partial \bar{p}_f}{\partial \eta}\bigg|_{\eta=\pi/2-} = 0 , \qquad \frac{\partial \bar{p}_f}{\partial \eta}\bigg|_{\eta=0} = 0 . \tag{4.16}$$

A convenient way to view the role of the delta function in **Eq. 4.15** is to consider two line sources producing from opposite wings of the fracture. If these sources produce at equal rates and are symmetrically placed about the well, the derivative of the pressure at the well will be zero. If we bring this pair of sources toward the well and place them an infinitesimal distance from it, we have accounted for the well production while imposing a zero gradient condition at $\eta = \pi/2$. This may seem rather contrived, but the delta function will simplify the analysis of Chapter **6** considerably.

The fracture formulation is now complete, although at a later stage we will make the assumption that κ_D is equal to zero. Before we attempt to solve the coupled fracture/reservoir differential equations we need to discuss Mathieu functions in some detail. These functions arise from applying separation of variables to the reservoir equation, **Eq. 4.7.** Mathieu functions are the topic of the next chapter.

Chapter 5

MATHIEU FUNCTIONS

In this chapter we interrupt the discussion of the elliptical fracture problem to give an overview of Mathieu functions. This is necessary because these functions are the separated solutions of the diffusivity equation in elliptical coordinates. The development will be fairly detailed because Mathieu functions are rarely used in petroleum engineering.

Mathieu functions will be introduced as separated solutions of the diffusivity equation. The angular functions, ce_{2n}, will be discussed at length, since they are the eigensolutions of the reservoir problem. There will be a lengthy digression which discusses the orthogonality properties of the Mathieu functions'and the Mathieu Fourier coefficients. These relations will be used to develop Fredholm sum equations in the next chapter. The chapter ends with a discussion of the radial functions, Fek_{2n}, and presentation of the reservoir pressure series.

5.1   Separation of Variables

In this section we discuss the method of separation of variables applied to the diffusivity equation in elliptical coordinates. The separated equations will be Mathieu's equations and their solutions will be the subjects of subsequent sections.

As was shown in Chapter 4, Eq. 4.7, reservoir pressure is governed by:

$$\frac{\partial^2 \bar{p}_R}{\partial \xi^2} + \frac{\partial^2 \bar{p}_R}{\partial \eta^2} = \frac{s}{2}[\cosh(2\xi) - \cos(2\eta)]\, \bar{p}_R \; . \tag{5.1}$$

This equation is subject to the boundary conditions discussed in Chapter 4: the solution must have η-derivative equal to zero at $\eta = 0$, $\pi/2$, π, and $3\pi/2$; it must decay as ξ approaches infinity, and it must equal the fracture pressure at $\xi = 0$. The zero-derivative condition in η is equivalent to the requirement, that $\bar{p}_R$ be n-periodic and even in η.

The first step in solving Eq. 5.1 is to assume that solutions exist in the form $R(\xi)\Theta(\eta)$, i.e., a function of ξ multiplied by a function of η. Inserting this product into Eq. 5.1 and rearranging yields:

$$-\frac{1}{\Theta}\frac{d^2\Theta}{d\eta^2} - \frac{s}{2}\cos(2\eta) = \frac{1}{R}\frac{d^2 R}{d\xi^2} - \frac{s}{2}\cosh(2\xi) = a. \tag{5.2}$$

Here we have set an expression that is only a function of η equal to an expression that is only a function of f t. Equality can hold only if both expressions are equal to a constant, the separation constant, **a.**

The equations in Eq. 5.2 are the "separated equations". The first of these:

$$\frac{d^2\Theta}{d\eta^2} + [a + \frac{s}{2}\cos(2\eta)]\,\Theta = 0, \tag{5.3}$$

is a form of Mathieu's equation. Equation 5.3 governs flow in the q-direction and so will be referred to as the angular Mathieu equation. This equation is subject to homogeneous derivative conditions at integral multiples of $\pi/2$.

The second separated equation is:

$$\frac{d^2 R}{d\xi^2} - [a + \frac{s}{2}\cosh(2\xi)]\,R = 0. \tag{5.4}$$

This equation is usually referred to as an associated Mathieu equation. Equation 5.4 governs flow in the ξ-direction and so we will refer to it as the radial Mathieu equation. The solutions we require must decay as ξ approaches infinity.

The discussion of the solutions of these two separated equations and the properties of these solutions comprise the remainder of this chapter.

5.2 The Angular Mathieu Functions, ce_{2n}

In this section we describe the even a-periodic angular Mathieu functions, ce_{2n} . Before we can discuss these functions, we need to discuss the separation constants, a_{2n}, which occur in the separated equations and also discuss the Fourier coefficients, A_{2r}^{2n}, which are used to express ce_{2n} by cosine series. The separation constants are intimately related to the eigenvalues of Eq. **5.3** which are the topic of the next subsection.

5.2.1 The Eigenvalues, λ_{2n}^2

In this subsection we discuss the eigenvalues, λ_{2n}^2 . The discussion will be largely qualitative, since we must defer the discussion of the quantitative aspects of the eigenvalues until we consider the Fourier coefficients.

The significance of the separation constant, a, is best illustrated by considering the angular Mathieu equation given in the previous section:

$$\frac{d^2\Theta_{2n}}{d\eta^2} + [a_{2n} + \frac{s}{2}\cos(2\eta)]\,\Theta_{2n} = 0. \tag{5.5}$$

Here we have added subscripts to Θ and a because there are an infinite number of these functions and constants that satisfy Eq. **5.5** and the symmetry conditions. Note that when $s = 0$, Eq. 5.5 becomes an equation with (constant coefficients. For $s = 0$, the only solutions which satisfy this equation and the: boundary conditions are $\cos(2n\eta)$.

Since, Θ_{2n} satisfy **a** homogeneous differential equation with homogeneous boundary conditions, they will play the role of the reservoir eigenfunctions. It is the properties of these eigenfunctions, principally orthogonality, which makes separation of variables such an effective tool.

Equation 5.5 is the defining equation for the eigenfunctions, ce_{2n} . Sturm-Liouville theory states that there exist only certain special values of a_{2n} for which these eigenfunctions exist. It is the determination of these constants which poses the first major problem in developing the eigensolutions.

We have made a point of referring to a_{2n} as separation constants and not eigen-
values. Technically, a_{2n} are not eigenvalues because Eq. 5.5 is not in standard Sturm-
Liouville form. This is because $\cos(2\eta)$ changes sign on the interval $(0, \pi)$. Equation
5.5 can be put into standard form by defining a new set of constants, $\lambda_{2n}^2 = a_{2n} + s/2$.
Using these new constants, which *are* the eigenvalues, and the half-angle identities of
cosines, puts Eq. 5.5 into Sturm-Liouville form:

$$\frac{d^2\Theta_{2n}}{d\eta^2} + [\lambda_{2n}^2 - s\sin^2(\eta)]\,\Theta_{2n} = 0. \tag{5.6}$$

In this form, Sturm-Liouville theory gives useful information about the eigenvalues,
λ_{2n}^2. The theory says that all of the eigenvalues are positive (or at least nonnegative).
It also states that there are an infinite number of them and. that they are all simple,
i.e., no two eigenvalues are equal. An unfortunate feature of the eigenvalues is that
they are functions not only of their index, but also of s. What is more, there is no
closed form expression for λ_{2n}^2 .

We can facilitate the discussion of the eigenvalues by examining a graph of λ_{2n}^2
versus s for various values of n. Figure 5.1 shows a graph of the first eleven eigenvalues.
This figure shows that each eigenvalue starts out at a value of $4n^2$ at $s = 0$. **As**
s increases each of the eigenvalues increases and each curve has a positive second
derivative until it reaches a point near the line $\lambda^2 = s$. At these points, each curve
has a point of inflection. After this, the second derivative becomes negative. The first
derivative remains positive, however, so that the eigenvalues are strictly increasing
functions of s.

The significance of the line, $\lambda_{2n}^2 = s$, is found by examining Eq. 5.6 with regard
to the coefficient of Θ_{2n}. If λ_{2n}^2 is greater than s, the coefficient is positive for all real
values of η. When the coefficient is positive we expect purely oscillatory solutions.
When s becomes greater than λ_{2n}^2, however, there are always certain ranges of η in
which the coefficient is negative. The values where the coefficient is zero are called
turning points. The existence of these turning points complicates the solution of
the differential equation, because they separate regions of oscillatory behavior from
those of exponential character. This difficulty is reflected in the determination of the
eigenvalues as well as the computation of the Mathieu functions.
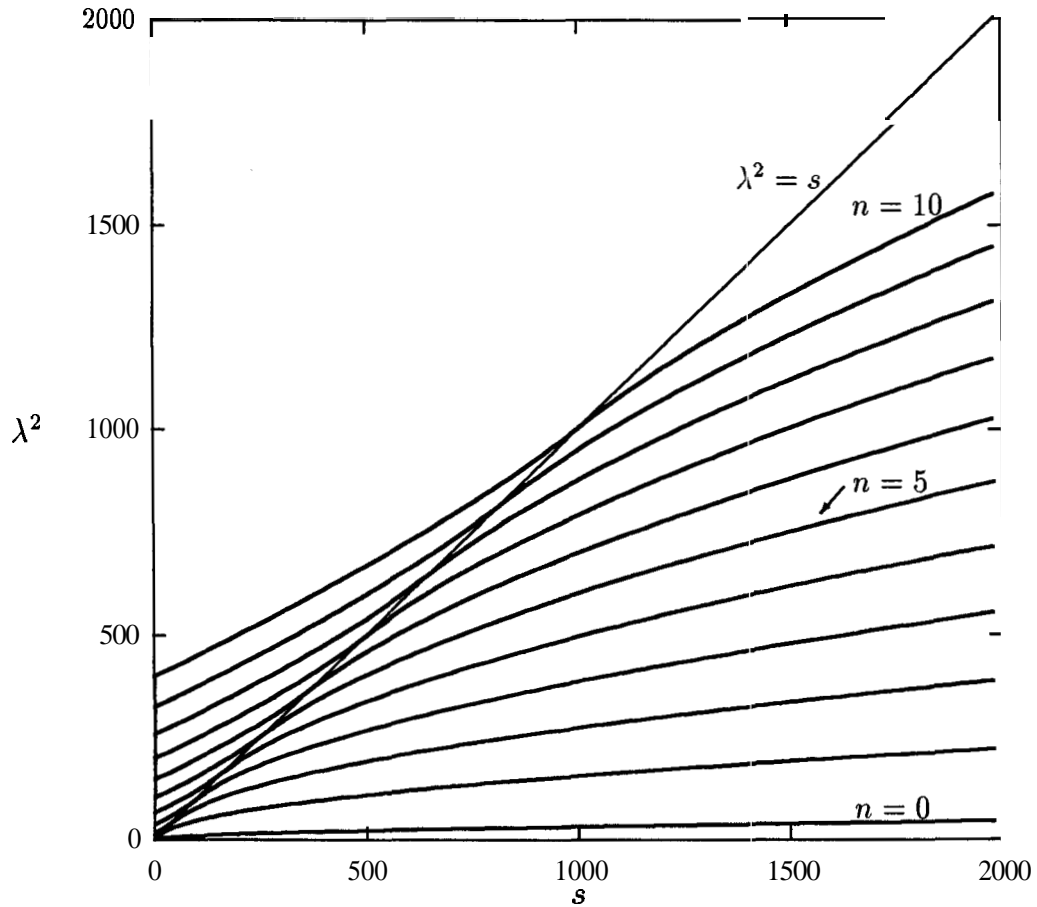
Figure 5.1: Eigenvalues, λ_{2n}^2, $n = 0 - 10$

The determination of the eigenvalues is somewhat involved. There are power series expansions for λ_{2n}^2, in powers of s, for each value of n. However, the radius of convergence of these series is less than $s = \lambda_{2n}^2$, i.e., the series converge to the left of the straight line on Fig. 5.1. Far to the right of this line, there is an asymptotic expansion which works fairly well. However, there is no satisfactory representation of the eigenvalues near the line, $\lambda^2 = s$. There is, however, a continued fraction which can be used to compute the eigenvalues for any value of s. This continued fraction will be discussed in some detail in Appendix B.

5.2.2   The Fourier Coefficients, A_{2r}^{2n}

This subsection is primarily concerned with the Fourier coefficients, A_{2r}^{2n}, which are used in the series representations of Mathieu functions. The discussion is aided by the construction of the solutions of the angular Mathieu equation, since the Fourier coefficients arise from the representation of ce_{2n} by cosine series. The Fourier coefficients are constrained by a set of recurrence relations derived from the Fourier series representation. The eigenvalues of Mathieu's equation are constrained by these same relations.

The reservoir eigenfunctions, ce_{2n}, satisfy the same periodicity requirements as $\cos(2n\eta)$ and become proportional to them as s approaches zero. So, it is not surprising that the solutions to the angular Mathieu equation are usually expressed by cosine series. In keeping with the literature, we shall refer to the solutions of Eq. 5.6, satisfying the homogeneous derivative conditions, as $ce_{2n}(\eta; -s/4)$. It is convenient, however, to solve Eq. 5.5 rather than Eq. 5.6 and to use a_{2n} rather than λ_{2n}^2.

The Mathieu functions, $ce_{2n}(\eta; -s/4)$, are usually represented as:

$$ce_{2n}(\eta; -s/4) = \sum_{r=0}^{\infty}(-1)^{r+n} A_{2r}^{2n}(s/4)\cos(2r\eta). \tag{5.7}$$

Here the coefficients, $A_{2r}^{2n}(s/4)$, have been written in this way to emphasize the **dependence** of the Fourier coefficients on s. Throughout this work we tacitly assume that the argument of the Fourier coefficients is $s/4$, unless otherwise specified. Also, note that "$2n$", which appears as a superscript, is a superscript and not a power.

Inserting Eq. 5.7 into Eq. 5.5, and equating coefficients of $\cos(2r\eta)$ to zero produces the recurrence relations:

$$4a_{2n}A_0^{2n} - sA_2^{2n} = 0 \ ,$$
$$4(a_{2n} - 4)A_2^{2n} - s(A_4^{2n} + 2A_0^{2n}) = 0 \ ,$$
$$r \geq 2 \quad 4(a_{2n} - 4r^2)A_{2r}^{2n} - s(A_{2(r+1)}^{2n} + A_{2(r-1)}^{2n}) = 0 \ . \tag{5.8}$$

Since these relations are all homogeneous, they define the Fourier coefficients only up to a multiplicative constant. This constant will be fixed by the normalization of ce_{2n} in the next section. The recurrence relations also constrain the separation

constants because the values of A_{2r}^{2n} are required to approach zero as r becomes infinite. It is interesting that this last requirement can only be fulfilled if a_{2n} takes on those same special values which allow solutions of Eq. 5.5 to be n-periodic and even. In Appendix B, we make this restriction on a_{2n} explicit by recasting the recurrence relations as a continued fraction.

In theory, once the eigenvalues have been found, the Fourier coefficients can be determined from the recurrence relations of Eq. 5.8. The recurrence relations are unstable in the forward direction, however, and so it is expedient to determine the coefficients from the continued fraction formulation used in determining the eigenvalues. This is also discussed in Appendix B.

Before discussing the properties of the "Fourier coefficients", A_{2r}^{2n}, we need to comment on their significance to Mathieu functions. We use the quotation marks to emphasize that, although we use many types of Fourier expansions in this work, the term Fourier coefficients is used to refer to A_{2r}^{2n} only. We introduced the Fourier coefficients through a cosine expansion of the angular Mathieu functions, but these coefficients are fundamental to all representations of Mathieu functions. They appear in all of the series expansions for the angular functions — cosine expansions as well as Bessel function expansions. They also appear in the expansions of the radial Mathieu functions. For our purposes they are essential, since the Fourier coefficients will be the building blocks of the sum equations of Chapter 6 independent of their role in the representation of Mathieu functions.

Analysis of the recurrence relations, Eq. 5.8, shows that convergence of the Fourier series, Eq. 5.7, is rapid. This is because the Fourier coefficients become proportional to $(-1)^r (s/16)^r/(r!)^2$, as r becomes infinite. It would be illustrative to show a graph of the Fourier coefficients. Since they are functions of r, n and s, there is no convenient way to do this. Therefore, we will give a qualitative appraisal of the coefficients in the cases of small and large s.

The behavior of the coefficients for small s is favorable from a computational standpoint. The previous discussion together with the normalization adopted in the

next section shows that ce_{2n} have the limiting form:

$$\lim_{s \to 0} ce_{2n}(\eta; -s/4) = \frac{\cos(2n\eta)}{\sqrt{\epsilon_n}} . \tag{5.9}$$

This implies that the Fourier coefficients have the limiting form:

$$\lim_{s \to 0} A_{2r}^{2n} = \frac{\delta_{nr}}{\sqrt{\epsilon_n}} . \tag{5.10}$$

In these last two relations, ϵ, is defined to be two, if $n = 0$, and is unity, otherwise. For small s and for r less than a fixed n, the coefficients increase factorially with r up to A_{2n}^{2n} and are all positive. For r greater than n, the coefficients decrease factorially with r and have alternating signs. This means that there is only a narrow range of r, centered at $r = n$, in which the coefficients differ significantly from zero.

The behavior for large s is less favorable. The large s behavior seems to begin at the straight line of Fig. 5.1, i.e., large s behavior starts with the appearance of turning points. As s increases a second region develops. Again we are considering n fixed. This region is again centered at n, but the coefficients no longer decay near $r = n$. In this second region the coefficients change magnitude and sign in an apparently random fashion. In addition, the coefficient, A_{2n}^{2n}, is no longer guaranteed to have the greatest magnitude and itself changes sign. The size of this secondary region increases with s, but the coefficients outside this region still decrease rapidly. This large s behavior not only makes the coefficients more difficult to calculate, simply because there are more of them, but this behavior also makes the resulting Fourier series converge more slowly.

This ends the discussion, in the main text, of the computational aspects of the Mathieu functions. Appendix B discusses the computation of the eigenvalues and the Fourier coefficients in detail.

5.2.3   Qualitative Aspects of ce_{2n}

Mathieu functions differ from those functions normally used in petroleum engineering. Most of the functions used in petroleum engineering: error functions, exponential integrals and Bessel functions, are of hypergeometric type. These hypergeometric functions possess power series expansions, integral representations, recurrence relations

and the like, all in terms of explicitly defined coefficients, integrands etc. This is not the case with Mathieu functions: the power series representations of Mathieu functions are not useful, no known integral representations exist {(insteadhere are integral equations which contain Mathieu functions themselves), and the recurrence relations for ce_{2n} have coefficients which are complicated functions of Mathieu functions.

As alluded to earlier, the functions, ce_{2n}, are similar to the trigonometric functions, $\cos(2n\eta)$. They have the same number of oscillations, in any interval of length π, as $\cos(2n\eta)$, but, for large values of s, the oscillations are confined to regions between turning points.

Typical behavior of Mathieu functions is shown in Fig. 5.2. This figure shows the function, ce_4, for s equal to 1, 10, 100 and 1000, for η between $-\pi/2$ and $\pi/2$. For low values of s, the function is closely approximated by $\cos(4\eta)$. For higher values of s the function changes shape: the appearance of turning points restricts the oscillatory behavior to a narrow range of η.

There is another property of Mathieu functions that is important in the solution of the finite conductivity fracture problem: for sufficiently large n, $ce_{2n}(\eta; -s/4)$ becomes equal to $\cos(2n\eta)$ to any tolerance desired. Another way of saying this is that a value of s, which is considered large for a function of low order, is considered small for a function of much higher order. This is illustrated by Fig. **5.3** where we have plotted $ce_{2n}(\eta; -25)$ for n equal to $1, 3, 5$, and 7. From this figure it is clear that the two lowest order eigenfunctions are not purely oscillatory — turning points have developed. However, the highest order eigenfunction looks much like $\cos($**1417**$)$. For higher values of n, ce_{2n} will resemble $\cos(2n\eta)$ even more closely. This is significant, since in later chapters we will equate a cosine series to a Mathieu function series. This property implies that for large n, the coefficients in the Mathieu function series must equal those in the cosine series.

This ends the discussion of the descriptive properties of the angular Mathieu functions. Before we describe analytic properties of these functions, however, we need to mention the second solutions of Mathieu's equation. Since Eq. **5.6** is a linear second order equation, there must be a second solution that is linearly independent of ce_{2n} . Since the first solution is analogous to cosine, we expect the second solution
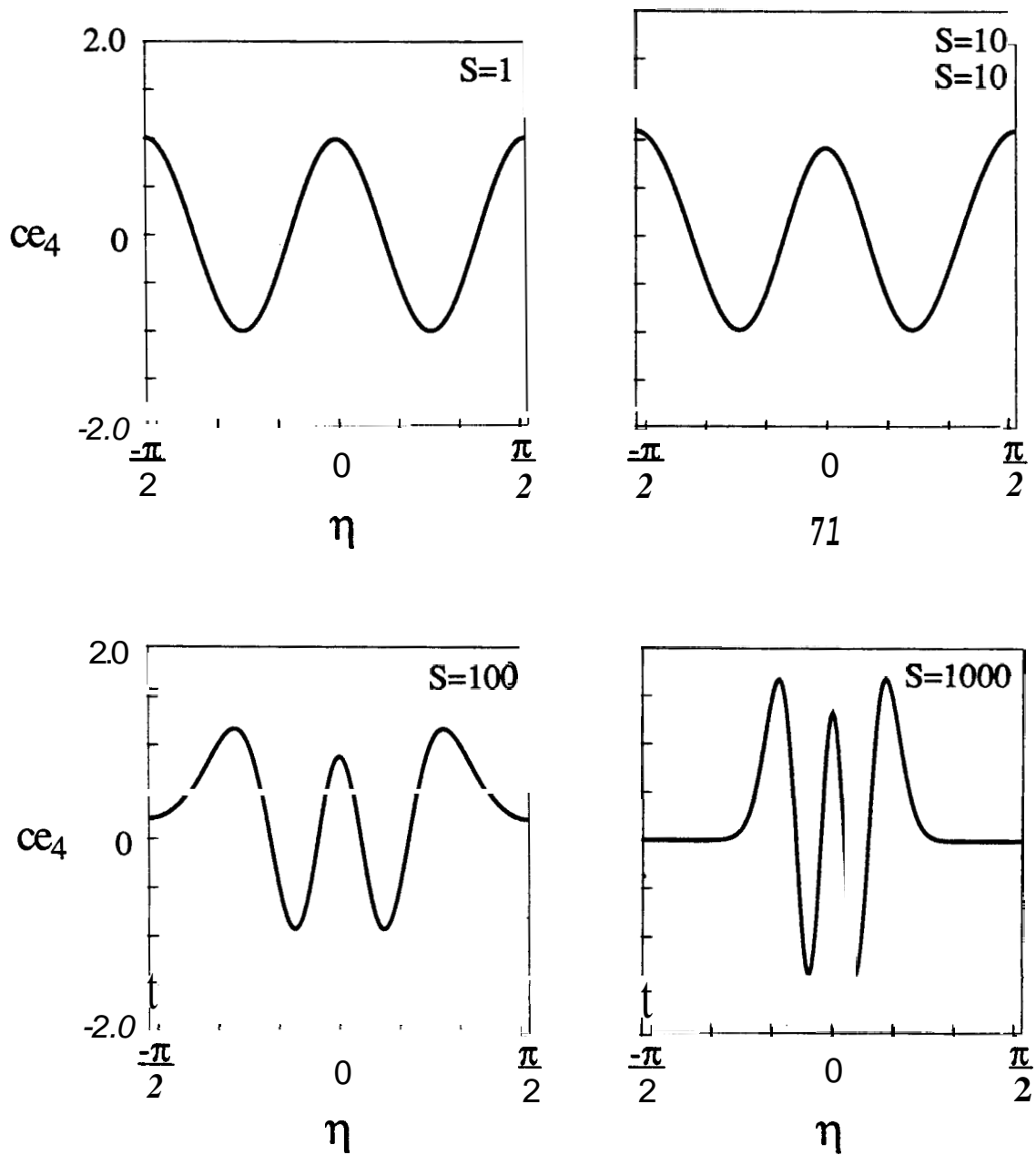
Figure **5.2:** ce_4 **as** a function of s
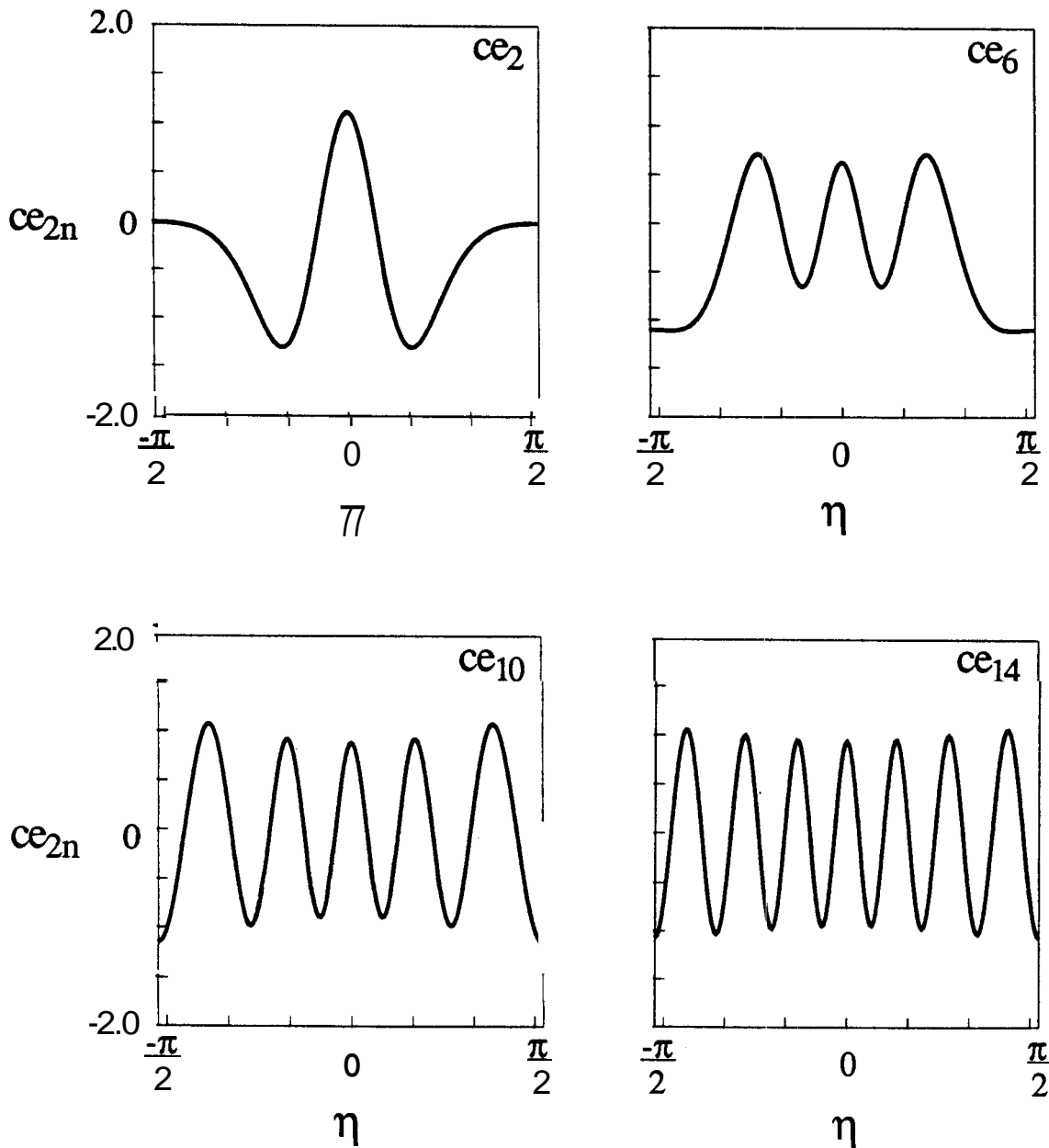
Figure **5.3:** ce_{2n} as a function of n, $s = 100$

to be analogous to sine. This is not the case. The second solution, denoted fe_{2n} by McLachlan (1947), is not oscillatory and bears little resemblance to any trigonometric function. It also does not satisfy the symmetry requirements and so must be discarded. In passing, it should be said that solutions analogous to $\sin(2n\eta)$ require a different set of separation constants. These separation constants are usually denoted b_{2n+2} and are constructed in a way analogous to that shown above.

5.2.4 Orthogonality Properties

In this subsection we discuss the orthogonality properties of the angular Mathieu functions, the Mathieu Fourier coefficients and the functions, $\cos(2r\eta)$. These properties will be used in the next chapter, where we derive the Fredholm sum equations which are the focus of this work.

The functions, ce_{2n}, possess an orthogonality relation because they satisfy a Sturm-Liouville problem. This orthogonality relation states that the integral of the product of two eigenfunctions over a period will be zero, if the functions are of different order, or a constant, if the functions are of the same order. This relation can be written as:

$$\int_0^{\frac{\pi}{2}} ce_{2m}(\eta; -s/4) ce_{2n}(\eta; -s/4) d\eta = \frac{\pi}{4} \delta_{mn} . \tag{5.11}$$

The Kronecker delta function, δ_{mn}, is defined to be zero unless $m = n$, in which case it is unity. Implicit in Eq. **5.11** is that ce_{2n} has norm $\pi/2$, i.e., the square integral of ce_{2n} over any interval of length π is equal to $\pi/2$. This normalization is the one most commonly used in the literature.

The analysis of related orthogonality properties is facilitated by the use of the cosine series representation, Eq. **5.7**:

$$ce_{2n}(\eta; -s/4) = \sum_{r=0}^{\infty} (-1)^{r+n} A_{2r}^{2n} \cos(2r\eta). \tag{5.12}$$

This form is useful because the functions, $\cos(2r\eta)$, also satisfy a Sturm-Liouville problem and, hence, possess an orthogonality relation:

$$\int_0^{\frac{\pi}{2}} \cos(2r\eta) \cos(2p\eta) d\eta = \epsilon_r \frac{\pi}{4} \delta_{rp} . \tag{5.13}$$

Recall, ϵ_r, is two, if $r = 0$, and unity, otherwise.

We can now demonstrate an orthogonality property of the Fourier coefficients, A_{2r}^{2n}, over summation. This discrete orthogonality relation is obtained by using **Eq. 5.12** to represent both Mathieu functions in Eq. **5.11.** Subsequent use of Eq. **5.13** yields:

$$\sum_{r=0}^{\infty} \epsilon_r A_{2r}^{2m} A_{2r}^{2n} = \delta_{mn} .\tag{5.14}$$

This is the first orthogonality property of Fourier coefficients over summation. A second expression of this type will be given later in this section.

For $n = m$, Eq. **5.14** shows that the Fourier coefficients satisfy the normalization:

$$2(A_0^{2n})^2 + \sum_{r=1}^{\infty} (A_{2r}^{2n})^2 = 1.\tag{5.15}$$

This normalization taken together with recurrence relations, Eq. **5.8,** fully constrains the magnitude of the Fourier coefficients. The sign of A_{2r}^{2n} is fixed by requiring A_0^{2n} to be positive.

In addition to its orthogonality properties, Sturm-Liouville theory states that the functions, ce_{2n}, comprise a complete set. This means that any even n-periodic function can be written as an infinite series of Mathieu functions. The same completeness property holds for $\cos(2r\eta)$. Hence, an arbitrary even n-periodic function, $f(\eta)$, can be written:

$$f(\eta) = \sum_{n=O}^{\infty} (-1)^n \gamma_{2n} ce_{2n}(\eta; -s/4) = \sum_{r=0}^{\infty} (-1)^r \beta_{2r} \cos(2r\eta).\tag{5.16}$$

The factors, $(-1)^r$ and $(-1)^n$, have been used because they simplify expressions derived below.

Application of the orthogonality relations to Eq. **5.16** shows that the coefficients, γ_{2n} and β_{2r}, can be expressed as integrals:

$$\gamma_{2n} = \frac{4(-1)^n}{\pi} \int_0^{\frac{\pi}{2}} f(\eta) ce_{2n}(\eta; -s/4) d\eta, \qquad \beta_{2r} = \frac{4(-1)^r}{\epsilon_r \pi} \int_0^{\frac{\pi}{2}} f(\eta) \cos(2r\eta) d\eta. \tag{5.17}$$

The orthogonality and completeness properties allow us to write Mathieu function series and cosine series in terms of each others coefficients. This requires the use of the relation:

$$\int_0^{\frac{\pi}{2}} ce_{2n}(\eta; -s/4) \cos(2r\eta) d\eta = (-1)^{n+r} \frac{\pi}{4} \epsilon_r A_{2n}^{2r} .\tag{5.18}$$

Equation *5.18* is derived by using the cosine series representation of ce_{2n}, Eq. *5.12*, and the orthogonality property of $\cos(2r\eta)$, Eq. *5.13*.

Applying the orthogonality property of $\cos(2r\eta)$ and Eq. *5.18*, to Eq. *5.16* gives:

$$\beta_{2r} = \sum_{n=0}^{\infty} A_{2r}^{2n}\gamma_{2n} \ . \tag{5.19}$$

Applying the orthogonality property of ce_{2n} and **Eq. *5.18*,** to Eq. *5.16* gives:

$$\gamma_{2n} = \sum_{r=0}^{\infty} \epsilon_r A_{2r}^{2n}\beta_{2r} \ . \tag{5.20}$$

These two relations allow us to write the coefficients of a cosine series in terms of the coefficients of a Mathieu function series, and *vice versa.*

As an application of these relations, we show the expansion of $\cos(2p\eta)$ as a series of Mathieu functions. In this case, $\beta_{2r} = (-1)^r \delta_{rp}$. Use of Eq. *5.20* gives:

$$\cos(2p\eta) = \sum_{n=0}^{\infty}(-1)^n \left(\sum_{r=0}^{\infty} \epsilon_r(-1)^r \delta_{rp} A_{2r}^{2n} \right) ce_{2n}(\eta) = \epsilon_p \sum_{n=0}^{\infty}(-1)^{n+p} A_{2p}^{2n} ce_{2n}(\eta). \tag{5.21}$$

Using this relation, to represent both cosine functions in Eq. *5.13,* and the orthogonality property of ce_{2n} gives a second orthogonality relation for the Fourier coefficients over summation:

$$\epsilon_r \sum_{n=0}^{\infty} A_{2r}^{2n} A_{2p}^{2n} = \delta_{rp} \ . \tag{5.22}$$

This discrete orthogonality relation, together with Eq. *5.14,* will be used in Chapter *6* to manipulate the sum equations.

The discrete orthogonality properties, Eqs. *5.14* and *5.22,* of the Fourier coefficients at first appear rather mystical. However, some reflection will show that they are equivalent to the continuous orthogonality properties of ce_{2n} and $\cos(2r\eta)$. The importance of the discrete orthogonality properties is that they can be used to manipulate expressions in which explicit η dependence has been removed, i.e., they can be used after the problem has been reduced to a relation between coefficients. This will enable us, in Chapter *6,* to derive equivalent forms of sum equations almost at will.

In this section we have concentrated on the relations between Mathieu functions and cosine functions. This is because, in the next chapter, we represent the fracture

pressure by a cosine series. The cosine series will arise naturally from the assumption of incompressible fracture flow.

5.3 The Radial Mathieu Functions, Fek$_{2n}$

The subject of this section is the radial functions, Fek_{2n} . In the previous section we dealt with the eigenfunctions, ce_{2n} . That discussion required some fairly delicate manipulations, because we were solving an eigenvalue problem which required the determination of eigenvalues. Discussion of the radial functions will be much more direct. It is simplified greatly because we have already discussed the Fourier coefficients.

The equation which determines the radial functions is the separated equation, **Eq. 5.4.** Substituting R_{2n} for R and a_{2n} for a yields:

$$\frac{d^2 R_{2n}}{d\xi^2} - \left[a_{2n} + \frac{s}{2}\cosh(2\xi)\right] R_{2n} = 0. \tag{5.23}$$

The requirement that reservoir pressure decays at infinity means that R_{2n} must vanish as ξ approaches infinity. Two linearly independent solutions of Eq. *5.23* are given by McLachlan *(1947)* as $Fek_{2n}(\xi; -s/4)$ and $Ce_{2n}(\xi; -s/4)$. The functions, Ce_{2n}, become infinite as ξ becomes infinite while, Fek_{2n} approach zero as ξ approaches infinity. So we use only the functions, Fek_{2n} .

The derivation of the representation of Fek_{2n} is fairly complex and will not be given here. The series representation is discussed in Chapter **13** of McLachlan *(1947)*. It is convenient to normalize the radial function by its value at zero and deal with the function, $Fek_{2n}(\xi; -s/4)/Fek_{2n}(0; -s/4)$. This radial function is represented by a ratio of two series of modified Bessel functions:

$$\frac{Fek_{2n}(\xi; -s/4)}{Fek_{2n}(0; -s/4)} = \frac{\sum_{r=0}^{\infty} A_{2r}^{2n} I_r(v_1) K_r(v_2)}{\sum_{r=0}^{\infty} A_{2r}^{2n} I_r(\sqrt{s}/2) K_r(\sqrt{s}/2)} . \tag{5.24}$$

In Eq. *5.24,* v_1 is equal to $\sqrt{s}e^{-\xi}/2$ and v_2 is equal to $\sqrt{s}e^{+\xi}/2$. Defined in this way, as a ratio, the radial solution has simple characteristics: it decays exponentially at infinity, it has a value of unity at $\xi = 0$, and decreases monotonically as ξ increases.

In this work, we are primarily interested in the derivative of the radial function with respect to ξ evaluated at the origin: $Fek'_{2n}(0; -s/4)/Fek_{2n}(0; -s/4)$. Because we shall use this ratio often, we denote it as $\mathcal{F}_{2n}$. The expression for this derivative is similar to Eq. *5.24:*

$$\mathcal{F}_{2n} = \frac{Fek'_{2n}(0; -s/4)}{Fek_{2n}(0; -s/4)} = \frac{-(-1)^n ce_{2n}(\pi/2; -s/4)}{\sum_{r=0}^{\infty} A_{2r}^{2n} I_r(\sqrt{s}/2) K_r(\sqrt{s}/2)} \; . \tag{5.25}$$

We have made use of Eq. **13.31 (13)** of McLachlan **(1947)** to simplify the numerator of this expression. For large s, Eq. *5.25* will prove difficult to evaluate. The computation of this derivative has proven to be a major obstacle in this iresearch and Appendix C is devoted to its computation.

It can be shown that as n becomes infinite, $\mathcal{F}_{2n}$ becoimes equal to $-2n$. This simplifying form also holds as s approaches zero, for $n \neq 0$. The limiting behavior for small s, explicitly stated is:

$$\begin{aligned} \lim_{s\to 0} \mathcal{F}_0 &= -1/\ln(4/\sqrt{s}\gamma') & n = 0, \\ \lim_{s\to 0} \mathcal{F}_{2n} &= -2n & n > 0. \end{aligned} \tag{5.26}$$

The constant, y', is the exponential of Euler's constant and is approximately equal to **1.781.**

This ends the discussion of the radial functions, Fek_{2n} . The next section will combine the radial functions with the angular functions to present **a** series representation of the reservoir pressure.

5.4 The Reservoir Solution

This chapter has dealt largely with the determination of the functions which satisfy the separated equations of the first section. The previous discussion indicates that the product, $ce_{2n}Fek_{2n}$, satisfies the reservoir equation, **Eq.** *5.1,* for any value of *n*. This product also satisfies the boundedness condition as ξ approaches infinity and the symmetry requirements at η equal to multiples of $\pi/2$.

Since the product, $ce_{2n}Fek_{2n}$, comprises a complete set, the full expression for the reservoir pressure can be written as an infinite sum of this product. For convenience

we represent the reservoir pressure as:

$$\bar{p}_R(\eta, \xi; s) = \sum_{n=0}^{\infty} \frac{(-1)^n \gamma_{2n} ce_{2n}(\eta; -s/4) Fek_{2n}(\xi; -s/4)}{Fek_{2n}(0; -s/4)} \tag{5.27}$$

Equation 5.27 gives the pressure anywhere in the reservoir, including the fracture. The only unknowns in this equation are the coefficients, γ_{2n} . The factor, $(-1)^n / Fek_{2n}(0)$, has been included to enable direct use of Eqs. 5.19 and 5.210.

We have thus reduced the problem of determining the reservoir pressure to the problem of finding the values of the coefficients in its series. It is a matter of some debate whether this is progress, but we shall concentrate our efforts on determining these coefficients. The path we shall follow is to insert the reservoir pressure series and the fracture pressure series (to be given in the next chapter) into the fracture equation. Manipulation of the resultant expression gives the sum equations whose solutions we pursue throughout the remainder of this work.

Chapter 6

THE FREDHOLM SUM EQUATIONS

In this chapter we derive relations which constrain the coefficients in the series representations of reservoir and fracture pressure. These constraining relations take the form of Fredholm sum equations. The solution of any one of these equations allows computation of pressures anywhere in the reservoir/fracture system.

The coefficients in the series expansions are not readily obtained using conventional methods. This is because the eigenfunctions of the reservoir and fracture problems differ from each other. The reason for this difference is that the diffusivities of the reservoir and fracture are unequal. To emphasize this point, the first section will consider a problem which is readily solvable using the orthogonality properties of ce_{2n} . This problem models the distinguished case of equal fracture and reservoir diffusivity. The equal diffusivity system does not model any physically realistic phenomenon, but it provides a means of illustrating some important points.

6.1   The Matched Diffusivity Problem

In this section we solve the composite problem in the case where fracture diffusivity is equal to reservoir diffusivity. The solution will not be of use in field applications, since the diffusivity ratio, κ_D, in the field is of the order 10^{-6} to 10^{-8}. The matched

diffusivity problem will be shown to have a straightforward solution in terms of a Mathieu function series. The solution will be used to give the limiting form of the coefficients as $s \to 0$ for any value of κ_D.

The matched diffusivity problem requires solution of the fracture equation, Eq. **4.15** of Chapter **4**:

$$\frac{\partial^2 \bar{p}_f}{\partial \eta^2} + \frac{2}{F_E} \frac{\partial \bar{p}_R}{\partial \xi}\bigg|_{\xi=0} - s\kappa_D \sin^2(\eta)\bar{p}_f = \frac{-\pi}{sF_E} \delta(\eta - \pi/2), \tag{6.1}$$

with κ_D equal to unity. In arriving at Eq. **6.1,** we have made use of the identity, $[1 - \cos(2\eta)]/2 = \sin^2(\eta)$. Equation **6.1** is subject to the boundary conditions:

$$\frac{\partial \bar{p}_f}{\partial \eta}\bigg|_{\eta=\pi/2} = \frac{\partial \bar{p}_f}{\partial \eta}\bigg|_{\eta=0} = 0. \tag{6.2}$$

The eigensolutions of Eq. **6.1,** can be shown to be $ce_{2n}(\eta; -\kappa_D s/4)$. Therefore, we choose to represent the solution of Eq. **6.1,** with $\kappa_D = 1$, as:

$$\bar{p}_f(\eta; s) = \sum_{r=0}^{\infty}(-1)^r \beta_{2r} ce_{2r}(\eta; -s/4). \tag{6.3}$$

The reservoir pressure series was presented as Eq. **5.27** of the last chapter, and will remain the reservoir solution throughout this work:

$$\bar{p}_R(\eta, \xi; s) = \sum_{n=0}^{\infty} \frac{(-1)^n \gamma_{2n} Fek_{2n}(\xi; -s/4)ce_{2n}(\eta; -s/4)}{Fek_{2n}(0; -s/4)} \tag{6.4}$$

Equations **6.3** and **6.4** contain two sets of undetermined 'constants and must fulfill two constraints: Eq. **6.4** evaluated at $\xi = 0$ must equal Eq. **6.3,** and the two series must satisfy the fracture differential equation, Eq. **6.1.**

If we set ξ equal to zero in Eq. **6.4,** the Fek_{2n} functions will cancel and it becomes identical in form to Eq. **6.3.** Therefore, $\beta_{2j} = \gamma_{2j}$ for all **j.** This relation satisfies the first constraint. By contrast, in the incompressible case, a single coefficient of one series will be represented as a weighted sum over all of the coefficients of the other series. This is because the incompressible case involves series representations containing different eigenfunctions.

The second constraint requires that the reservoir and fracture series combine to satisfy Eq. 6.1. Inserting Eq. 6.4 and Eq. 6.3 into Eq. 6.1, setting $\beta_{2j} = \gamma_{2j}$, and κ_D equal to unity gives:

$$\sum_{n=0}^{\infty}(-1)^n\gamma_{2n}ce_{2n}''(\eta; -s/4) + \frac{2}{F_E}\sum_{n=0}^{\infty}(-1)^n\gamma_{2n}\mathcal{F}_{2n}ce_{2n}(\eta; -s/4)$$

$$-s\sin^2(\eta)\sum_{n=0}^{\infty}(-1)^n\gamma_{2n}ce_{2n}(\eta; -s/4) = \frac{-\pi}{sF_E}\delta(\eta - \pi/2). \tag{6.5}$$

Here we have used the notation $\mathcal{F}_{2n} = Fek_{2n}'(0; -s/4)/Fek_{2n}(0; -s/4)$ and assumed the validity of interchanging the orders of summation and differentiation. This termwise differentiation is valid because the Dirac delta function has been used to account for well production.

The defining equation for ce_{2n} is Eq. 5.6 of Chapter 5:

$$ce_{2n}''(\eta; -s/4) - s\sin^2(\eta)ce_{2n}(\eta; -s/4) = -\lambda_{2n}^2 ce_{2n}(\eta; -s/4) . \tag{6.6}$$

This equation allows us to combine the first and third terms in Eq. 6.5. Making this substitution and rearranging the result gives:

$$\sum_{n=0}^{\infty}(-1)^n\gamma_{2n}\left(\frac{2}{F_E}\mathcal{F}_{2n} - \lambda_{2n}^2\right)ce_{2n}(\eta; -s/4) = \frac{-\pi}{sF_E}\delta(\eta - \pi/2) . \tag{6.7}$$

It is now a simple matter to remove the summation sign using the orthogonality property of Mathieu functions. Before doing this, however, we should pause and consider the reason that **Eq.** 6.7 has such a simple form. The reason is simple—we were able to use Eq. 6.6 to remove both the second derivative and the sine term from Eq. 6.5 because we had set κ_D equal to unity in the fracture equation. Had we not set $\kappa_D = 1$, a sine term would have remained in Eq. 6.7 and orthogonality would not be of much use. A similar difficulty will arise in the incompressible case and will be the reason we are forced to solve sum equations.

If we multiply Eq. 6.7 by $ce_{2m}(\eta; -s/4)$, integrate from 0 to $\pi/2$, use the orthogonality property of the Mathieu functions and the sifting property of the delta function, the coefficients are determined explicitly. The result of these manipulations is:

$$\gamma_{2n} = \frac{4(-1)^n ce_{2n}(\pi/2; -s/4)}{s(F_E\lambda_{2n}^2 - 2\mathcal{F}_{2n})} \tag{6.8}$$

We will not use Eq. 6.8 for any computations, since it is the solution to an unrealistic problem. However, Eq. 6.8 can be used to give an important limiting form for any value of diffusivity ratio.

Taking the limit of Eq. 6.8 as s approaches zero gives the late time form of the coefficients, γ_{2n}. Using Eq. 6.8, the limiting forms, Eqs. 5.9 and 5.26 of the last chapter, and inserting the result into Eq. 6.3 gives the small s form of the fracture pressure:

$$\bar{p}_f(\eta; s \to 0) = \frac{\ln(4/\gamma'\sqrt{s})}{s} + \frac{1}{s}\sum_{r=1}^{\infty}\frac{(-1)^r\cos(2r\eta)}{r^2 F_E + r} \tag{6.9}$$

It is not a coincidence that this equation is essentially the steady-state solution given by Prats (1961) (though there seems to be an error in his Eq. A-27). Equation 6.9 was derived for the equal diffusivity case, but it can be shown to be the limiting form of the solution for any nonnegative value of κ_D. This is important because as n becomes arbitrarily large, ce_{2n} approach their low s forms, i.e., $\cos(2n\eta)$, for any value of s. This means that no matter what are the values of s and κ_D, only a finite number of terms of the exact solution will differ significantly from those of **Eq.** 6.9.

The above derivation was straightforward because the eigenfunctions of the reservoir and fracture problems were identical. This is because the eigenfunctions of the fracture equation, Eq. 6.1, are $ce_{2r}(\eta; -s\kappa_D/2)$. If κ_D is not equal to unity, the Mathieu functions in the reservoir and fracture series will have different parameters. Mathieu functions of different parameters are different functions and are not orthogonal to each other (see Riley (1990)). This idea will be brought out in the following section where we consider the case $\kappa_D = 0$ and represent the fracture pressure by a cosine series. This representation makes sense when we recall that $\cos(2r\eta)$ are proportional to $ce_{2r}(\eta; 0)$.

6.2 The Sum Equations

In this section we derive the sum equations to which we have been referring for some time. We present four equivalent expressions which seem to be primary—other expressions can be derived from these. Each sum equation comprises an infinite

set of algebraic relations which fully constrain the coefficients of one of the series. Sum equations result from solving the composite flow problem for cases where κ_D is not equal to unity. The sum equations are the crux of this work—solution of any one of them enables determination of pressure anywhere in the fracture/reservoir system. In the remainder of this work, we treat only the case of κ_D equal to zero, i.e., incompressible fracture flow.

The sum equations result from inserting the reservoir and fracture pressure series into Eq. 6.1. We consider the fracture flow to be incompressible, so we set κ_D equal to zero:

$$\frac{\partial^2 \bar{p}_f}{\partial \eta^2} + \frac{2}{F_E} \frac{\partial \bar{p}_R}{\partial \xi}\bigg|_{\xi=0} = \frac{-\pi}{sF_E}\,\delta(\eta - \pi/2). \tag{6.10}$$

The boundary conditions are unchanged:

$$\frac{\partial \bar{p}_f}{\partial \eta}\bigg|_{\eta=0} = \frac{\partial \bar{p}_f}{\partial \eta}\bigg|_{\eta=\pi/2} = 0. \tag{6.11}$$

The fracture pressure series is found by determining the eigenfunctions of Eq. 6.10. To determine the eigenfunctions, we consider the related homogeneous problem, i.e., the homogeneous form of Eq. 6.10 is set equal to the product of the eigenfunction and an eigenvalue:

$$\frac{\partial^2 \phi}{\partial \eta^2} = \lambda^2 \phi \tag{6.12}$$

The only functions which satisfy this equation and Eq. 6.11 are proportional to $\cos(2r\eta)$, for integer r. Thus, fracture pressure can be represented by:

$$\bar{p}_f(\eta; s) = \sum_{r=0}^{\infty} (-1)^r \beta_{2r} \cos(2r\eta). \tag{6.13}$$

The factor $(-1)'$ has been included to facilitate equating Eq. 6.13 to Eq. 6.4 at the fracture face.

Inserting Eqs. 6.4 and 6.13 into Eq. 6.10 and interchanging the orders of summation and differentiation, yields:

$$\sum_{r=0}^{\infty}(-1)^r(-4r^2)\beta_{2r}\cos(2r\eta) + \frac{2}{F_E}\sum_{n=0}^{\infty}(-1)^n\gamma_{2n}\mathcal{F}_{2n}ce_{2n}(\eta; -s/4)$$
$$= \frac{-\pi}{sF_E}\delta(\eta - \pi/2). \tag{6.14}$$

This equation will be recast as Fredholm sum equations in the next two subsections.

6.2.1   Sum Equations Involving β_{2r}

In this subsection we present two equivalent forms of sunn equation involving β_{2r}. The first equation results from removing the η dependence of Eq. **6.14,** using the orthogonality properties of $\cos(2r\eta)$, and writing γ_{2n} in terms of β_{2r}. The second sum equation is derived from the first using the discrete orthogonality properties of the Fourier coefficients.

Multiplying Eq. **6.14** by $\cos(2p\eta)$, using the orthogonality properties of these functions, the sifting properties of the delta function and the relations:

$$\gamma_{2n} = \sum_{r=0}^{\infty} \epsilon_r A_{2r}^{2n} \beta_{2r} \ , \qquad \int_0^{\frac{\pi}{2}} ce_{2n}(\eta) \cos(2r\eta) d\eta = (-1)^{n+r} \epsilon_r \frac{\pi}{4} A_{2r}^{2n}, \qquad (6.15)$$

developed in Chapter **5,** gives:

$$2 F_E r^2 \beta_{2r} - \sum_{p=o}^{\infty} \epsilon_p \mho_{2p}^{2r} \beta_{2p} = \frac{2}{s \epsilon_r} \ . \qquad (6.16)$$

The kernel of Eq. **6.16,** $\mho$, is defined by the sum:

$$\mho_{2p}^{2r} = \mho_{2r}^{2p} = \sum_{m=0}^{\infty} A_{2r}^{2m} A_{2p}^{2m} \mathcal{F}_{2m} \ . \qquad (6.17)$$

Equation **6.16** is the first sum equation. It comprises an infinite set of linear relations which fully constrain the values of the coefficients; β_{2r}. In Eq. **6.16,** β_{2r} is the unknown, $\mho_{2p}^{2r}$ is the kernel, and $2/s\epsilon_r$ is the inhomogeneity. We refer to this set of linear relations as an inhomogeneous Fredholm sum equation of the second kind. This is because of the close resemblance of Eq. **6.16** to the inhomogeneous Fredholm *integral* equation of the second kind:

$$\phi(x) + \lambda \int_a^b K(x, x') \phi(x') dx' = f(x). \qquad (6.18)$$

In the integral equation: $\phi(x)$ is the unknown function, while $K(x, x')$ and $f(x)$ are the known kernel and inhomogeneity, respectively. The theory of integral equations is fairly well developed, however no theory of sum equations is known to this author. In considering the sum equations we shall borrow heavily from the theory of integral equations: we shall assume that the solutions of the sum equations exist and are

unique, and in Chapter 7 we shall use the discrete analogy of the Neumann series to derive a series solution for β_{2r}.

Equation 6.16 is amenable to solution for large values of F_E. This will be discussed in Chapter 7. We now derive a second sum equation from Eq. 6.16, which is amenable to solution for low values of F_E. This derivation requires the inverse of the kernel, $\mho$. This inverse kernel, which we call Ω, can be found by inspection to be:

$$\Omega_{2p}^{2r} = \Omega_{2r}^{2p} = \sum_{m=0}^{\infty} \frac{A_{2r}^{2m} A_{2p}^{2m}}{\mathcal{F}_{2m}} .\tag{6.19}$$

Summing the product of the two kernels, R and $\mho$, using the discrete orthogonality relations given in Chapter 5:

$$\epsilon_r \sum_{n=0}^{\infty} A_{2r}^{2n} A_{2p}^{2n} = \delta_{rp} , \qquad \sum_{r=0}^{\infty} \epsilon_r A_{2r}^{2m} A_{2r}^{2n} = \delta_{nm} ,\tag{6.20}$$

and the definitions of the kernels, shows that they are orthogonal in the sense:

$$\sum_{q=0}^{\infty} \epsilon_q \, \Omega_{2q}^{2r} \, \mho_{2q}^{2p} = \frac{\delta_{rp}}{\epsilon_r} .\tag{6.21}$$

To derive the second sum equation we need only to multiply Eq. 6.16 by $\epsilon_r \Omega_{2r}^{2q}$ and sum over r. We can simplify the resultant expression by noting:

$$\sum_{r=0}^{\infty} \Omega_{2r}^{2q} = \sum_{r=0}^{\infty} \sum_{m=0}^{\infty} \frac{A_{2r}^{2m} A_{2q}^{2m}}{\mathcal{F}_{2m}} = \sum_{m=0}^{\infty} \frac{A_{2q}^{2m}}{\mathcal{F}_{2m}} \sum_{r=0}^{\infty} A_{2r}^{2m} =$$
$$= \sum_{m=0}^{\infty} \frac{(-1)^m A_{2q}^{2m} ce_{2m}(\pi/2; -s/4)}{\mathcal{F}_{2m}} = -\frac{I_q(\sqrt{s}/2) K_q(\sqrt{s}/2)}{\epsilon_q} .\tag{6.22}$$

The fourth term in Eq. 6.22 uses the cosine series representation of ce_{2n} . The final expression in Eq. 6.22 results from applying Eq. 6.20 to Eq. 5.25 of Chapter 5.

Performing the steps outlined above, gives the second sum equation:

$$\beta_{2r} - 2F_E \sum_{p=1}^{\infty} p^2 \beta_{2p} \Omega_{2r}^{2p} = \frac{2}{s} \frac{I_r(\sqrt{s}/2) K_r(\sqrt{s}/2)}{\epsilon_r} .\tag{6.23}$$

This equation is equivalent to Eq. 6.16, but is amenable to solution for low values of F_E. Solution to either Eq. 6.16 or Eq. 6.23 will give the fracture pressure using

Eq. **6.13.** Since the first relation of Eq. **6.15** gives γ_{2n} in terms of β_{2r}, the reservoir pressure can be obtained from Eq. **6.4.**

Because we are primarily interested in well pressures and because the reservoir pressures can be found from the coefficients, β_{2r}, the remaining chapters concentrate on obtaining the coefficients, β_{2r}. However, for the sake of completeness, sum equations for the coefficients, γ_{2n}, are derived in the next subsection.

6.2.2 Sum Equations Involving γ_{2n}

We can derive two sum equations involving γ_{2n} in the same way as those involving β_{2r}. The first equation is found using Eq. **6.14** and the orthogonality properties of Mathieu functions. The second equation is derived from the first.

Multiplying Eq. **6.14** by ce_{2m}, integrating from zero to $\pi/2$, using Eq. **6.15** and the relation;

$$\beta_{2r} = \sum_{n=O}^{\infty} A_{2r}^{2n}\gamma_{2n} \; , \tag{6.24}$$

gives the sum equation:

$$\gamma_{2n}\mathcal{F}_{2n} - 2F_E \sum_{m=0}^{\infty} \gamma_{2m}\Delta_{2m}^{2n} = -\frac{2}{s}(-1)^n ce_{2n}(\pi/2; -s/4). \tag{6.25}$$

The kernel of this equation, **A,** is defined by the sum:

$$\Delta_{2m}^{2n} = \Delta_{2n}^{2m} = \sum_{r=1}^{\infty} r^2 A_{2r}^{2n} A_{2r}^{2m} \; . \tag{6.26}$$

A second sum equation can be obtained from Eq. **6.25** by using the kernel which is the inverse of **A.** This inverse kernel, **V,** can be found by inspection and is:

$$\nabla_{2m}^{2n} = \nabla_{2m}^{2n} = \sum_{r=1}^{\infty} \frac{A_{2r}^{2n} A_{2r}^{2m}}{r^2} \; , \tag{6.27}$$

The two kernels, **A** and **V,** are orthogonal in the sense:

$$\sum_{l=0}^{\infty} \Delta_{2l}^{2n}\nabla_{2l}^{2m} = \delta_{nm} - 2A_0^{2n} A_0^{2m}. \tag{6.28}$$

This orthogonality relation can be verified by using Eq. **6.20** and the definitions of **A** and **V.**

Multiplying Eq. 6.25 by ∇_{2l}^{2n} and summing over l from zero to infinity, gives the final sum equation:

$$2F_E\gamma_{2n} - 4F_E A_0^{2n} \sum_{m=0}^{\infty} A_0^{2m}\gamma_{2m} - \sum_{m=0}^{\infty} \nabla_{2m}^{2n} \mathcal{F}_{2m}\gamma_{2m} = \frac{2}{s} \sum_{r=1}^{\infty} \frac{A_{2r}^{2n}}{r^2} \ . \tag{6.29}$$

The form of this last sum equation differs from the previous three in that it has two sums involving, γ_{2n}.

We have now completed the development of the four Fredholm sum equations which we consider to be primary. We can derive other forms by combining these four equations. The solution of the first two of these sum equations, Eqs. 6.16 and 6.23, will be derived in the next chapter.

Before we end this chapter it should be noted that the four sum equations were derived, directly or indirectly, from the governing differential equations. This work has also examined equivalent formulations in terms of various integral and differential-difference equations. None of the alternative forms allow for efficient solution and all of them, when expanded in terms of eigenfunctions, give the same Fredholm sum equations already presented. For these reasons, the alternative formulations will not be discussed.

Chapter 7

SOLUTION OF SUM EQUATIONS

In this chapter we develop the solutions to the Fredholm sum equations involving β_{2r} derived in Chapter 6. When β_{2r} is known, pressure can be determined anywhere in the reservoir/fracture system.

We consider only the equations containing coefficients of the cosine series for two reasons: (1) we are primarily interested in determining well pressures, and (2) the Mathieu function coefficients, γ_{2n}, can be obtained directly from the cosine series coefficients. There may be advantages to pursuing solutions to the sum equations involving γ_{2n}. However, time constraints have limited our investigations to determining β_{2r}.

In the first section we develop a series solution in powers of F_E which is useful for low fracture conductivities. In the second section we develop a power series in terms of $1/F_E$ which is useful for high fracture conductivities. These two series have restricted regions of applicability, but the first terms of both series will be used as the starting values for the iterative procedure of the third section.

The third section develops two solutions which iterate on the late time solution. The two iterative solutions converge for all values of s and F_E. These solutions are analogous to continued fractions, except that the unknown terms are sums and the number of tails of the fractions grow with iteration level. It is these iterative solutions

which are the most generally valid and which are used for numerical calculation.

The two Fredholm sum equations we solve in this chapter are Eqs. *6.23* and *6.16* of Chapter **6:**

$$\beta_{2r} - 2F_E \sum_{p=1}^{\infty} p^2 \beta_{2p} \Omega_{2r}^{2p} = \frac{2}{s} \frac{I_r(\sqrt{s}/2) K_r(\sqrt{s}/2)}{\epsilon_r} \tag{7.1}$$

and

$$2F_E r^2 \beta_{2r} - \sum_{p=0}^{\infty} \epsilon_p \mho_{2p}^{2r} \beta_{2p} = \frac{2}{s\epsilon_r} . \tag{7.2}$$

These two expressions are equivalent and we need solve only one. However, the expressions are amenable to solution for differing ranges of F_E; Eq. *7.1* for small values of F_E and Eq. *7.2* for large values of F_E. It is the presence of the summation which complicates solution. So Eq. *7.1* is preferred for low conductivities, since F_E multiplies this sum. Equation *7.2* is preferred for high conductivities for similar reasons.

7.1 The Low Conductivity Solution

In this section we develop the low conductivity series solution of Eq. *7.1*. The procedure uses the method of successive substitution, where a power series is developed by inserting Eq. 7.1 into itself. The resulting series consists of terms of the form, $2^j F_E^j Q_j$, where Q_j is a j-fold series containing the kernel Ω_{2j}^{2k}.

We can write Eq. *7.1* in the form:

$$\beta_{2r} - \beta_{2r}^0 = 2F_E \sum_{p=1}^{\infty} p^2 \beta_{2p} \Omega_{2r}^{2p} , \tag{7.3}$$

where β_{2r}^0 is the Bessel function term:

$$\beta_{2r}^0 = \frac{2}{s} \frac{I_r(\sqrt{s}/2) K_r(\sqrt{s}/2)}{\epsilon_r} \tag{7.4}$$

This form indicates that if F_E is zero, β_{2r} is given by β_{2r}^0. This first approximation can be shown to be the coefficient in the cosine series representation of the line source solution, K_0/s. This is encouraging, because the solution of Eq. *7.3* must degenerate to the line source solution for zero fracture conductivity.

The power series is developed by solving Eq. 7.3 for β_{2r} in terms of β_{2r}^0 and the sum on the right hand side of Eq. 7.3. Redefining indices and substituting the result back into Eq. 7.3 gives:

$$\beta_{2r} = \beta_{2r}^0 + 2F_E \sum_{p=1}^{\infty} p^2 \Omega_{2r}^{2p} \left(\beta_{2p}^0 + 2F_E \sum_{q=1}^{\infty} q^2 \beta_{2q} \Omega_{2p}^{2q} \right), \tag{7.5}$$

or:

$$\beta_{2r} = \beta_{2r}^0 + 2F_E \sum_{p=1}^{\infty} p^2 \Omega_{2r}^{2p} \beta_{2p}^0 + 4F_E^2 \sum_{p=1}^{\infty} \sum_{q=1}^{\infty} p^2 q^2 \Omega_{2r}^{2p} \Omega_{2p}^{2q} \beta_{2q} . \tag{7.6}$$

This expression gives the first two terms in the power series expressed in terms of known quantities. The unknown, β_{2q}, appears in the last term only. Equation 7.6 **is** equivalent to Eq. 7.3—we merely substituted the equation into itself.

This procedure can be repeated indefinitely, each time substituting **Eq.** 7.3 into its extended form. Successive use of this procedure yields the kth iteration:

$$\beta_{2r} = \beta_{2r}^0 + 2F_E \sum_{\alpha_1=1}^{\infty} \alpha_1^2 \Omega_{2r}^{2\alpha_1} \beta_{2\alpha_1}^0 + 4F_E^2 \sum_{\alpha_1=1}^{\infty} \sum_{\alpha_2=1}^{\infty} \alpha_1^2 \alpha_2^2 \Omega_{2r}^{2\alpha_1} \Omega_{2\alpha_1}^{2\alpha_2} \beta_{2\alpha_2}^0$$

$$+ \ldots + (2F_E)^k \sum_{\alpha_1=1}^{\infty} \sum_{\alpha_2=1}^{\infty} \ldots \sum_{\alpha_k=1}^{\infty} \alpha_1^2 \ldots \alpha_k^2 \Omega_{2r}^{2\alpha_1} \Omega_{2\alpha_1}^{2\alpha_2} \ldots \Omega_{2\alpha_{k-1}}^{2\alpha_k} \beta_{2\alpha_k}^0 +$$

$$(2F_E)^{k+1} \sum_{\alpha_1=1}^{\infty} \sum_{\alpha_2=1}^{\infty} \ldots \sum_{\alpha_k=1}^{\infty} \sum_{\alpha_{k+1}=1}^{\infty} \alpha_1^2 \ldots \alpha_{k+1}^2 \Omega_{2r}^{2\alpha_1} \Omega_{2\alpha_1}^{2\alpha_2} \ldots \Omega_{2\alpha_{k-1}}^{2\alpha_k} \Omega_{2\alpha_k}^{2\alpha_{k+1}} \beta_{2\alpha_{k+1}} . \tag{7.7}$$

For any finite value of k, all of the series in Eq. 7.7 converge. Thus, Eq. 7.7 is an exact expression for β_{2r}. The problem with this representation is the final term which contains the unknown, $\beta_{2\alpha_{k+1}}$ (recall that all of the β_{2j}^0 are known). This final term can be considered a residual, i.e. the difference between the exact solution and the first k terms of its power series. The difficulty arises because this residual term will only approach zero, as k $\rightarrow \infty$, if F_E is within the radius of convergence of the power series. If F_E is too large, the residual term will grow without bound, while if F_E is small, it converges rapidly.

The low conductivity series, Eq. 7.7, should be useful for low values of F_E. How low these values need to be, has not been determined. In the third section we discuss the radius of convergence as we develop the final solution. Before doing this, however, we develop a series solution that is useful for high values of F_E.

7.2   The High Conductivity Solution

In this section we derive a series solution in powers of $1/F_E$. This solution should be valid for high values of F_E. Unfortunately, the derivation lacks a neat exposition and the series appears to have a finite radius of convergence.

The development of the series for high F_E starts with Eq. *7.2:*

$$2F_E r^2 \beta_{2r} - \sum_{p=0}^{\infty} \epsilon_p \mho_{2p}^{2r} \beta_{2p} = \frac{2}{s\epsilon_r} . \tag{7.8}$$

We cannot employ the method of successive substitutions in this case because it will require division by r^2 and summation beginning with $r = 0$ will be undefined.

The obvious way to solve Eq. *7.8* is to allow F_E to approach infinity and assume that the summation is small in comparison to the other terms. This is not the best approach because, as F_E becomes infinite, all of the β_{2r} terms approach zero except β_0. We know this because, as the fracture conductivity becomes infinite, the fracture becomes an isobar and the pressure in the fracture becomes equal to its average pressure. Since the zero order term in a cosine series is equal to the average of the function, β_0 must be the only nonzero term.

This observation indicates a better way to approach the solution. Let F_E approach infinity and set r equal to zero in Eq. *7.8.* This will result in the left hand side of the equation being reduced to a single term, $-\epsilon_r \mho_0^0 \beta_0$. We then put the resulting expression back into Eq. *7.8* and let r differ from zero, but keep F_E arbitrarily large. This will give the first approximation to the remaining coefficients. This process is then repeated to give a power series expression for all of the coefficients.

If we let F_E approach infinity in Eq. *7.8,* set $r = 0$, and solve for β_0, we obtain:

$$-1 \tag{7.9}$$

This is the expression for the pressure of an infinite conductivity fracture given by Kucuk and Brigham *(1979).*

Assigning r to be nonzero and assuming the only significant term in the summation of Eq. *7.8* is β_0, gives the leading order behavior for higher values of r:

$$\beta_{2r}^1 = \frac{2\mho_0^0 - \mho_0^{2r}}{s2F_E r^2 \mho_0^0} , \qquad r > 0. \tag{7.10}$$

We denote the first approximation for $r \neq 0$ by the superscript "1" and not by zero because the final representations for β_{2r} will be:

$$\beta_0 \sim \sum_{j=0}^{k} \beta_0^j , \qquad \beta_{2r} \sim \sum_{j=1}^{k} \beta_{2r}^j . \qquad (7.11)$$

Using this ordering of superscripts means that each β^j term will contain $1/F_E^j$.

The above procedure can be repeated indefinitely. At each stage we set $r = 0$ and assume that the coefficients in the summation, except β_0, are given by their values at the previous iteration level. Solving the resulting expression for β_0 (the right hand side of Eq. 7.8 is omitted from higher iterations, since it was accounted for in the first iteration), gives:

$$\beta_0^j = \frac{-1}{2\mathcal{U}_0^0} \sum_{p=1}^{\infty} \mathcal{U}_{2p}^0 \beta_{2p}^j, \qquad j > 0. \qquad (7.12)$$

Inserting this term into the summation of Eq. 7.8, letting r differ from zero, assuming the other β_{2r} terms in the sum take on their values at the previous iteration level, and solving for β_{2r}, gives:

$$\beta_{2r}^j = \frac{\mathcal{U}_0^{2r} \beta_0^{j-1}}{F_E r^2} + \frac{\sum_{p=1}^{\infty} \mathcal{U}_{2p}^{2r} \beta_{2p}^{j-1}}{2 F_E r^2}, \qquad r > 0, \;\; j > 1 . \qquad \textbf{(7.13)}$$

The high conductivity series is of limited usefulness because it has a finite radius of convergence. The value of this radius of convergence is unknown. In the next section we will discuss the radius of convergence as we develop the final form of solution.

7.3   The Final Solution

In this section we develop a computationally efficient method of determining the coefficients, β_{2r}. The method consists of iterating on the late time solution. The advantage of this approach is that it accounts for the singularities of β_{2r}, when β_{2r} is considered as a function of F_E. Thus, the iterative procedure has an infinite radius of convergence. Two forms of solution are given. Their usefulness depends on the magnitude of F_E, although technically they converge for all values of F_E.

We begin by showing the late time limiting form of the solution. We do this for three reasons: first, to bolster the claim, made in Chapter **6,** that the long time

solution was independent of diffusivity ratio; second, to give an indication of the difficulties of evaluating the power series of the previous two sections; and third, to derive an iterative procedure which gives computationally useful solutions to the sum equations.

To derive the limiting form, we need only take the limit of any of the sum equations as $s \to 0$. For definiteness we choose Eq. *7.2*. Before we take the limit we factor β_{2r} from the left hand side and divide by the factored term. This gives:

$$\beta_{2r} = \frac{2}{s\epsilon_r \left(2F_E r^2 - \sum_{p=0}^{\infty} \epsilon_p \mho_{2p}^{2r} \beta_{2p}/\beta_{2r} \right)} , \qquad (7.14)$$

This form will be important later. Because Eq. *7.14* expresses β_{2r} as a ratio, it will be referred to as a "rational form."

Using the definition of the kernel, $\mho_{2p}^{2r}$, Eq. *6.17* of Chapter *6*, and the limiting forms given in Chapter *5*, Eqs. *5.10* and *5.26*, shows:

$$\lim_{s \to 0} \mho_{2p}^{2r} = -2r \, \delta_{rp} , \qquad r > 0;$$

$$\lim_{s \to 0} \mho_{2p}^{0} = -\frac{1}{2\ln(4/\gamma'\sqrt{s})} \, \delta_{0p} . \qquad (7.15)$$

Note that the appearance of the Kronecker delta function in these two expressions causes the β_{2p} coefficients in the right hand side of Eq. *7.14* to be multiplied by zero, except when $r = p$. This term cancels with the β_{2r} which divides it. So, in the limit **as** s approaches zero, all of the β_{2r} and β_{2p} terms vanish in the right hand side, leaving:

$$\lim_{s \to 0} \beta_{2r} = \frac{1}{s(F_E r^2 + r)} , \qquad r > 0;$$

$$\lim_{s \to 0} \beta_0 = \frac{\ln(4/\gamma'\sqrt{s})}{s} . \qquad (7.16)$$

This is the same expression as Eq. *6.9* of Chapter *6* for the equal diffusivity case.

In the first two sections, we developed power series in terms of F_E and $1/F_E$. Equation *7.16* gives an idea of the radii of convergence of these series. We know, from the theory of Taylor series, that the radius of convergence of a power series is equal to the distance from the origin to the nearest singularity of the function being expanded. Thus, in the limit of small s, the radii of convergence are given by the

points where $F_E r^2 + r = 0$, at least for $r > 0$. So, the radii of convergence of the two series, in the limiting case, are $F_E = |-1/r|$ and $1/F_E = |-r|$. For s different from zero, it is unclear whether the radii of convergence increase or decrease, but we are not optimistic.

We will not pursue the investigation of the power series further. We merely wished to show the reason for their limited usefulness: power series do a poor job of accounting for singularities.

This observation indicates a much better way of developing a solution. The **rational** form, Eq. 7.14, accounts for the singularity of β_{2r} as $s \to 0$. For larger s it is unclear where the singularity, or singularities, lie; but it turns out that Eq. 7.14 accounts for them remarkably well. In the process of evaluatiing Eq. 7.14, it was found that it gave reasonable results as long as a reasonable guess for β_{2r} (and equivalently β_{2p}) was inserted into the right hand side. Indeed, experience with the rational form indicated that when approximate values were inserted for β_{2r}, the result was always closer to the correct β_{2r} value.

This observation indicates an iterative procedure which takes the form:

$$\beta_{2r}^{new} = \frac{2}{s\epsilon_r(2F_E r^2 - \sum_{p=0}^{\infty} \epsilon_p \mho_{2p}^{2r} \beta_{2p}^{old}/\beta_{2r}^{old})} , \qquad (7.17)$$

This procedure seems to converge for all s and for all F_E. Convergence is more rapid as F_E increases.

The iteration of Eq. 7.17 is initiated using the leading order terms of the high conductivity solution, Eq. 7.9 and 7.10:

$$\beta_0^{old} = \frac{-1}{s2\mho_0^0} ;$$

$$\beta_{2r}^{old} = \frac{2\mho_0^0 - \mho_0^{2r}}{s2F_E r^2 \mho_0^0} , \qquad r > 0. \qquad (7.18)$$

This first approximation works reasonably well, but a more refined first guess would enhance convergence.

An analogous procedure can be used for low values of F_E. This iterative procedure uses the rational form of Eq. 7.1:

$$\beta_{2r}^{new} = \frac{2I_r(\sqrt{s}/2)K_r(\sqrt{s}/2)}{s\epsilon_r(1 - 2F_E \sum_{p=1}^{\infty} p^2 \beta_{2p}^{old}\Omega_{2r}^{2p}/\beta_{2r}^{old})} . \qquad (7.19)$$

The starting values for this procedure are the zero order terms in the low conductivity power series of Eq. 7.4:

$$\beta_{2r}^{old} = \frac{2}{s} \frac{I_r(\sqrt{s}/2)K_r(\sqrt{s}/2)}{\epsilon_r} \qquad (7.20)$$

Again, more refined starting values will result in enhanced convergence.

Equations 7.17 and 7.19 give computationally independent means of calculating β_{2r}. Equation 7.19 is preferred for F_E less than about 2. Equation 7.17 is preferred for higher F_E. One reason we believe that these two iterative procedures represent exact solutions is that they converge to the same result — this has been checked numerically in the range $0.1 < F_E < 20$.

We choose to leave Eqs. 7.17 and 7.19 in iterative form because of the typographical difficulty of showing more explicit forms. The explicit forms result from successive substitution in much the same way as in the first section. The first substitution re-sults in a two-fold rational form—each β_{2r} term and β_{2p} term in the denominator of Eq. 7.17 (or Eq. 7.19) is replaced by a rational form. This new form resembles a continued fraction of summations with two tails. Further substitution results in a $j + 1$-fold rational form or equivalently a continued fraction of summations with $2j$ tails.

The computation of the solutions presented above are fairly straightforward, how-ever, computation of the kernels requires some explanation. This is because the evaluation of the series containing the kernels requires filling out a matrix. The computation of the kernels is discussed in Appendix B.

The convergence of the solutions is slowest for $1.0 < F_E < 5.0$ and for large s. In this range of F_E, for s equal to 10^4, both methods require about thirty iterations to obtain ten significant figures of precision in Laplace space. The required number of iterations increases with s. For this reason alternative methods of computing well pressures, for very large s, are presented in Chapter 8.

Pressure computation from the solution is also a problem. If the cosine series, Eq. 6.13 of the last chapter, were summed directly, it would require excessive computa-tional time and storage space. For this reason we choose to accelerate the convergence of the series by means of the Kummer transformation of series. The acceleration of

the solution is the subject of the next subsection.

7.3.1   Accelerating Convergence of the Cosine Series

In this subsection we deal with the problem of accelerating convergence of the cosine series, so that the solutions can be computed with only a relatively small number of terms. The method we employ is the Kummer transformation of series. It is useful and conceptually simple. Using it we have been able to obtain accuracies using one hundred terms which would otherwise require over ten thousand.

We wish to enhance convergence of the series:

$$\bar{p}_f(\eta; s) = \sum_{r=0}^{\infty} (-1)^r \beta_{2r} \cos(2r\eta). \tag{7.21}$$

Before showing the Kummer transformation, we need to consider why direct computation of Eq. *7.21* is impractical. **As** r becomes large, β_{2r} is closely approximated by the limiting forms of Eq. *7.16.* Hence, the cosine series will ultimately converge as $1/r^2$. Thus, to compute the series to eight significant figures (which is necessary for numerical Laplace inversion), we must calculate at least ten thousand terms.

Kummer's transformation entails adding and subtracting a comparison series to and from Eq. 7.21:

$$\bar{p}_f(\eta; s) = \sum_{r=0}^{\infty} (-1)^r (\beta_{2r} - \chi_{2r}) \cos(2r\eta) + \sum_{r=0}^{\infty} (-1)^r \chi_{2r} \cos(2r\eta). \tag{7.22}$$

In this transformation we are free to choose any comparison series which possesses **a** sum. However, it is desirable to choose a comparison series whose ultimate convergence matches that of the original series. This will accelerate the convergence of the first series in Eq. 7.22. The comparison series should also contain easily calculable terms. For example, we can choose $\chi_{2r} = 1/s(F_E r^2 + r)$. This will accelerate convergence dramatically and is itself simple to compute. In fact, we use an expression similar to this as the final comparison series.

The method of finding the final comparison series was a numerical trial and error procedure. This procedure assumed initially that $\chi_{2r} = 1/s(F_E r^2 + r)$. This χ_{2r} value was subtracted from β_{2r} and the terms were examined for large values of r. The form

of χ_{2r} was then altered to account for the new dominant behavior. Proceeding in this way, the final comparison series was chosen to have terms:

$$\chi_{2r} = \frac{1}{s(F_E r^2 + \sqrt{r^2 + s/4} + g(s,r))} \; , \tag{7.23}$$

where $g(s,r)$ is:

$$g(s,r) = \frac{s}{32r^3/9 - 32r/5 - 32/45 + 55sr/64 - 6s} \; . \tag{7.24}$$

This expression is completely empirical. However, it ensures that the difference, $\beta_{200} - \chi_{200}$, is essentially zero for s less than 10^4 and F_E greater than 0.1. Other, more analytic, methods have been used to find comparison series, but none have been found to be as useful as Eq. *7.23*.

Using this acceleration procedure, we are able to efficiently calculate well pressures for all conductivities and s less than 10^4. However, even with the acceleration procedure, the solutions require more computational time than desired. For example, computation of six log cycles of well pressure with twenty-four points per cycle in the range, $10^{-3} \le t_{Dx_f} \le 10^3$, requires approximately five minutes of real time using an Apollo 10000 computer. It is hoped that acceleration procedures superior to the one used in this work will be found in the future that will allow the evaluation of the solution in much fewer than one hundred terms.

A t_{Dx_f} value of 10^{-3} corresponds roughly to $s = 10^4$. Computation of the solution for such large values of s becomes difficult because the kernels of the sum equations become time consuming to compute. For this reason we have developed alternative means of obtaining accurate well pressures for very early times. These procedures will be developed in Chapter 8.

Chapter *8*

LIMITING FORMS FOR WELLBORE PRESSURE

The main objective of this research is to enable the computation of wellbore pressures for any value of fracture conductivity at any time. The iterative solutions of the last chapter theoretically give exact results for any values of fracture conductivity and Laplace parameter, s. However, these solutions become cornputationally demanding as s becomes large. Therefore, we devote this chapter to the computation of wellbore pressures at very early times.

The early time well pressures will be presented as a pair of composite solutions comprising three cases: the infinitely long fracture, the bilinear/linear flow model, and the infinite conductivity fracture. These composite solutions accurately predict well pressures for t_{Dx_f} less than 10^{-3} and all values of fracture conductivity.

8.1   Wellbore Pressures for Very Low F_E

In this section we present an approximate solution that gives wellbore pressures for fractures of very low conductivity. The solution assumes that the fracture is infinitely long. We use this solution as part of the composite solution of the third section. However, this solution gives accurate well pressures for all values of s when $F_E \leq 0.1$.

As fracture conductivity decreases, the amount of influx at the fracture tips becomes negligible and the wellbore pressure behaves as if the fracture were infinitely long. The case of an infinitely long rectangular fracture is readily solved, as shown by Wilkinson *(1989)* in terms of a Fourier integral. Evaluated at the wellbore, Wilkinson's solution simplifies to a combination of elementary functions.

We are concerned with a very low conductivity *elliptical* fracture. However, as the conductivity decreases, well pressure is only affected by the influx in the immediate vicinity of the wellbore. In this region, the elliptical fracture is essentially rectangular and so Wilkinson's solution can be used directly.

Wilkinson's solution, evaluated at the well, is:

$$\bar{p}_{low} = \frac{1}{Rs}\left[\frac{B_1}{2}\ln\left(\frac{A_1 + B_1}{A_1 - B_1}\right) + B_2 \arctan\left(\frac{B_2}{A_2}\right)\right], \qquad (8.1)$$

where $R = \sqrt{1 + F_E^2 s}$, $A_1 = 1 + F_E\sqrt{s} + R$, $A_2 = 1 + F_E\sqrt{s} - R$, $B_1 = \sqrt{2(R+1)}$, and $B_2 = \sqrt{2(R-1)}$.

Equation 8.1 is in a slightly different form than that given by Wilkinson, but should be equivalent to his expression for the case of incompressible fracture flow. Examination of Eq. 8.1 shows that, aside from an overall factor of $1/s$, F_E and s appear only in the combination $F_E\sqrt{s}$. Use of the change of scale property of the Laplace transform, as in Chapter **3,** shows that the real space solution is only a function of t_{Dx_f}/F_E^2.

Figure 8.1 presents the wellbore solution, Eq. *8.1,* as a solid curve, graphed as a function of t_{Dx_f}/F_E^2. Overlain on this graph is the iterative solution of the last chapter evaluated for F_E equal to 0.1. The data for these two cases are given in Table **D.5** of Appendix D. The two solutions agree to within 1.0 percent.

The method of presentation used in Figure 8.1, p_{Dw} versus t_{Dx_f}/F_E^2, is equivalent to that used by Cinco et al. (1987), p_{Dw} versus $t_{Dr'_w}$. This is because, for very low conductivity fractures, dimensionless time based on equivalent well radius is proportional to t_{Dx_f}/F_E^2.

The very low conductivity case exhibits a bilinear flow period followed immediately by pseudoradial flow. Reservoir linear flow does not develop. For linear flow to develop a significant amount of production must enter the fracture near its tips. For cases
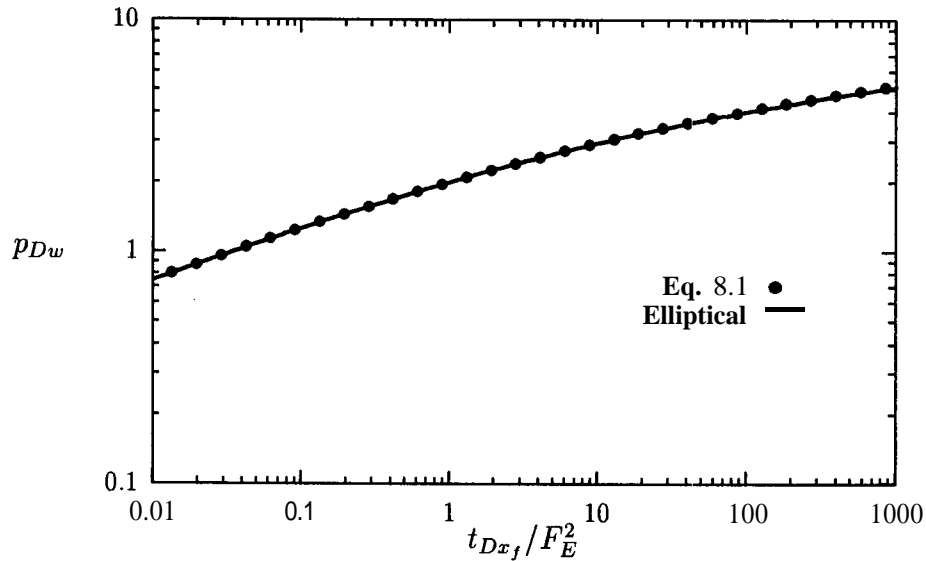
Figure 8.1: The Low Conductivity Case

of higher conductivity, the wellbore pressures will exhibit some reservoir linear flow. For these cases, the early time behavior can be found by assuming that the flow in the reservoir is one-dimensional.

8.2   Linear and Bilinear Flow

In this section we develop analytic expressions for the bilinear aad reservoir linear flow regimes of the elliptical fracture. These regimes for the elliptical fracture are similar to those for a rectangular fracture. The greatest difference between the elliptical and rectangular cases occurs in the transition region between the two regimes.

As in Chapter **3,** we assume that reservoir flow is one-dimensional. Thus, reservoir pressure is approximated by **Eq. 3.23:**

$$\bar{p}_R = \bar{p}_f(x_D)\exp(-\sqrt{s}y_D) = \bar{p}_f(\eta)\exp[-\sqrt{s}\sinh(\xi)\sin(\eta)] \ . \tag{8.2}$$

Using this expression to give the reservoir influx term in the fracture equation, **Eq.**

6.10 of Chapter 6, yields:

$$\frac{d^2 \bar{p}_f}{d\eta^2} - \frac{2\sqrt{s}\sin(\eta)}{F_E} \bar{p}_f = 0, \tag{8.3}$$

subject to the boundary conditions:

$$\frac{d\bar{p}_f}{d\eta}\bigg|_{\eta=\pi/2} = \frac{\pi}{sF_E}, \qquad \frac{d\bar{p}_f}{d\eta}\bigg|_{\eta=0} = 0. \tag{8.4}$$

In this case it is not convenient to use the Dirac delta function to account for well production. So, we have specified an inhomogeneous boundary condition.

Equation **8.3** is of Mathieu type because of the factor, $\sin(\eta)$. Full solution of this equation will be quite difficult to obtain. However, since we are only interested in pressures at the wellbore, we can simplify the procedure by recasting the problem as a Riccati equation.

To write Eq. **8.3** in Riccati form, we make the substitution:

$$z(\eta) = \frac{1}{\bar{p}_f} \frac{d\bar{p}_f}{d\eta}. \tag{8.5}$$

Making this substitution, the fracture problem becomes:

$$\frac{dz}{d\eta} + z^2 = B^2 \sin(\eta), \qquad z(\eta = 0) = 0. \tag{8.6}$$

In this equation B is defined as $\sqrt{2\sqrt{s}/F_E}$.

Equation 8.6 is a first-order nonlinear ordinary differential equation that is no less difficult to solve than the original second-order equation. However, it is much more amenable to solution by perturbation. Moreover, to determine well pressure we need only find $z(\pi/2)$ and use the definition of z:

$$\bar{p}_{BL} = \bar{p}_f(\pi/2) = \frac{1}{z(\pi/2)} \frac{d\bar{p}_f}{d\eta}\bigg|_{\eta=\pi/2} = \frac{\pi}{sF_E z(\pi/2)}. \tag{8.7}$$

In this equation, $\bar{p}_{BL}$ is the well pressure during the bilinear and linear flow regimes.

To determine $z(\pi/2)$ for B ranging from zero to infinity, we consider two cases: B small and B large. For small B, we assume that z^2 in Eq. 8.6 is negligible to a first approximation and iterate. For large B, we assume that $dz/d\eta$ is negligible to a first approximation and iterate. These two perturbative approaches are fundamentally different: the low B solution takes the form of an ascending series, while the high B solution is purely asymptotic.

8.2.1 The Small B Approach

In this subsection we develop a perturbative solution of the Riccati equation for small values of B. We assume that z^2 is small and solve a succession of first-order linear ordinary differential equations. Using the final iterate, we develop a power series solution for $z(\pi/2)$. Examination of this series shows that it has a small radius of convergence, so we recast it as a continued fraction.

The low B perturbation approach proceeds as follows. We assume initially that z^2 is zero in Eq. 8.6 and obtain the zero-order solution, z_0. We then obtain a better approximation by assuming that z^2 is given by z_0^2 and solving the full equation. At each stage we are solving a first-order linear equation and so each higher approximation requires an additional integration.

At each stage we solve the equation:

$$\frac{dz_k}{d\eta} = B^2 \sin(\eta) - z_{k-1}^2, \qquad z_k(\eta = 0) = 0, \tag{8.8}$$

or, equivalently, integrate:

$$z_k(\eta) = \int_0^\eta [B^2 \sin(\eta') - z_{k-1}^2(\eta')]d\eta'. \tag{8.9}$$

It should be kept in mind that this is an iterative procedure and so we do not sum the z_k. At each iteration level z_k is updated, so z_k is the approximation to z.

The first two iterations can be performed by hand:

$$z_0 = -B^2(\cos(\eta) - 1)$$
$$z_1 = -B^2(\cos(\eta) - 1) - B^4\left(\frac{3\eta}{2} - 2\sin(\eta) + \frac{\sin(2\eta)}{4}\right). \tag{8.10}$$

Higher order iterations are straightforward and involve only integration of powers and trigonometric functions, but the manipulations become tedious. For this reason, the procedure was programmed into MATHEMATICA (see Wolfram (1988)), a symbolic manipulation software package. Use of MATHEMATICA enabled calculation of terms through z_{17}. This final term is complicated and will not be shown. However, since we are interested only in $z(\pi/2)$, we expand it in a power series and use $z_{17}(\pi/2)$ to

k	a_k
1	+1 00000000(0 000
2	-0.35619449019234492884698253745962716314778770495313 3
3	+0.15537933669048629103563571670096901611354984 5
4	-0.068825856026139185331998076943892487837219921 4
5	+0.0305399630045774866754590358788940459319574015
6	-0.0135544095268710697101 7375684187000286692476540
7	+0.0060159610143377565146566756669855141784208655 4
8	-0.002670121551763249055732460223269923039141919 9
9	+0.0011851061779774621965525286009857713911649 96
10	-0.00052599730590446916296257668666625373471 682549
11	+0.000233458548506845809 22 195836793771845275
12	-0.0001036181997875659709698378045100308861302099
13	+0.000045989882989675213410214069003858355108452
14	-0.000020412 14132054465547841828921015648808724 1
15	+0.0000090597210996267824227653785824726251950 3
16	-0.00000402106496883980837312488277569767473695
17	+0.00000 1784708746089045859213366568608253254 72

Table 8.1: Coefficients for Ascending Series, Eq. 8.11

give the first seventeen terms in the series. The first seventeen coefficients, a_k, in the power series:

$$z(\pi/2) = \sum_{k=1}^{\infty} a_k B^{2k},\qquad\qquad (8.11)$$

are given in table 8.1. The entries of this table are reproduced as given by MATHE-MATICA. In implementing MATHEMATICA, we requested fifty significant figures of precision. This seems like extraordinary precision, but, as we shall see, it is actually only marginal precision. It is not known why the coefficients in Table 8.1 seem to lose and gain precision—we are assuming MATHEMATICA knows what it's doing.

Examination of the ascending series, Eq. 8.11, was performed using the methods of Van Dyke (1974). Use of these methods and discussions with Professor Van Dyke (Van Dyke (1990)) indicate that the series represents a function with simple poles symmetrically placed on the imaginary B-axis. The distance from the origin to the first pole (and consequently the radius of convergence of the series) is about 1.501.

This means that the utility of the power series is restricted to a small region near $B = 0$. However, the terms of the power series can be manipulated to give a much better representation in terms of a continued fraction. Continued fractions seem to have extraordinary convergence properties, and there is a simple recipe for generating the terms.

The continued fraction representation assumes that $z(\pi/2)$ can be written as:

$$z(\pi/2) = \frac{d_0 B^2}{1+} \frac{d_1 B^2}{1+} \frac{d_2 B^2}{1+} \frac{d_3 B^2}{1+} \frac{d_4 B^2}{1+} \cdots .$$ (8.12)

This is the conventional way of writing a continued fraction. The breaks in the bar and the lone addition sign in each denominator indicate that each successive term belongs in the denominator of the term which precedes it.

Bender and Orzag (1982) give recursive formulae for the d_j's, in **Eq.** 8.12, in terms of the a_k's of Table 8.1:

$$
\begin{aligned}
D_k^0 &= a_k, \quad k = 1, 2, 3, ..., 17 \\
D_k^1 &= -\frac{D_{k+1}^0}{D_1^0}, \quad k = 1, 2, 3, ..., 16 \\
D_k^{j+1} &= \frac{D_{k+1}^{j-1}}{D_1^{j-1}} - \frac{D_{k+1}^j}{D_1^j}, \quad k = 1, 2, ..., 16 - j \\
d_j &= D_1^j \cdot
\end{aligned}
$$ (8.13)

Using these relations, the coefficients from Table 8.1 and MATHEMATICA gave the coefficients, d_j, shown in Table 8.2. These coefficients are given to at most 16 significant figures, since this is the significance used in double precision Fortran. Note that even though we calculated the power series coefficients to high precision, the coefficients in the continued fraction lose significance rapidly. In fact, MATHEMATICA was only able to calculate the first fourteen coefficients in Table 8.2. The remaining coefficients were extrapolated from the first fourteen.

Using the coefficients of Table 8.2 in the continued fraction of **Eq.** 8.12, enables the computation of $z(\pi/2)$, for B up to 11.0, to nine significant figures. This result has been verified numerically using a Runge-Kutta solution of the Riccati equation. To calculate $z(\pi/2)$ for values of B exceeding 11.0 we are forced to use another approach.

j	d_j
1	+1.000000000000000
2	+0.3561944901923449
3	+0.08002600442165511
4	+0.03670273499100588
5	+0.02097049584855654
6	+0.01357049453376811
7	+0.009499608396674833
8	+0.007021542075008946
9	+0.00540122208992925
10	+0.00428374369506396
11	+0.00348054939937352
12	+0.002883887762
13	+0.002428539254
14	+0.0020731
15	+0.001787
16	+0.00154
17	+0.0013

Table 8.2: Coefficients for Continued Fraction, Eq. 8.12

8.2.2   The Asymptotic Series

In this subsection we develop an expression for $z(\pi/2)$ useful for B greater than 11.0. This approach assumes that the derivative term in **Eq.** 8.6 is small. Since this method ignores the boundary condition at $\eta = 0$, it must be purely asymptotic.

In this method, we assume initially that $dz/d\eta$ is zero and represent z at each stage by:

$$z_k(\eta) = \sqrt{B^2 \sin \eta - \frac{dz_{k-1}}{d\eta}} \; . \tag{8.14}$$

This procedure is more straightforward than that of the previous subsection, since it involves only differentiation. The fact that it does not make use of the boundary condition must mean that, as B becomes very large, the boundary condition has little effect on the solution away from $\eta = 0$.

The first two terms are readily calculable:

$$z_0(\eta) \;=\; B\sqrt{\sin(\eta)} \; ,$$

$$z_1(\eta) = \sqrt{B^2 \sin(\eta) - \frac{B\sqrt{\cos(\eta)\cot(\eta)}}{2}} \tag{8.15}$$

Using the iterative procedure to develop a power series representation for $z(\pi/2)$, shows that the series involves inverse powers of B^2 and that, except for the first, it takes two iterations to achieve an additional term. Although the procedure is simple in principle, the complexity of the successive terms increases rapidly. Using MATHEMATICA with 5.5 MegaBytes of memory enabled the calculation of z_k only through k equal to eight. The power series for $z(\pi/2)$ using this last iterate is:

$$z(\pi/2) \sim B \left(1 - \frac{1}{8B^2} - \frac{15}{128B^4} - \frac{419}{1024B^6} - \frac{98389}{32768B^8} \cdots \right). \tag{8.16}$$

This series enables computation of $z(\pi/2)$, for all values of B greater than 11.0, to at least 9 significant figures. This has been verified numerically using a Runge-Kutta solution.

8.2.3 Comparison with Rectangular Fracture

At this point, we pause in the development of approximate well solutions, and compare the bilinear and reservoir linear regimes of the rectangular fracture to those of the elliptical fracture. The behavior of these regimes in the rectangular case was found to be very close to that of the elliptical case. The greatest percentage difference between the two cases occurs in the transition region separating bilinear flow from linear flow.

In Chapter 3, **Eq.** 3.26, we gave the equation governing the bilinear and linear flow regimes in the rectangular case, as:

$$\bar{p}_w = \frac{\pi}{sF_D B_D} \coth(B_D), \tag{8.17}$$

Here we use the term, B_D, to represent $\sqrt{2\sqrt{s}/F_D}$.

In Chapter 3, we used the change of scale property of the Laplace transform to show that Eq. 8.17 represented a single curve when $p_{Dw}F_D$ was graphed versus $F_D^2 t_{Dxf}$. We can apply the change of scale property to the elliptical case, and show the analogous result that the product of F_E and wellbore pressure is a single valued function of $t_{Dxf}F_E^2$ during bilinear and linear flow.
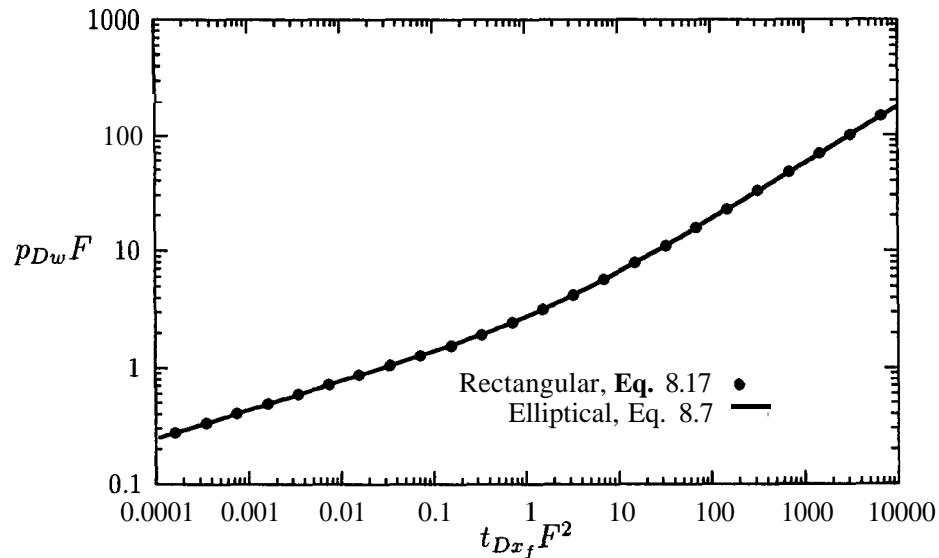
Figure 8.2: The Bilinear/Linear Flow Case

Figure 8.2 is a log-log graph of Fp_{Dw} versus $F^2 t_{Dxf}$ for the elliptical fracture, shown as the solid curve, and for the rectangular fracture, shown as dots. This figure shows the two solutions are remarkably similar — the agreement is within two percent. The fact that the curves merge for early times is as expected, because the flux distribution is concentrated around the wellbore at early times and F_E is defined so as to match F_D at the well. The merging of the curves at late times is also expected, since linear flow develops only for high conductivity fractures and, in this case, the shape of the fracture is unimportant. In the transition region the elliptical fracture has a slightly higher pressure drop because it has a conductivity that decreases along its length.

Figure 8.2 indicates that the bilinear and linear representations for the rectangular fracture also apply to elliptical fracture. However, there is a minor difference during reservoir linear flow:

$$p_{Dw} = \sqrt{\pi t_{Dxf}} + \frac{0.356\pi}{F_E} \; . \tag{8.18}$$

Recall that the constant term for the rectangular case, given in Chapter **3,** was $\pi/3F_E$.

Equation **8.18** was found by expanding Eq. **8.7** using Eq. **8.11** aad neglecting decaying terms.

The well pressure during bilinear flow is exactly the same as in the rectangular fracture case:

$$p_{Dw} = \frac{\pi (t_{Dxf})^{1/4}}{\sqrt{2F_E}\ \Gamma(5/4)} \simeq \frac{2.451(t_{Dxf})^{1/4}}{\sqrt{F_E}} \tag{8.19}$$

We had hoped that the early time behavior, i.e., $t_{Dxf} \leq 10^{-3}$, would be fully accounted for by the bilinear/linear flow model. This has not proven to be the case. The reason for the inadequacy of this model is that it does not achieve pseudoradial flow. Apparently there is some effect of pseudoradial flow even at $t_{Dxf} = 10^{-3}$. For this reason we couple the solution of this section with two models which do achieve pseudoradial flow: the infinitely long fracture model and the infinite conductivity model.

8.3   The Composite Early Time Solutions

In this section we combine the results of the two special cases presented earlier with the infinite conductivity solution to produce composite solutions accurate for early times. A discussion of the method of composite solutions is given in Van Dyke **(1975).**

Before we present the composite solution, we need an accurate early time approximation of the infinite conductivity fracture pressure. Trial and error manipulation of the known early time limiting form for the infinite conductivity case, $p_{fD} = \sqrt{\pi t_{Dxf}}$, indicates that a very accurate approximation is:

$$\bar{p}_{inf} \simeq \frac{\pi}{s(2\sqrt{s}+1)} \ . \tag{8.20}$$

This expression is a very good approximation for s as low as **10** and will be more than suitable for our purposes since we are concerned with s values greater than 10^4. A comparison of Eq. **8.20** with the exact infinite conductivity solution is given in Tables D.3 and **D.4** of Appendix D.

To give an expression for well pressures at early times, we consider two cases: F_E greater than **45** and F_E less than **45.** For F_E less than **45** we add the low conductivity

solution of the first section to the bilinear/linear flow solution of the second section. Since these terms are equal in the limit as time approaches zero, we must subtract the part they have in common: the bilinear flow regime. The composite low conductivity wellbore solution is:

$$\bar{p}_{comp} = \bar{p}_{low} + \bar{p}_{BL} - \frac{\pi}{\sqrt{2F_E}s^{5/4}} \ , \qquad F_E \leq 45, \tag{8.21}$$

where $\bar{p}_{low}$ is given by Eq. 8.1 and $\bar{p}_{BL}$ is given by Eq. 8.7.

The composite solution for high conductivity fractures is similar. The difference is that we use the infinite conductivity solution rather than the very low conductivity solution. The common part of these two solutions is now linear flow, so we subtract it:

$$\bar{p}_{comp} = \bar{p}_{inf} + \bar{p}_{BL} - \frac{\pi}{2s\sqrt{s}} \ , \qquad F_E > 45 \ . \tag{8.22}$$

The obvious way to utilize these two expressions is to use them for dimensionless times less than 10^{-3} and to use the iterative solution for times greater than this. When used in this way the composite solutions are accurate, to within one half of one percent. A better way to use the composite solutions is to use them in Laplace space, when s is greater than 10^4. So, numerical Laplace inversion will use some parts of the composite solution and some parts of the exact solution for dimensionless times in the neighborhood of 10^{-3}. This last approach has not been checked but it should be the more accurate of the two.

Chapter 9

RESULTS AND FUTURE WORK

In this chapter we do two things. First, we compare the well pressures from the elliptical and rectangular models. Second, we outline extensions of the present model.

9.1   Comparison of Wellbore Pressures

In this section we compare the wellbore pressures calculated for the elliptical fracture to those for the rectangular fracture. The data for the elliptical case were generated using the iterative solutions of Chapter **7,** while the data for the rectangular case are taken from Cinco et al. (1978). We compare the wellbore pressures in three ways: the first two are graphical, and the third is tabular. The comparison of the well pressures shows good agreement between the two cases.

In their paper, Cinco and Samaniego (1981) showed that type-curves for finite conductivity fractures are best presented in two ways. The first method shows the pressures on a log-log graph of $p_{Dw}F_D$ versus $t_{Dx_f}F_D^2$. When graphed in this way, all of the data start from a single curve which represents bilinear/linear flow as was shown in Figure 3.1 of Chapter 3. The second method employs a log-log graph of well pressures versus dimensionless time based on equivalent well radius, $t_{Dr'_w}$. When graphed in this way all of the data end on a curve representing pseudoradial flow.
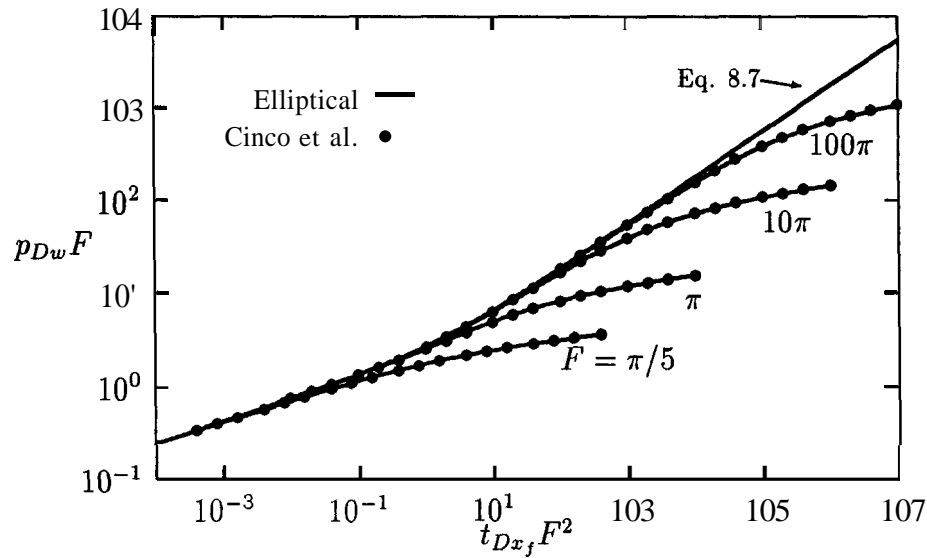
Figure 9.1: Comparison Using Cinco and Samaniego's Type Curves

The first of these graphs is shown in Figure 9.1. Figure 9.1 shows a log-log graph of $p_{Dw}F$ versus $t_{Dx_f}F^2$. The solid curves correspond to the elliptical fracture and the dots represent data for the rectangular fracture. The heavy solid curve is the representation of bilinear/linear flow for the elliptical fracture given by **Eq.** 8.7 of Chapter 8.

Figure 9.1 shows two important ideas. First, the data of the elliptical case all begin on the bilinear/linear curve and deviate only at late times. Second, the high degree of correlation between the two geometries shows that the elliptical case **mimics** the rectangular case. This second point will be brought out more clearly in the comparison of tabular data.

The second method of presentation is shown in Figure 9.2. This figure is a log-log graph of well pressures versus time based on equivalent well radius. This figure shows that all of the data fall on a single curve at late times. It also shows good agreement between the elliptical and rectangular cases.

The equivalent wellbore radii for the rectangular fracture were computed using
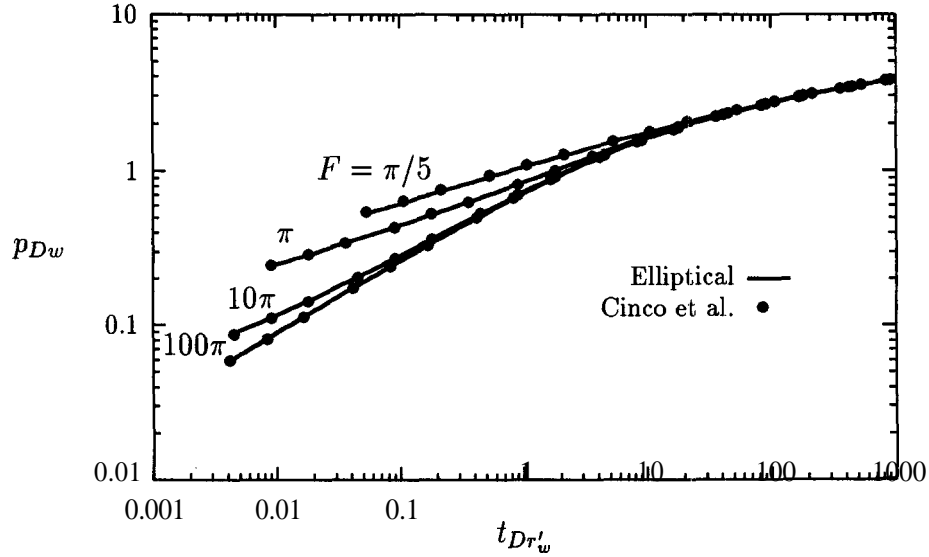
Figure 9.2: Equivalent Wellbore Radius Comparison

the late time data of Cinco et al. (1978) and the formula:

$$p_{Dw} = \tfrac{1}{2}\left(\ln(t_{Dx_f} x_f^2/r_w'^2) + 0.80907\right) . \tag{9.1}$$

The equivalent well radius, for the elliptical case, is given by:

$$r_w' = \frac{x_f}{2}\exp\left[-\Psi\left(1 + \frac{1}{F_E}\right) - \gamma\right]. \tag{9.2}$$

This expression is essentially a rearrangement of Eq. 9.1 using **Eq.** 6.9 of Chapter *6* and the expression of the Ψ-function as an infinite sum:

$$\Psi(x) = -\gamma - \frac{1}{x} + \sum_{k=1}^{\infty}\frac{x}{k(x+k)} . \tag{9.3}$$

The Ψ-function is the logarithmic derivative of the Γ-function and γ is Euler's constant. The Ψ-function is fairly simple to compute and is available as an *IMSL* subroutine (see IMSL Inc. (1990)).

Equation 9.2 demonstrates one advantage of the elliptical fracture formulation — it gives an explicit formula for the equivalent wellbore radius and hence, the apparent

t_{Dx_f}	$F = 100\pi$		$F = 10\pi$		$F = \pi$		$F = \pi/5$	
	Rect.	Ellip.	Rect.	Ellip.	Rect.	Ellip.	Rect.	Ellip.
0.001	0.0590	0.0589	0.0866	0.0882	0.2443	0.2464	0.5449	0.5398
0.01	0.1742	0.1735	0.2047	0.2062	0.4341	0.4424	0.9313	0.9315
0.1	0.4975	0.4947	0.5316	0.5320	0.8170	0.8355	1.5387	1.553
1.0	1.2192	1.213	1.2577	1.256	1.5865	1.613	2.4371	2.469
10	2.2745	2.267	2.3147	2.312	2.6581	2.687	3.5414	3.578
100	3.4148	3.407	3.4553	3.453	3.8005	3.830	4.6878	4.725
1000	4.5650	4.557	4.6055	4.603	4.9509	4.980	5.8383	5.876

Table 9.1: Comparison of Rectangular and Elliptical Well Pressures

skin. No such explicit form has been found (or is likely to be found) for the rectangular fracture.

Figures 9.1 and 9.2 show that all well pressures start on a single curve when graphed in one way and end on a single curve when graphed in another. This suggests the possibility of finding a composite solution that will give accurate well pressures for all fracture conductivities and for all times. We have expended considerable effort to find a method of computing wellbore pressures without resorting to the exact solution. We have not found an alternative well solution which is satisfactory for all values of time.

Both Figures 9.1 and 9.2 show a high degree of correlation between the wellbore pressures. This comparison is made explicit in Table 9.1 which shows well pressures for the rectangular and elliptical fractures. The well pressures in this table agree to within two and one-half percent. A more exhaustive tabulation of the elliptical case is given in Tables D.1 and D.2 of Appendix D.

Table 9.1 has one troubling feature; some tabulated pressures for the rectangular fracture are higher than those for the elliptical fracture. The elliptical fracture conductivity, F_E, is defined to match the rectangular fracture conductivity, F_D, at the well. Moreover, the rectangular fracture has a constant cross section, while the elliptical fracture tapers toward its ends. So, the rectangular fracture pressures should always be *lower* than the elliptical fracture pressures. We assume that the discrepancies in Table 9.1 are due to inaccuracies in Cinco et al.'s data.

We have now completed the presentation of the elliptical finite conductivity fracture problem and solutions. We have shown a method that theoretically allows the computation of pressures anywhere in the fracture/reservoir system. However, we have concentrated our efforts on obtaining accurate well pressures.

The accurate and efficient computation of reservoir pressures is a topic which we have not fully investigated. Neither have we considered the computation of pressures for the case of fracture face skin. These topics fall under the category of future work and will be discussed in the next section.

9.2   Extensions

The purpose of this section is to discuss aspects of the elliptical fracture problem which we were not able to develop fully. Here we give only a brief outline of the topics we see as logical outgrowths of this work.

9.2.1   Fracture and Reservoir Pressure

In this subsection we discuss the computation of reservoir pressures using the present model. In Chapter 7, we developed a method to determine the fracture pressure by means of the series:

$$\bar{p}_f(\eta; s) = \sum_{r=0}^{\infty} (-1)^r \beta_{2r} \cos(2r\eta). \tag{9.4}$$

We also showed how to accelerate the convergence of this series by using the behavior of the large r terms.

Determination of reservoir pressure requires evaluation of

$$\bar{p}_R(\eta, \xi; s) = \sum_{n=0}^{\infty} \frac{(-1)^n \gamma_{2n} Fek_{2n}(\xi; -s/4) ce_{2n}(\eta; -s/4)}{Fek_{2n}(0; -s/4)} \tag{9.5}$$

This series requires the computation of angular and radial Mathieu functions, but should converge as $\exp(-2n\xi)/n^2$.

To evaluate the coefficients in *Eq.* 9.5, γ_{2n}, we can use the expression:

$$\gamma_{2n} = \sum_{r=0}^{\infty} A_{2r}^{2n} \beta_{2r} , \tag{9.6}$$

given in Chapter **5.** Another possibility is to develop iterative solutions for the two sum equations involving γ_{2n}, Eqs. **6.25** and **6.29** of Chapter **6.** These solutions should be analogous to those involving β_{2r}. There is also a possibility that manipulation of these sum equations will give insights into the problem which we have overlooked.

We also need to consider the determination of pressures for large values of s. **We** have already developed early time solutions for well pressures. The method for determining the bilinear/linear flow behavior could be extended to account for pressures in the reservoir using the method of geometrical optics (see the notes of Keller **(1989)**).

9.2.2   Fracture Face Skin

Fracture face skin can be easily included if we define the skin so that it is consistent with the elliptical fracture formulation.

The usual way of defining the skin effect is to specify that the pressure drop across an infinitesimally thin skin region is equal to the product of the dimensionless skin factor and the flux density, q'. For fracture face skin, the equation takes the form:

$$\bar{p}_f(\eta; s) = \bar{p}_R(\eta, 0; s) + Sq' = \bar{p}_R(\eta, 0; s) - \frac{S}{\pi \sin(\eta)} \left.\frac{\partial \bar{p}_R}{\partial \xi}\right|_{\xi=0}. \qquad (9.7)$$

The last expression in this equation uses the definition of q' given by Eq. **3.15** of Chapter **3** and the relation:

$$\left.\frac{\partial \bar{p}_R}{\partial y_D}\right|_{y_D=0+} = \frac{1}{\sin(\eta)} \left.\frac{\partial \bar{p}_R}{\partial \xi}\right|_{\xi=0}. \qquad (9.8)$$

The presence of $\sin(\eta)$ in Eq. **9.7** will complicate the solution process considerably. Thus, it is advantageous to specify a skin effect which is elliptically distributed on the fracture face. This entails the use of the derivative of reservoir pressure with respect to ξ rather than the normal derivative:

$$\bar{p}_f(\eta; s) = \bar{p}_R(\eta, 0; s) - \frac{S_E}{\pi} \left.\frac{\partial \bar{p}_R}{\partial \xi}\right|_{\xi=0}. \qquad (9.9)$$

Equation **9.9** should model the physical system better than Eq. **9.7.** This is because fracture face skin arises from fluid invasion during fracturing and this invasion is greatest near the well. Equation **9.9** implicitly specifies a skin effect which is proportional to $\sin(\eta)$.

Equation **9.9** gives the matching condition for reservoir and fracture pressure, since the two pressures are no longer equal at the fracture face. The rest of the elliptical fracture problem is unchanged: the diffusivity equation and the fracture flow equations are as specified in earlier chapters. The main difference in the new formulation is that the relation between γ_{2n} and β_{2r} is no longer given by Eq. **9.6.** Equation **9.9** indicates that the new form of Eq. 9.6 will contain an additional term. This means that the Fredholm sum equations will also contain additional terms.

The exact solution of the new sum equations should be essentially the same as in the third section of Chapter 7. This solution will undoubtedly have computational difficulty at early times. To circumvent this difficulty, we can use the methods of Chapter 8 to develop early time wellbore solutions. It should be no problem to include a skin term in the infinite length fracture model or the bilinear/linear flow model. However, the effect of skin on the infinite conductivity fracture may be difficult to determine.

9.2.3   Miscellaneous Problems

Wellbore Storage

Since we have developed solutions in Laplace space, wellbore storage can be included in the well pressure solution simply:

$$\bar{p}_w C_D = \frac{\bar{p}_w}{1 + C_D s^2 \bar{p}_w} \; . \tag{9.10}$$

This expression is due to Van Everdingen and Hurst **(1949)** and assumes that the wellbore storativity is constant.

Bounded Reservoirs

It does not appear that the elliptical formulation can be easily modified to include linear barriers. The method of images will produce a zero gradient condition along the barrier. However, the image fracture will cause a pressure gradient along the original fracture which does not satisfy the fracture differential equation.

The only boundaries which can be handled readily are those which correspond to constant values of ξ in the elliptical coordinate system. Solving problems where the reservoir is externally bounded by an ellipse will be straightforward. The acceptable radial solutions will be both Fek_{2n} and Ce_{2n}. The constant which multiplies the additional radial function is readily determined because the outer boundary condition will give an explicit relation between the coefficients of the two radial functions.

Double Porosity Systems

The solutions presented in earlier chapters can be modified to account for double-porosity behavior using any of the double-porosity formulations currently in use. This is because the solutions in this work are presented in Laplace space and the flow within the fracture is incompressible.

The current double-porosity formulations use an $sf(s)$ term in place of s in the single-porosity solution and multiply the solution by $f(s)$ (see, for example, Bourdet and Gringarten (1980)). Double-porosity behavior is included in the present case in exactly the same way:

$$\bar{p}_{dp}(s) = f(s)\bar{p}(sf(s)). \tag{9.11}$$

The $f(s)$ term accounts for interporosity flow. It takes different forms depending on whether interporosity flow is pseudosteady or transient.

Layered Systems

A layered system can be incorporated into the present model as long as the models do not account explicitly for flow in the z-direction. In most of the models used at present, the layers either do not communicate or the communication is accounted for by coupling equations representing two-dimensional flow. Extending the present model to these cases should not pose a problem.

However, if the fracture affects the flow in the z-direction, the solution of a three-dimensional problem will be required. The solution of this type of problem will require a reformulation of the basic governing equations used in this work.

Chapter 10

CONCLUSIONS

This chapter concludes the present work. It consists primarily of a list of conclusions reached in the course of this research. Before proceeding with the listing, however, we review the reasons for undertaking this project.

It was not the intent of this work to usurp the groundbreaking and exhaustive efforts of Cinco and others. The purpose was to develop a model that approximated the physical situation as well as, or better than, the rectangular fracture and was exactly solvable.

There were other aims. Primary among these was to determine if various linear-type flow regimes, which arise naturally from a rectangular fracture formulation, would arise in the case of a different fracture geometry. These regimes were found to occur in the elliptical fracture formulation.

Another aim of this work was to find an accurate, readily calculable wellbore solution valid for all times and conductivities. This general simplified solution was never found. So, determination of the wellbore pressure requires computation of the exact solution, at least for dimensionless times greater than 10^{-3}.

It needs to be emphasized that the present solutions are analytic. The only impediment to writing the solutions in explicit form is that they are typographically unwieldy. We have no mathematical proof of the exactness of the solution, but we have verified that the two computationally independent solutions converge to the same value.

We feel the need to emphasize the exactness of the solutions because we never expected to find them. Indeed, we happened upon them largely by chance. It was assumed that this work would have to rely on the power series solutions of Chapter 7 which have restricted ranges of applicability. The exact solutions, although not trivial to calculate, can be computed using standard computing machinery (in our case an Apollo 10000). The data presented in the graphs of Chapter 9 consist of 125 data points over six log cycles of time. Each data set required approximately five minutes of real time for computation.

1. This work poses and solves the problem of a vertical finite conductivity fracture of elliptical cross section producing at constant rate. The flow within the fracture is assumed to be incompressible and the reservoir is assumed to be infinite in extent.

2. Two iterative solutions are presented. These solutions bear some resemblance to continued fractions and contain Mathieu functions and Mathieu Fourier coefficients. The two solutions converge to the same value! for all values of fracture conductivity, F_E, and Laplace parameter, s. For practical calculations, the choice of solution depends on the magnitude of F_E.

3. The difficulty in computation of the solutions varies directly with the magnitude of s. This is because the kernels used in computing the solutions are represented by diagonally dominant square matrices which fill as s increases. Asymptotic solutions are presented for wellbore pressures when s is greater than 10^4.

4. The wellbore pressure for an elliptical fracture exhibits the same flow regimes as a rectangular fracture. The bilinear and reservoir linear regimes have similar representations for the two geometries. The pseudoradial flow regimes differ slightly in the two cases. There is an explicit expression for the apparent skin during pseudoradial flow to an elliptical fracture. No such explicit form has been found for the rectangular fracture.

5. The present solution procedures can be applied to related problems. These applications are limited to two-dimensional problems whose geometries can be

represented by elliptical coordinates.

6. Mathieu functions *are* computationally useful. Also, the **work** of Blanch (**1966**) reduces the determination of eigenvalues and Fourier coefficients to a straight-forward procedure.

Bibliography

[1] Abramowitz, M., and Stegun, I.A., Editors: *Handbook of Mathematical Functions*. National Bureau of Standards, Appl. Math. Series, No. 55, U.S. Government Publications, Washington (1972).

[2] Agarwal, R.G., Carter, R.D., and Pollock, C.B.: "Evaluation and Performance Prediction of Low-Permeability Gas Wells Stimulated by Massive Hydraulic Fracturing," *J. Pet. Tech.* (Mar. 1979), 362-372.

[3] Barker, B., and Ramey, H.J. Jr.: "Transient Flow to Finite Conductivity Fractures," paper SPE 7489, presented at the 53rd Annual Technical Conference and Exhibition of SPE, held in Houston, TX, Oct. 1-3, 1978.

[4] Bender, C.M., and Orszag, S.A.: *Advanced Mathematical Methods for Scientists and Engineers.* (McGraw-Hill Book Co., New York, N'Y, 1978).

[5] Blanch, G.: "Numerical Aspects of Mathieu Eigenvalues," *Rend. Circ. Matem. Palermo* - Serie II -Tomo XV - Anno 1966, 51-97.

[6] Bourdet, D., and Gringarten, A.C.: "Determination of Fissure Volume and Block Size in Fractured Reservoirs by Type-Curve Analysis," paper SPE 9293, presented at the 55th Annual Technical conference and Exhibition of SPE, held in Dallas, TX, Oct. 21-24, 1980.

[7] Cinco-Ley, H.: "Evaluation of Hydraulic Fracturing by Transient Pressure Analysis Methods," paper SPE 10043, presented at the International Petroleum Exhibition and Technical Symposium of the SPE, held in Beijing, China, 18-26 March 1982.

[8] Cinco-Ley, H., and Meng, H.Z.: "Pressure Transient Analysis of Wells with Finite Conductivity Vertical Fractures in Double Porosity Reservoirs," paper SPE 18172, presented at the 63rd Annual Technical Conference and Exhibition of the SPE, held in Houston, TX, Oct. 2-5, 1988.

[9] Cinco-Ley, H., Ramey, H.J. Jr., Samaniego-V, F., and Rodriguez, F.: "Behavior of Wells with Low-Conductivity Vertical Fractures," presented at the 62nd Annual Technical Conference and Exhibition of the SPE, held in Dallas, TX, Sept. 27-30, 1987.

[10] Cinco-Ley, H., and Samaniego-V., F.: "Effect of Wellbore Storage and Damage on the Transient Pressure of Vertically Fractured Wells," paper SPE 6752, presented at the 52nd Annual Technical conference and Exhibition of the SPE, held in Denver, CO, Oct. 9-12, 1977.

[11] Cinco-Ley, H., and Samaniego-V., F.: "Transient Pressure Analysis for Fractured Wells," *Soc. Pet. Eng. J.* (Sept. 1981), 1749-1766.

[12] Cinco-Ley, H., Samaniego-V., F. and Dominguez A., N.: "Transient Pressure Behavior for a Well with a Finite-Conductivity Vertical Fracture," *Soc. Pet. Eng. J.* (Aug. 1978), 253-264.

[13] Cinco-Ley, H., Samaniego-V, F., and Rodrigues, F.: "Application of the Pseudo-linear Flow Model to the Pressure Transient Analysis of Fractured Wells," paper SPE 13059, presented at the 59th Annual Technical Conference and Exhibition of the SPE, held in Houston, TX, Sept. 16-19, 1984.

[14] Delft Analysis Group: "On the Computation of Mathieu Functions," **J. *Eng. Math.*, 7,**(1973), 39-61.

[15] Dingle, R.B., and Muller, H.J.W.: "Asymptotic Expansions of Mathieu Functions and their Characteristic Numbers," **J.** *Reine Angew. Math.,* **211,** (1962), 11-32.

[16] Erdelyi, A., et al.: *Higher Transcendental Functions.* (McGraw-Hill Book Co., Inc., New York, NY, 1955), 3 volumes.

[17] Gringarten, A.C., Ramey, H.J. Jr., and Rhagavan, R.: "Unsteady-State Pressure Distributions Created by a Well with a Single Infinite-Conductivity Vertical Fracture," *Soc. Pet. Eng. J.* (Aug. 1974), 347-360.

[18] IMSL Inc.: *User's Manual — IMSL SFUN/Library.* (IMSL Inc., Houston, TX, 1990).

[19] Keller, J.B., and Rubinow, S.I.: "Asymptotic Solution of Eigenvalue Problems," *Annals of Physics,* **9,** (1960), 24-75.

[20] Keller, J.B.: Course Notes distributed in Math 274, "Wave Propagation," Winter quarter 1989-1990, Stanford University.

[21] Kuchuk, F.J.: "New Methods fo Estimating Parameters of Low Permeability Reservoirs," paper SPE 16394, presented at the SPE/DOE Low Permeability Reservoirs Symposium, held in Denver, CO, May 18-19, 1987.

[22] Kuchuk, F.J., Goode, P.A., Wilkinson, D.J., and Thambynayagam, R.K.M.: "Pressure Transient Behavior of Horizontal Wells With and Without Gas **Cap** or Aquifer," paper SPE 17413, presented at the California Regional Meeting of the SPE, held in Long Beach, CA, Mar. 23-25, 1988.

[23] Kucuk, F.J., and Brigham, W.E.: "Transient Flow in Elliptical Systems," *Soc. Pet. Eng. J.* (Dec. 1979), 401-410.

[24] Lee, S.T., and Brockenbrough, J.R.: "A New Approximate Analytic Solution for Finite-Conductivity Vertical Fractures," *Soc. Pet. Eng. Form. Eval.* (Feb. 1986), 75-88.

[25] Matthews, C.S., and Russell, D.G.: *Pressure Buildup and Flow Tests in Wells.* SPE Monograph Series, **1,** Dallas, TX (1967).

[26] McLachlan, N.W.: *Theory and Application of Mathieu Functions.* (Clarendon Press, Oxford, England, 1947).

[27] Meixner, J., and Schafke, F.W.: *Mathieusche Funktionen und Spharoidfunktionen.* (Springer-Verlag, Berlin, Germany, 1954). *In German.*

[28] Meixner, J., Schafke, F.W., and Wolf, G.J.: *Mathieu Functions and Spheroidal Wave Functions and Their Mathematical Foundations.* (Springer-Verlag, Berlin, 1980).

[29] Morse, P.M., and Feshbach, H.: *Methods of Theoretical Physics.* (McGraw-Hill Book Co., New York, NY, 1953), 2 Volumes.

[30] Muskat, M.: *Flow of Homogeneous Fluids Through Porous Media.* (McGraw-Hill Book Co., New York, NY, 1937).

[31] Obut, S.T., and Ertekin, T.: **"A** Composite System Solution in Elliptical Flow Geometry,'' *Soc. Pet. Eng. Form. Eval.* (Sept. 1987), 227-238.

[32] Olver, F.W.J.: "Second-Order Linear Differential Equations with Two Turning Points," *Phil. Trans. R. Soc. Lond. A,* **278,** (1975), 13'7-174.

[33] Papatzacos, P.: "Exact Solutions for Infinite-Conductivity Wells," *Soc. Pet. Eng. Reser. Eng.* (May 1987), 217-226.

[34] Prats, M.: "Effect of Vertical Fractures on Reservoir Behavior—Incompressible Fluid Case," *Soc. Pet. Eng. J.* (Jun. 1961), 103-118.

[35] Prats, M.: "Effect of Vertical Fractures of Reservoir Behavior — Compressible Fluid Case," *Soc. Pet. Eng. J.* (Jun. 1962), 87-94.

[36] Riley, M.F.: "Discussion of A Composite System Solution in Elliptic Flow Geometry," *Soc. Pet. Eng. Form. Eval.* (Sept. 1990), 325-326.

[37] Rubin, H.: "Anecdote on Power Series Expansions of Mathieu Functions," **J.** *Math. and Phys.,* **43,** (1964), 339-341.

[38] Sips, R.: "Reprksentation Asymptotique des Fonctions de Mathieu et des Fonctions d'Onde Sphéroidales," *Trans. Amer. Math. Soc.,* **66,** (1949) , 93-134. *In French*

[39] Stehfest, H.: "Algorithm 368 — Numerical Inversion of Laplace Transforms [D5]," *Comm. of ACM,* **13,** No. 1, (Jan. 1970), 47-49. *ERRATA Comm. of ACM,* **13,** No. 10, 624.

[40] Tranter, C.J.: "Heat Conduction in the Region Bounded Internally by an Elliptical Cylinder and an Analogous Problem in Atmospheric Diffussion," *Quart.* **J.** *Mech. Appl. Math.,* **4** (1951), 461-465.

[41] Van Dyke, M.: "Analysis and Improvement of Perturbation Series," *Quart.* **J.** *Mech. Appl. Math.,* **27,** (1974), 423-450.

[42] Van Dyke, M: *Perturbation Methods in Fluid Mechanics.* (Parabolic Press, Stanford, CA, 1975).

[43] Van Dyke, M: *Personal Communication.* Dept. of Aero. and Astro., Stanford University, Stanford, CA, June, 1990.

[44] Van Everdingen, A.,F., and Hurst, W.: "The Application of the Laplace Transformation to Flow Problems," *Trans.,* AIME, **198,** (1949), 171-176.

[45] van Kruysdijk, C.P.J.W.: "Semianalytical Modeling of Pressure Transients in Fractured Reservoirs," paper SPE 18169, presented at the 63rd Annual Technical Conference and Exhibition of the SPE, held in Houston, TX, Oct. 2-5, 1988.

[46] Wilkinson, D.J.: "New Results for Pressure Transient Behavior of Hydraulically Fractured Wells," paper SPE 18950, presented at the SPE Joint Rocky Mountain Regional/Low Permeability Reservoirs Symposium and Exhibition held in Denver, CO, Mar. 6-8, 1989.

[47] Wolfram, S.: *Mathematica: A System for Doing Mathematics by Computer.* (Addison-Wesley Pub. Co., Redwood City, CA, 1988).

[48] Yeh, C.: "The Diffraction of Waves by a Penetrable Ribbon," **J.** *Math. Phys.,* **4,** No. 1, (Jan. 1963), 65-71.

Appendix A

NOMENCLATURE

a_{2n} Separation constant in Mathieu's equation, Chapt. 5

A_{2r}^{2n} Mathieu function Fourier coefficient, Chapt. 5

B Parameter in Riccati equation, $\sqrt{2\sqrt{s}/F_E}$, Chapt. 8

ce_{2n} Angular n-periodic Mathieu function, Chapt. 5

Ce_{2n} Radial Mathieu function, Chapt. 5

c_t Total isothermal compressibility

D_p Parabolic cylindrical function, App. C

F_D Rectangular fracture conductivity, $k_f w/k_R x_f$, Chapt. 3

F_E Elliptical fracture conductivity, $2k_f \xi_0/k_R$, Chapt. 4

Fek_{2n} Radial Mathieu fiinrtinn, Chapt 5

$\mathcal{F}_{2n}$ $Fek'_{2n}(0; -s/4)/Fek_{2n}(0; -s/4)$, Chapt. 5

G_{2r} Fourier coefficient ratio, $A_{2r}^{2n}/A_{2r-2}^{2n}$, App. B

h Reservoir thickness

h Parameter, $\sqrt{s}/2$, App. C

h_η, h_ξ Scale factors of coordinate transformation, Chapt. 5

I_r Modified Bessel function of the first kind

k Permeability

K_r Modified Bessel function of the third kind

$\mathcal{L}(f)$ Laplace transformation of f

p Index of parabolic cylindical function, $-\lambda_{2n}^2/4h - 1/2$, App. C

99

p_D	Dimensionless pressure $2\pi k_R h(p_i - p)/q\mu$
q	Well flowrate
q'	Fracture flux density, Chapt. **3**
r	Radius, $\sqrt{x^2 + y^2}$
r_D	Dimensionless radius, r/x_f
R	Separated radial solution, Chapt. 5
s	Parameter of Laplace transformation
S	Dimensionless skin factor, Chapt. 9
S_E	Elliptical dimensionless skin factor, Chapt. 9
t	Time
t_{Dx_f}	Dimensionless time, $k_R t/\phi_R \mu c_{tR} x_f^2$
V_{2r}	Term in continued fraction, $4(a_{2n} - 4r^2)/s$, App. B
w	Rectangular fracture width
x_D	Dimensionless distance, x/x_f
x_f	Fracture half length
y_D	Dimensionless distance, y/x_f
z	Dependent variable in Riccati equation, $(d\bar{p}_f/d\eta)/\bar{p}_f$, Chapt. 8

GREEKS

α_i	Indices of summation in Low F_E series, Chapt. 7
β_{2r}	Coefficients in fracture pressure series, Chapt. 6
γ_{2n}	Coefficients in reservoir pressure series, Chapt. **5**
γ	Euler's constant, 0.5771.. .
γ'	Exponential of Euler's constant, 1.781...
Γ	Γ-function
$\delta(x - x')$	Dirac delta function, Chapt. **4**
δ_{ij}	Kronecker delta function
$\Delta_{2n}^{2m}, \nabla_{2n}^{2m}$	Kernels of Fredholm sum equation, Chapt. 6
ϵ_r	$1 + \delta_{0r}$, Chapt. 5
η	Angular elliptical coordinate, Chapt. **4**
θ_{2n}	Parameter in elliptical integral formulation, App. B

Θ	Separated angular solution, Chapt. 5
κ_D	Diffusivity ratio, $k_R \phi_f c_{tf} / k_f \phi_R c_{tR}$, Chapt. 3
λ_{2n}^2	Mathieu eigenvalue, $a_{2n} + s/2$, Chapt. 5
μ	Fluid viscosity
ξ	Radial elliptical coordinate, Chapt. 4
ξ_0	Coordinate of fracture ellipse, Chapt. 4
ρ	Fluid density
ϕ	Porosity
χ_{2r}	Term in comparison series of Kummer's transformation, Chapt. 7
$\Psi(x)$	@-function, $\Gamma'(x)/\Gamma(x)$
$\Psi'(x)$	Derivative of Ψ function
$\Omega_{2r}^{2p}, \mho_{2r}^{2p}$	Kernels of Fredholm sum equation, Chapt. 6

SUBSCRIPTS AND SUPERSCRIPTS

f	Fracture quantity
$i, j, k, l, m,$	
n, p, q, r, α_i	Integer indices
R	Reservoir quantity
w	Wellbore value
$\bar{}$	Laplace transformed variable

Appendix B

MATHIEU EIGENVALUES AND COEFFICIENTS

In this appendix we illustrate the computational aspects of the separation constants, a_{2n}, the Fourier coefficients, A_{2r}^{2n}, and the kernels of the sum equations of Chapter 6.

Mathieu functions are rarely mentioned without reference to their computational difficulties. We have found that these computational difficulties have been overstated. The computation of Mathieu functions, except in extreme cases, is accomplished by summing series involving the Fourier coefficients, A_{2r}^{2n}. The paper of Blanch (1966) makes the computation of these coefficients straightforward.

B.1 Evaluation of a_{2n}

This section discusses the computation o the separation constants, a_{2n}. We work primarily with, a_{2n}, rather than the eigenvalues, λ_{2n}^2, because the separation constants appear in the continued fraction. Recall that the relation between the eigenvalues and separation constants is: $\lambda_{2n}^2 = a_{2n} + s/2$.

B.1.1   The Continued Fraction

In this subsection we discuss an iterative procedure for computing the eigenvalues from a continued fraction. This subsection is essentially an. overview of the work of Blanch (1966).

The derivation of the continued fraction starts from the recurrence relations given in Chapter **5**:

$$4a_{2n}A_0^{2n} - sA_2^{2n} = 0 ,$$

$$4(a_{2n} - 4)A_2^{2n} - s(A_4^{2n} + 2A_0^{2n}) = 0 ,$$

$$r \geq 2 \quad 4(a_{2n} - 4r^2)A_{2r}^{2n} - s(A_{2(r+1)}^{2n} + A_{2(r-1)}^{2n}) = 0 . \tag{B.1}$$

Defining G_{2r} as the ratio of coefficients, $A_{2r}^{2n}/A_{2(r-1)}^{2n}$, and V_{2r} by:

$$V_{2r} = \frac{4(a_{2n} - 4r^2)}{s} , \tag{B.2}$$

transforms the recurrence relations into:

$$G_2 = V_0 ,$$

$$G_4 = V_2 - 2/G_2 ,$$

$$r \geq 2 \quad G_{2(r+1)} = V_{2r} - 1/G_{2r} . \tag{B.3}$$

Solving the second of these relations for G_2 and setting it equal to the first gives a relation between G_4, V_0 and V_2. Repeating this process using the third relation with $r = 2$ gives a relation between G_6, V_0, V_2 and V_4. This procedu ɛ can be repeated indefinitely and ultimately yields the continued fraction:

$$0 = V_0 - \frac{2}{V_2-} \frac{1}{V_4-} \frac{1}{V_6-} \frac{1}{V_8-} \frac{1}{K0-} \cdots . \tag{B.4}$$

Equation **B.4** is a transcendental equation for a_{2n}, since each "V" given by Eq. B.2, contains the unknown, a_{2n}, and no other unknown terms.

The roots of Eq. **B.4** are the separation constants, a_{2n}. The obvious way of finding these roots is to apply the Newton method of successive approximation directly to Eq. **B.4.** This was attempted and found to be inadequate. The reason for this inadequacy
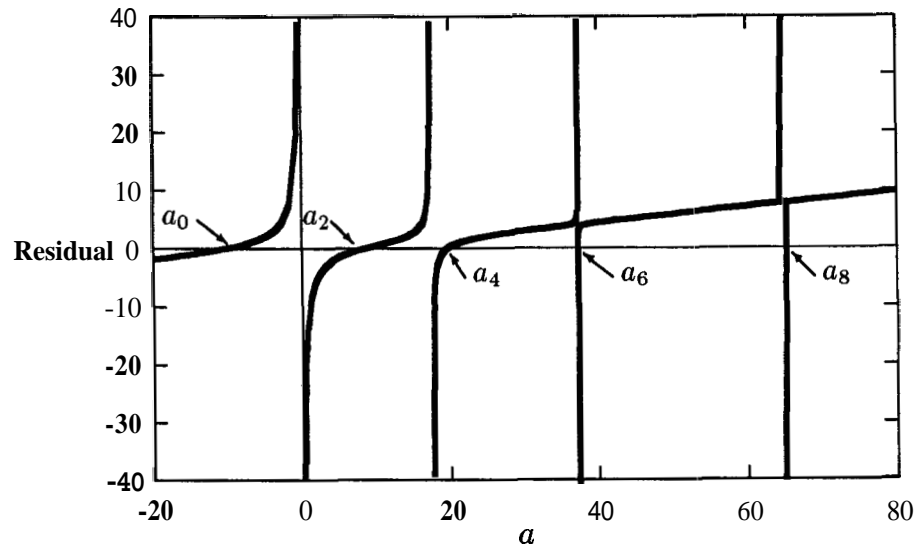
Figure **B.1:** Continued Fraction, Nonterminating Fraction Only

is illustrated by a representative example. In this example we attempt to find a_{2n} for all n and $s = 32$. Figure **B.1** shows a graph of the right hand side of Eq. **B.4,** termed the residual, versus a for s equal to **32.** The separation constants, a_{2n}, are the points where the residual is zero, i.e., at the intersection of the heavy curves with the horizontal line.

Newton's method is able to find the first two roots, $a_0 = $ **-10.6** and $a_2 = $ **+8.1,** with no difficulty. The next root, $a_4 = $ **19.3,** is more difficult to obtain, and the higher roots are virtually impossible to find. The reason for this difficulty is that as n increases, the zeroes and infinities of Eq. **B.4** approach each other. Since Newton's method relies on the slope of the function, if the initial guess is close to the eigenvalue, but not close enough, the first iteration will return a value that is on the more shallow slope. The next iterations will move along the shallow slope to one of the lower roots.

To overcome this difficulty, the recurrence relations of Eq. **B.3** are used to develop a second *terminating* continued fraction. This is accomplished by using the recurrence relations in reverse order. For example, to generate a terminating fraction for G_8, r is set equal to **3** and the first two relations of Eq. **B.3** are inserted into the third.
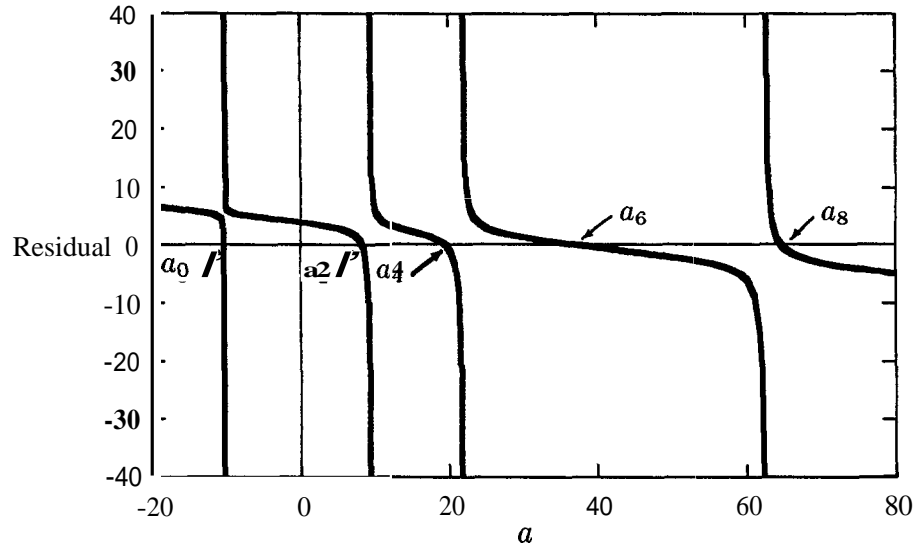
Figure B.2: Continued Fraction, Nonterminating aad Terminating

Then r is set equal to **4** and the expression for G_6 is inserted into the third relation of Eq. **B.3.** This gives:

$$G_{8,1} = V_6 - \frac{1}{V_4-} \frac{1}{V_2-} \frac{2}{V_0} \cdot \qquad \text{(B.5)}$$

Here we are using the notation of Blanch, the subscript, 1, refers to the terminating fraction. The infinite continued fraction for G_8 is denoted 'by $G_{8,2}$ and is derived in the same way as Eq. **B.4,** except that we start with G_8 rather than G_2. This gives

$$G_{8,2} = \frac{1}{V_8-} \frac{1}{V_{10}-} \frac{1}{V_{12}-} \frac{1}{V_{14}-} \frac{1}{V_{16}-} \cdots \cdot \qquad \text{(B.6)}$$

When $a = a_{2n}$, $G_{8,1}$ equals $G_{8,2}$, i.e., the difference between the two continued fractions, $G_{8,2} - G_{8,1}$, is zero.

The reason that this formulation is so valuable is shown in Fig. B.2. Figure B.2 is a graph of $G_{8,2} - G_{8,1}$, the residual, versus a for s equal **32.** .As before, the separation constants occur at the intersection of the heavy curves with the horizontal line. Here the fourth eigenvalue, at $a_6 = $ **36.9,** is easily found by Newton's method. We can find higher values in the same way by a judicious choice of r in $G_{2r,2} - G_{2r,1}$.

The discussion of the previous paragraphs outlines the gist of Blanch's method: the determination of r such that $G_{2r,2} - G_{2r,1}$ is essentially linear in the area of the desired eigenvalue. This allows Newton's method to converge to the desired eigenvalue. Blanch refers to this as the "chaining r" (actually in her nomenclature, it is the "chaining m", m_1) and gives a method for finding it using a first guess to a_{2n}. So, if an inaccurate first guess is used, $G_{2r,2} - G_{2r,1}$ may be linear near an undesired eigenvalue and Newton's method will converge to the wrong eigenvalue.

Once the chaining r has been found, the Newton method of successive approximation uses the relation:

$$a_{2n}^{new} = a_{2n}^{old} - \frac{G_{2r,2} - G_{2r,1}}{G'_{2r,2} - G'_{2r,1}} \qquad (B.7)$$

The primes in this equation refer to the derivatives with respect to **a.** The evaluation of these derivatives is outlined by Blanch. It is not necessary that these derivatives be computed to a high degree of accuracy.

Equation B.7 is iterated until a desired tolerance is met. In this work we check the ratio, $(a_{2n}^{old} - a_{2n}^{new})/(a_{2n}^{old} + s/2)$, i.e. we check the convergence of the eigenvalues, λ_{2n}^2, rather than a_{2n}. We do this because the separation constants become zero for certain values of s while the eigenvalues are always positive.

Equation B.7 converges quickly, usually in three iterations, but it requires a fairly accurate first guess. Before giving the correlations for the first guess we need to comment on a paper which has evaluated the above technique. A paper by the Numerical Analysis group at Delft University of Technology, Delft (1973), states that the method given by Blanch "in some cases will not produce the correct result." We have not had any problems using Blanch's method.

B.1.2 Obtaining a First Guess

The drawback of the continued fraction approach is that it requires an accurate first guess. The determination of the first guess is something that is not discussed in the literature and turns out to be the major difficulty with the method. If the guess is not close enough to the desired eigenvalue, the iterative procedure will converge to the wrong eigenvalue. The applicability of Blanch's technique is limited solely by the
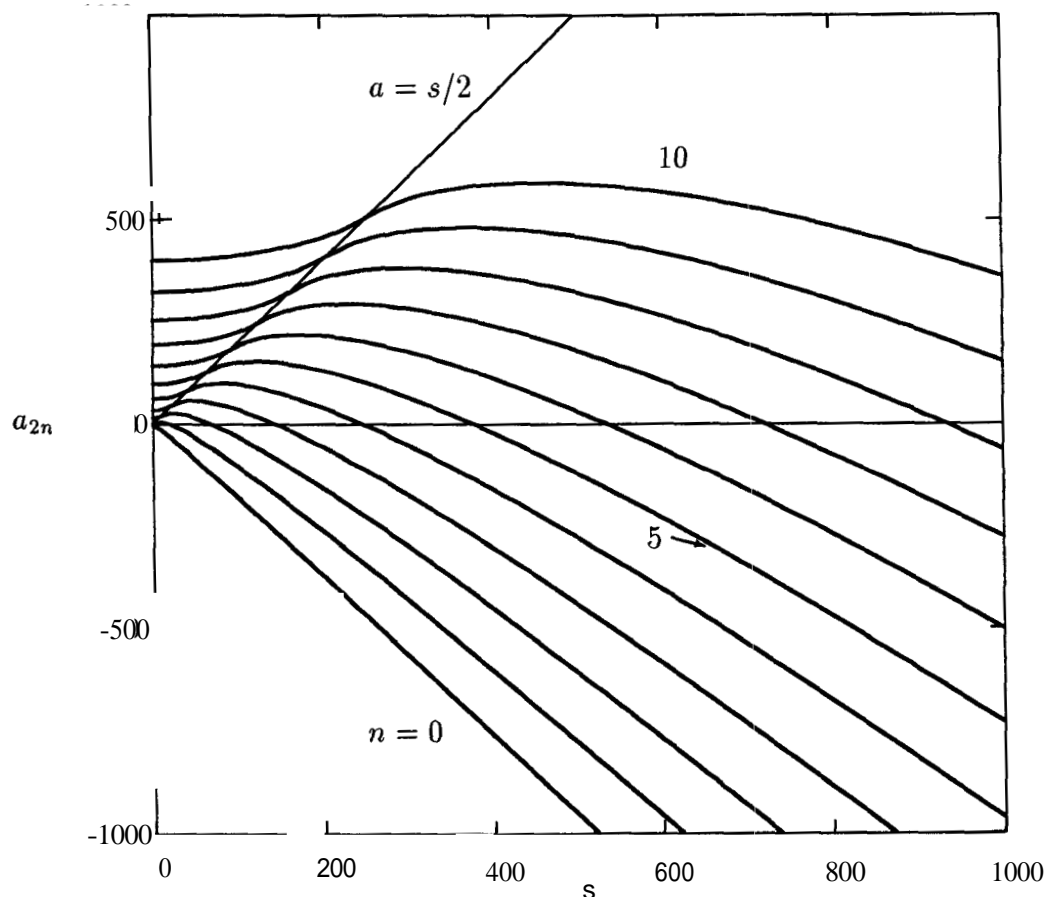
Figure **B.3:** Separation Constants, a_{2n}, $n = 0 - 10$

ability to give an accurate approximation to a_{2n}. The continued fraction approach has no limitation, *per* se.

The difficulty in finding a first guess is illustrated by Fig. **B.3.** Figure **B.3** is a graph of a_{2n} as a function of s for n ranging from 0 to 10. We show this graph because separation constants are usually displayed over a more limited range of s. Figure **B.3** clearly illustrates the points of inflection near $a = s/2$. The nature of the curves changes character dramatically as they cross this line. It is this change in character which complicates approximation of a_{2n}.

In the course of this work it was found that the point **of** equality, i.e., the value

of s where $a_{2n} = s/2$, is well approximated by:

$$s_{app} = \left(n + \frac{1}{8}\right)^2 \pi^2. \tag{B.8}$$

The difference between s_{app} and the actual point of equality appears to grow logarithmically. For n = 1 the difference is 0.154, while for n = 100 it is 0.617.

Using Eq. B.8 to approximate the point of equality, and the ascending and asymptotic series given by McLachlan (1947), the following (fairly rough) correlations were developed for $n \geq 1$:

$$a_{2n} \simeq 4n^2 + As^2 , \qquad s \leq s_{app} ;$$

$$a_{2n} \simeq -\frac{s}{2} + (4n+1)\sqrt{s} - \frac{(4n+1)^2 + 1}{8} + \frac{B}{\sqrt{s}} , \qquad s \geq s_{app} . \tag{B.9}$$

In **Eq.** B.9, A and B are given by:

$$A = \frac{\pi^2(n+1/8)^2 - 8n^2}{2\pi^4(n+1/8)^4} ,$$

$$B = \pi(n+1/8)\left[\pi^2(n+1/8)^2 - (4n+1)\pi(n+1/8) + \frac{(4n+1)^2 + 1}{8}\right] . \tag{B.1O}$$

For n = 0, we use the correlation:

$$a_0 \simeq -\frac{s^2}{32} + \frac{7s^4}{32768} - \frac{29s^6}{9437184} + \frac{68687s^8}{(65536)(18874368)} , \qquad s \leq 7.0 ;$$

$$a_0 \simeq -\frac{s}{2} + \sqrt{s} - \frac{1}{4} , \qquad s \geq 7.0 . \tag{B.11}$$

The correlations of Eqs. B.9 and B.11 have been checked thoroughly and give correct results when used in Newton's method for $0 \leq n \leq 150$ and for $0 < s \leq 10^4$. These correlations should give correct results for higher values of n, but approximation of a_{2n} for higher values of s will require more sophisticated correlations.

B.1.3 Checking the Order of a_{2n}

While investigating the asymptotic approximations to Mathieu functions (for example, see Keller and Rubinow (1960)), a relation was found which gives the order of the
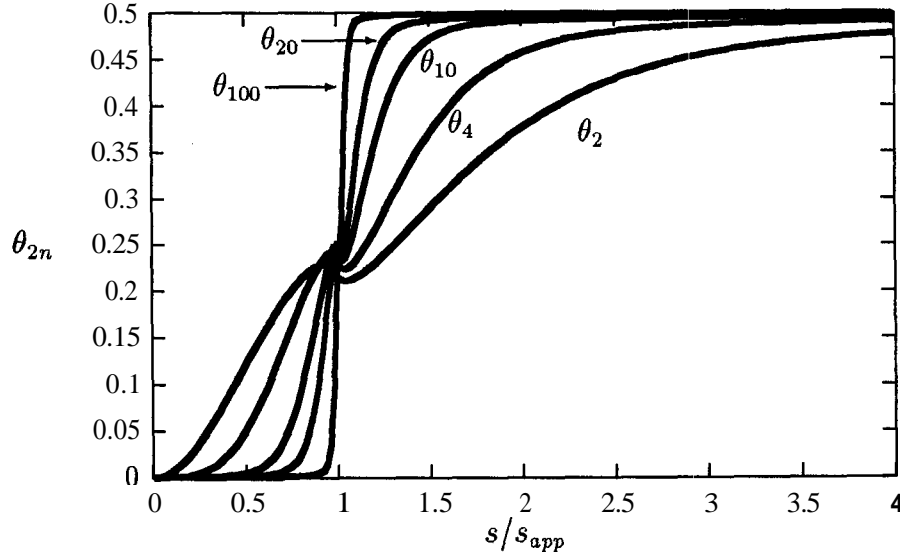
Figure B.4: Elliptical Integral Parameter, θ_{2n}

eigenvalue explicitly. This provides a means of checking whether the iterative procedure has converged to the eigenvalue of the desired order. This procedure employs
the observation that the integral of the square root of the coefficient in Mathieu's
equation, $\lambda_{2n}^2 - s\sin^2(\eta)$, gives the order of the eigenvalue explicitly.

More concretely put, θ_{2n} in the relation:

$$\int_0^{\eta_t} \sqrt{\lambda_{2n}^2 - s\sin^2(\eta)}\,d\eta = \frac{\pi}{2}(2n + \theta_{2n}). \tag{B.12}$$

has been found to vary between zero and one-half. In Eq. B.12, η_t is defined to be
$\pi/2$ for λ_{2n}^2 greater than s and $\arcsin(\lambda_{2n}/\sqrt{s})$, otherwise. Figure B.4 shows a graph
of θ_{2n} for various values of n.

Equation B.12 can be written in terms of the complete elliptic integrals $\mathbf{E}$ and
$\mathbf{K}$. Both of these elliptic integrals are available as *IMSL* subroutines (see IMSL Inc.
(1990)). For λ_{2n}^2 less than s, Eq. B.12 gives:

$$n = \frac{1}{\pi}\lambda_{2n}\mathbf{E}(\sqrt{s}/\lambda_{2n}) - \frac{1}{2}\theta_{2n}. \tag{B.13}$$

For λ_{2n}^2 greater than s it becomes:

$$n = \frac{\sqrt{s}}{\pi} \left\{ \mathbf{E}(\lambda_{2n}/\sqrt{s}) - \left(1 - \frac{\lambda_{2n}^2}{s}\right) \mathbf{K}(\lambda_{2n}/\sqrt{s}) \right\} - \frac{1}{2}\theta_{2n}. \tag{B.14}$$

Once an eigenvalue has been found, these two expressions give its order explicitly. This is because the unknown on the right hand side of these expressions, $\theta_{2n}/2$, varies between zero and one-quarter.

B.2   The Fourier Coefficients, A_{2r}^{2n}

The Fourier coefficients can theoretically be computed using the recurrence relations of Eq. B.l. In practice this is not feasible because the recurrence relations are unstable in the forward direction. To overcome this difficulty, Blanch (1966) uses the continued fraction formulations of the last section. The details are given in her paper.

The procedure for determining A_{2r}^{2n} is to employ the $G_{2r,1}$ and $G_{2r,2}$ used in finding the eigenvalues to compute a set of unnormalized coefficients. The sign of these coefficients is determined by requiring that A_0^{2n} be positive. This requirement is equivalent to requiring $ce_{2n}(0; -s/4) > 0$.

The final normalization is achieved by using the relation of Chapter *5:*

$$2(A_0^{2n})^2 + \sum_{r=1}^{\infty}(A_{2r}^{2n})^2 = 1. \tag{B.15}$$

This normalization also makes the sum over n of the squares equal to $1/\epsilon_r$, **as** shown in Chapter 5. Thus, the expression:

$$\sum_{n=0}^{\infty}(A_{2r}^{2n})^2 = \frac{1}{\epsilon_r}, \tag{B.16}$$

provides a convenient check on the Fourier coefficients. Recall that ϵ is defined to be unity for $r \neq 0$ and to be two for $r = 0$.

B.3   Computation of the Kernels and Their Sums

The computation of the iterative solutions given in Chapter 7 is uncomplicated once the sums involving the kernels have been calculated. Although, the computation of

these sums does not appear complex, certain pitfalls are present which have cost us weeks in lost time. For this reason we devote this subsection to the computation of the kernel, Ω_{2p}^{2r}, and the sum containing this kernel. The computation of the other kernels and their corresponding sums can be accomplished using the same procedure.

The kernel, Ω_{2p}^{2r}, is defined as:

$$\Omega_{2p}^{2r} = \Omega_{2r}^{2p} = \sum_{n=0}^{\infty} \frac{A_{2r}^{2n} A_{2r}^{2n}}{\mathcal{F}_{2n}} . \tag{B.17}$$

To compute this series efficiently, we sum only over the indices for which the Fourier coefficients differ significantly from zero. Once this has been accomplished, we need to compute the sum containing the kernel so that only nonzero terms are used.

The crux of the method involves calculating the Fourier coefficients, A_{2r}^{2n}, and noting the extremum of r and n for which the coefficients are nonzero. **As** was noted in Chapter 5, the nature of the Fourier coefficients is such that there is a band centered at A_{2n}^{2n} outside of which the coefficients become transcendentally small. It is only necessary to calculate the coefficients in this band and to note the values of the indices on its edges. **A** schematic of the nonzero values of A_{2r}^{2n} for a given value of s is shown as a matrix in Fig. B.5. Here the nonzero elements (those greater than 10^{-12}) are denoted by dots and the transcendentally small elements are omitted. In the exposition that follows, we assume that Fig. B.5 represents the matrix we are computing. Note that this figure only shows the upper left hand corner of the matrix — the matrix is infinite in both dimensions.

The first step in the procedure is to fill the matrix of the Fourier coefficients, which we call $A2r2n(r,n)$. The ultimate reason behind the computations of this appendix is to enable computation of β_{2r} for r up to 100. To achieve this goal, we set the dimensions of $A2r2n$ to 125 rows and columns. We do this because the sum involving Ω_{2p}^{2r} makes use of p values greater than r.

We also define a pair of two column matrices, mt and $mlow$, each with 125 rows, as:

$mlow(n,1) = $ lowest nonzero value of r, n fixed,
$mlow(r,2) = $ highest nonzero value of n, r fixed,
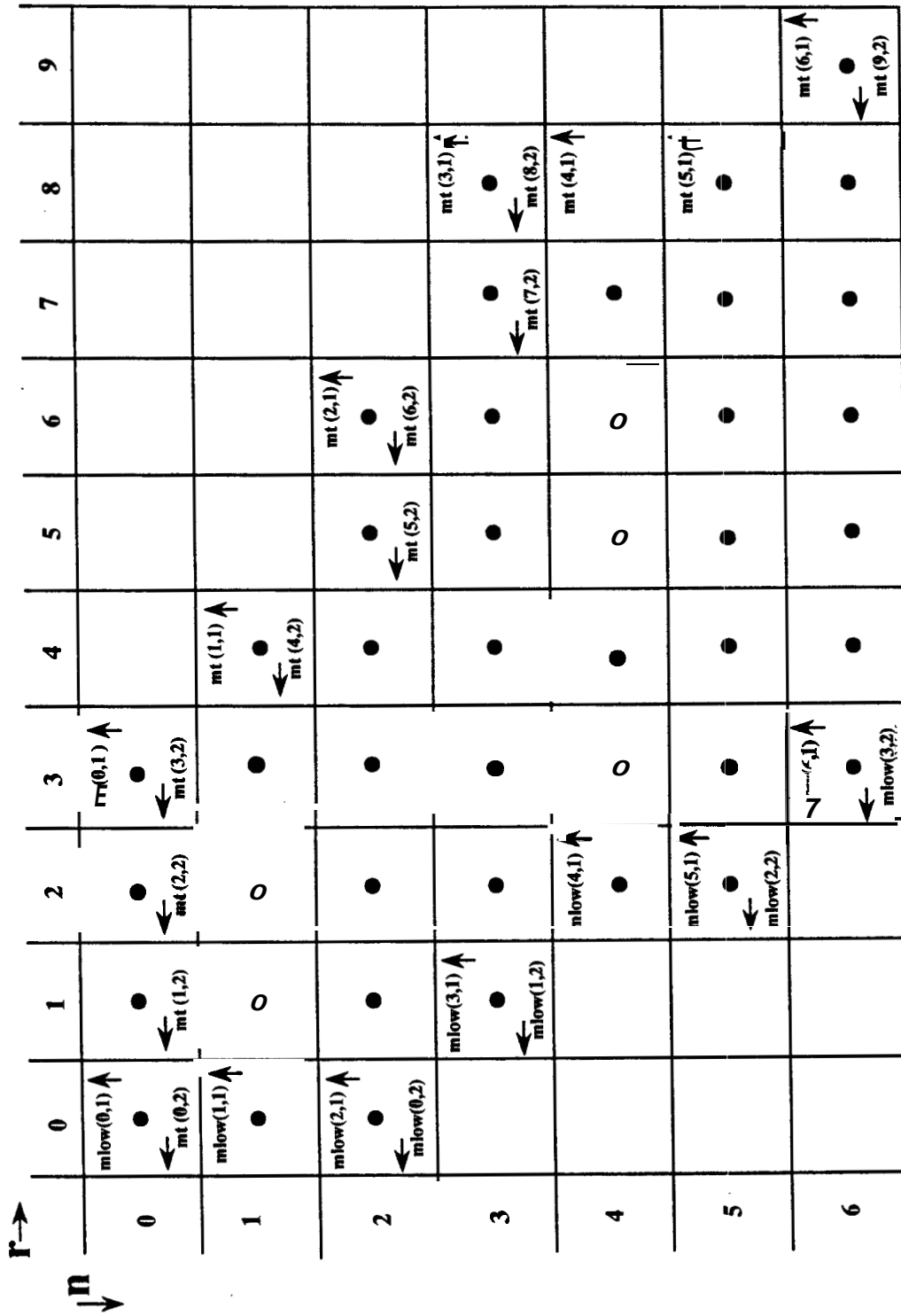
Figure **B.5:** Nonzero Values of A_{2r}^{2n}

$mt(\text{n},1) = $ highest nonzero value of r, n fixed,

$mt(\text{r},2) = $ lowest nonzero value of n, r fixed.

Since the Fourier coefficients are calculated from a recursion relation involving r, we start with $n = 0$ and calculate all of the nonzero values of A^0_{2r}. We then proceed to higher n. At each stage we find $mlow(\text{n},1)$ and $mt(\text{n},1)$ explicitly because we determine the starting and ending r values while computing A^{2n}_{2r}, although we may have to reassign them at a later stage. The values, $mlow(\text{r},2)$ and $mt(\text{r},2)$, are more difficult to determine. For each $A2r2n(\text{r},\text{n})$, n fixed, we only know if it is the first or last nonzero term in a column by comparing with coefficients of other rows, i.e. with other values of n.

In order to determine if a $A2r2n(\text{r},\text{n})$ value is the first nonzero value of a column, i.e., if $n = mt(\text{r},2)$, we compare r with $mt(\text{n-1},1)$. If there are any nonzero values for $r > mt(\text{n-1},1)$ in row n, then $mt(\text{r},2)$ is set equal to n for all of these values of r. The only problem with this procedure is where there are irregularities on the right side of the band. In Fig. B.5, the location n $= 3, r = 8$ is an irregularity because the coefficients immediately above and below it are zero. To overcome this difficulty, we artificially place a dot in the gap, $n = 4, r = 8$, and treat it as a nonzero term. This is accomplished by putting a check in the assignment of $mt(\text{n},1)$ to see if it is greater than or equal to $mt(\text{n-1},1)$. If it is less than $mt(\text{n-1},1)$ we reassign it to be equal to $mt(\text{n-1},1)$. In this way we fill out the gaps on the right side of the band.

The calculation of $mlow(\text{r},2)$ can be performed in a way analogous to that of the last paragraph. In practice, however, we have found that the machinations used to determine $mt(\text{r},2)$ are not needed for the determination of $mlow(\text{r},2)$. So we opt for a simpler method. This method assumes that $r = mlow(\text{n},1)$ and the next ten higher r values are at the bottom of a column. If they are not at the bottom of the column, they will be reassigned automatically at higher values of n. It has not been found necessary to fill in the gaps on the left side of the band nor do there appear to be irregularities which extend more than ten spaces.

The result of the above procedure is that we have filled the matrix of elements, $A2r2n(\text{r},\text{n})$, and know the locations of the extremal values. We now proceed to calculate the elements of the matrix of kernel elements, Ω^{2r}_{2p}. In order to fill the matrix,

$\text{OMEGA}(r,p)$, we start at a value of $r = 0$ and calculate a double loop for each value of r up to $r = 125$. In essence what the computation entails is multiplying a column corresponding to a value to r by a column corresponding to a value of p. In order **to** avoid unnecessarily computing zero values, we only multiply columns connected by a row of nonzero values and we sum only over values of n such that the p and r columns have nonzero elements. Otherwise we would be multiplying nonzero values of A_{2r}^{2n} by zero values **of** A_{2p}^{2n} and *vice versa.* So, at each value of r we start with a value of p equal to the lowermost nonzero position in the row corresponding to the uppermost nonzero position in column r, i.e., we start with p equal to $mlow(mt(r,2),1)$. For this value of p, we sum Eq. B.17 over the nonzero values of the column for this value of p downward in the column, i.e., we sum from n equal to $mt(r,2)$ to $mlow(p,2)$. We next increment p by one and perform the sum over n in the next column to the right. We repeat this procedure until we reach a value of p equal to r. Because is symmetric in p and r, at each value of p we set Ω_{2r}^{2p} equal to Ω_{2p}^{2r}. We need go no further than $p = r$ because higher order coefficients will be filled in symmetrically at higher values of r. At this point r is incremented by one and the procedure is repeated until $r = 125$, at which point the matrix, $\text{OMEGA}(r,p)$, is filled.

Once the matrix, $\text{OMEGA}(r,p)$, is filled we need to evaluate the sum containing it:

$$\sum_{p=1}^{\infty} p^2 \Omega_{2p}^{2r} \beta_{2p} \ . \tag{B.18}$$

We proceed in much the same way as in the preceding paragraph, i.e., we sum only indices such that the corresponding columns are joined by a row of nonzero elements. The terms, p^2 and β_{2p}, are slowly varying and so don't affect the magnitude of the terms significantly. In computing a sum over p we are given a value of r which is the same as the subscript of the coefficients, β_{2r}, outside of the summation. The sum is carried out from p equal to $mlow(mt(r,2),1)$ up to p equal to $mt(mlow(r,2),1)$. **At** this point the sum is complete.

Appendix C

COMPUTATION OF $\mathcal{F}_{2n}$

In this appendix we illustrate the computation of the derivative of the radial Mathieu function, Fek_{2n}, at $\xi = 0$. In this work, it has been convenient to consider the ratio $\mathcal{F}_{2n} = Fek'_{2n}(0; -s/4)/Fek_{2n}(0; -s/4)$. The methods outlined in this section allow computation of $\mathcal{F}_{2n}$ to at least seven significant figures of accuracy.

This appendix consists of four sections. The first section uses the relations given by McLachlan (1947) to express $\mathcal{F}_{2n}$ as a ratio of two series. This ratio is computationally useful for low values of s only. For higher values of s, truncation errors make the method inaccurate.

The second section gives a fairly rigorous and very tedious derivation in terms of parabolic cylindrical functions. The final expression for $\mathcal{F}_{2n}$ is given in terms of Γ-functions, Ψ-functions and derivatives of Ψ-functions. An argument is made that this final expression is actually a Taylor series expansion of a sum of Γ-functions.

The third section presents a simplistic, yet tedious derivation which gives accurate results for n greater than ten. The added benefit of this solution is that, for these high n values, it approximates both late and early time behavior.

The fourth section gives the ranges of applicability of the three solutions.

C.1   The Fourier Series Representation

The expression given as Eq. 5.25 in Chapter 5 can be written as:

$$\mathcal{F}_{2n} = \frac{-\sum_{p=0}^{\infty} A_{2p}^{2n}}{\sum_{r=0}^{\infty} A_{2r}^{2n} I_r(\sqrt{s}/2) K_r(\sqrt{s}/2)} , \tag{C.1}$$

where I_r and K_r are modified Bessel functions.

This expression is useful for small s. **As** s increases, the truncation errors, associated with computing each series in Eq. C.1, grow. This is because both series become transcendentally small for large s, although they sum terms of order unity. For this reason, alternative formulations are needed which give $\mathcal{F}_{2n}$ directly. These formulations are discussed in the next two sections.

C.2   Parabolic Cylindrical Function Derivation

This section derives expressions for $\mathcal{F}_{2n}$ directly from the governing differential equation. The solutions derived in this section are valid for large values of s and all n, although we make use of them for n less than or equal to ten only. The method takes into account that the differential equation contains turning points. The derivation is extremely tedious, so only the highlights and the final expressions will be given. Much of the approach used in this section is taken from Sips (1949).

We seek a solution of the radial separated equation, Eq. 5.23 of Chapter *5:*

$$\frac{\partial^2 y}{\partial x^2} - \left[a_{2n} + \frac{s}{2} \cosh(2x) \right] y = 0, \tag{C.2}$$

which approaches zero as x approaches infinity and has a value of unity at x equal *to* zero. Once this problem is solved, $\mathcal{F}_{2n}$ is the derivative of y at x equal to zero.

The difficulty with using asymptotic methods to solve Eq. C.2 is that it contains turning points: values of x such that the coefficient of y is equal to zero. It does not matter that these values are not real, they will still have an effect on the solution for real x. It does matter, however, that the turning points appear in complex conjugate pairs. This means that we must approximate Eq. C.2 by an equation which possesses a *double* turning point (see Olver(1975)).

The simplest differential equation which possesses a double turning point is the equation governing parabolic cylinder functions:

$$L[y; p] = \frac{\partial^2 y}{\partial z^2} + (p + \tfrac{1}{2} - \frac{z^2}{4})y = 0. \tag{C.3}$$

The solutions of this equation which vanish at infinity are the parabolic cylindrical functions, $D_p(z)$. There is not a great deal of literature on these functions, but Abramowitz and Stegun **(1972)** and Erdelyi et al. (Vol. **2,1955)** give some discussion.

Because we seek solutions of Eq. **C.2** valid in the region of the origin, we expand the hyperbolic cosine in a power series, make the substitutions, $h = \sqrt{s}/2$, $z = 2\sqrt{h}x$, and $p = -\lambda_{2n}^2/4h - 1/2$, and rearrange. These steps transform Eq. **C.2** into:

$$\frac{\partial^2 u}{\partial z^2} + (p + \tfrac{z}{2} - \tfrac{z^2}{4})y = y\left(\frac{z^4}{48h} + \frac{z^6}{1440h^2} + \frac{z^8}{80640h^3} \cdots\right). \tag{C.4}$$

In order to develop a perturbative solution, we assume a that y can be represented as:

$$y(z; p, h) = y_0(z; p) + \frac{y_1(z; p)}{h} + \frac{y_2(z; p)}{h^2} + \frac{y_3(z; p)}{h^3} + \ldots . \tag{C.5}$$

It may seem strange that we are considering p and h to be independent parameters, especially since we are assuming that **h** is large. The usual way to handle this type of problem is to expand p in inverse powers of **h** and then to equate powers of **h.** By assuming that p is independent of h, however, we develop a solution that is more accurate for low values of s.

The perturbation procedure consists of inserting Eq. **C.5** into Eq. **C.4** and equating powers of **h.** This results in an infinite set of differential equations which are solved sequentially. All of the solutions must approach zero as z approaches infinity and all of the solutions, except for y_0, must have a value of zero at z equal to zero. The solution, yo, is to have a value of unity at z equal to zero. In this way, we insure that Eq. **C.5** satisfies the differential equation and boundary conditions, at least formally.

The first approximation, y_0, is the solution of Eq. **C.3** having a value of unity at z equal to zero and approaching zero for large z. Since, the only solution which satisfies the differential equation and approaches zero for large z is proportional to $D_p(z)$, we must have:

$$y_0(z; p) = \frac{D_p(z)}{D_p(0)} . \tag{C.6}$$

To obtain the first approximation to $\mathcal{F}_{2n}$, we differentiatethis expression with respect to x using the chain rule and the relations:

$$\frac{dD_p(z)}{dz} = \frac{zD_p(z)}{2} - D_{p+1}(z),$$

$$D_p(0) = \frac{\sqrt{\pi}\, 2^{p/2}}{\Gamma(-(p-1)/2)}. \qquad (C.7)$$

This gives the pproximation:

$$\mathcal{F}_{2n} \sim -\frac{2\sqrt{2h}\,\Gamma(-(p-1)/2)}{\Gamma(-p/2)} + O(1/\sqrt{h}). \qquad (C.8)$$

The next approximation, y_1, is found by considering the terms of order $1/h$ and solving the equation:

$$L[y_1; p] = \frac{z^4 y_0}{48}. \qquad (C.9)$$

L is the differential equation defined by Eq. C.3. The term z^4 will prove troublesome, so we remove it through repeated use of the recurrence relation:

$$zD_p(z) = D_{p+1}(z) + pD_{p-1}(z), \qquad (C.10)$$

together with Eq. C.6. This procedure transforms Eq. C.9 into:

$$48D_p(0)L[y_1; p] = D_{p+4}(z) + 2(2p+3)D_{p+2}(z) + 3(2p^2 + 2p + 1)D_p(z)$$

$$+2p(p-1)(2p-1)D_{p-2}(z) + p(p-1)(p-2)(p-3)D_{p-4}(z). \qquad (C.11)$$

This form is advantageous because we have eliminated all of the coefficients which contain z. This enhances the solution procedure considerably. We can now find **a** particular solution to Eq. C.11 by manipulating Eq. C.3. For example, the definition:

$$L[D_{p+m}(z); p + m] = 0, \qquad (C.12)$$

implies that:

$$L\left[-\frac{D_{p+m}(z)}{m}; p\right] = D_{p+m}(z). \qquad (C.13)$$

This equation does not hold for m equal to zero. For this case, we need to differentiate L with respect to its order, p, and rearrange to get:

$$L\left[-\frac{\partial D_p(z)}{\partial p}; p\right] = D_p(z). \qquad (C.14)$$

These last two relations are used to find the particular solution of Eq. **C.11.** To find the general solution we need to add the homogeneous solution $C_1 D_p(z)$. The form of the solution automatically satisfies the boundedness condition at infinity. In order to satisfy the inner boundary condition, we need to specify C_1 such that $y_1(0)$ equals zero.

Solving for C_1, gives y_1 as:

$$
\begin{aligned}
y_1(z) &= \frac{1}{48 D_p(0)} \left(-\frac{D_{p+4}(z)}{4} - \frac{2(2p+3)D_{p+2}(z)}{2} - 3(2p^2 + 2p + 1)D_p^{(p)}(z) \right. \\
&+ \frac{2p(p-1)(2p-1)D_{p-2}(z)}{2} + \frac{p(p-1)(p-2)(p-3)D_{p-4}(z)}{4} \\
&- \left. \frac{9(2p+1)D_p(z)}{4} + \frac{3(2p^2+2p+1)D_p^{(p)}(0)D_p(z)}{D_p(0)} \right).
\end{aligned}
\tag{C.15}
$$

In this equation, the superscript, *(p)*, denotes differentiation with respect to order. The second term in the approximation of $\mathcal{F}_{2n}$ is found by differentiating Eq. **C.15** with respect to x and setting x equal to zero. We defer showing this second approximation until we present the third, and final, term.

The third term, y_2, is found by solving the equation:

$$
L[y_2(z); p] = \frac{z^4 y_1(z)}{48} + \frac{z^6 y_0(z)}{1440}.
\tag{C.16}
$$

Repeated use of the recurrence relation, Eq. C.10, results in an expression equivalent to Eq. C.16, but whose coefficients do not contain z. This expression consists of nineteen terms and will not be shown. It contains parabolic cylindrical functions and derivatives of parabolic cylindrical functions with respect to order. The method of solving the resulting equation is the same as in the previous approximation. The particular solutions for functions involving derivatives with respect to order are found by taking the derivative of Eqs. **C.13** and **C.14** with respect to order. In order to find the general solution, we add $C_2 D_p(z)$ to the particular solution and specify C_2 such that $y_2(0)$ is equal to zero. The resulting expression for y_2 consists of twenty-two terms and will not be shown. The solution is in terms of parabolic cylindrical functions and their first and second derivatives with respect to order.

The final expression for $\mathcal{F}_{2n}$ consists of adding the derivative of y_2 to the previous two approximations. At this point we need to simplify the resultant expression.

Since this expression contains parabolic cylindrical functions and their derivatives with respect to order, we use Eq. C.7 and its derivatives. The derivatives of the Γ-function are best expressed as @-functions:

$$\Psi(u) = \frac{d\Gamma(u)}{d\ln(u)} = \frac{\Gamma'(u)}{\Gamma(u)} \; . \tag{C.17}$$

Using the Γ-function, the @-function, and its derivative; the expression for $\mathcal{F}_{2n}$ becomes:

$$\mathcal{F}_{2n} = \frac{-\sqrt{8h}\,\Gamma(A)}{\Gamma(B)} \left(1 + \frac{1}{32h}\left[2p + 1 + (2p^2 + 2p + 1)\left(\Psi(A) - \Psi(B)\right)\right]\right.$$
$$+ \frac{1}{2048h^2}\left[-36p^2 - 36p - 19 - 2(10p^2 + 10p + 7)(2p + 1)(@(A) - \Psi(B))\right.$$
$$\left.\left. + (2p^2 + 2p + 1)^2\left(@\,'(A) - \Psi'(B) + (@(A) - \Psi(B))^2\right)\right]\right) + O(h^{-5/2}), \quad \text{C.18}$$

where Ψ' is the derivative of the Ψ-function, $A = 1/2 - p/2$, and $B = -p/2$.

Close examination of Eq. C.18 reveals that it is equivalent to a Taylor series expansion of three ratios of Γ-functions:

$$\mathcal{F}_{2n} = -2\sqrt{2h}\,\frac{\Gamma[-(p-1)/2 + (2p^2 + 2p + 1)/32h]}{\Gamma[-p/2 + (2p^2 + 2p + 1)/32h]}$$
$$- \sqrt{2h}\frac{(2p+1)\,\Gamma[-(p-1)/2 - (10p^2 + 10p + 7)/32h]}{16h\quad\Gamma[-p/2 - (10p^2 + 10p + 7)/32h]}$$
$$+ \sqrt{2h}\frac{(36p^2 + 36\text{P} + 19)\,\Gamma[-(p-1)/2]}{1024h^2\quad\Gamma[-p/2]} + O(h^{-5/2}). \tag{C.19}$$

Equation C.19 is no more accurate than Eq. C.18 but it is computationally preferable. It also indicates that there may be a much simpler method for determining the asymptotic expansion for $\mathcal{F}_{2n}$.

C.3 Exponential Approximation

In this section we derive an approximation to $\mathcal{F}_{2n}$ using exponential functions. This approximation ignores the presence of turning points, but is adequate for approximating the function for large values of n and **all** values of s. This approximation was derived before we became acquainted with the Riccati equation. It appears that the

method we employ is equivalent to the "Large B" Riccati equation method used in Chapter 8.

In this section, we take advantage of the fact that we are only interested in the point, $x = 0$, by rearranging **Eq.** C.2 so that the right hand side is zero at this point and the left hand side has constant coefficients. Thus, the present approach solves the equation:

$$LL[y; \lambda] = \frac{\partial^2 y}{\partial x^2} - \lambda_{2n}^2 y = 2h^2(\cosh(2x) - 1)y , \qquad (\text{C.20})$$

where h is $\sqrt{s}/2$.

The perturbation method is slightly different than that of the previous section. We initially ignore the right hand side of Eq. C.20 and seek a solution which has a value of unity at x equal to zero and approaches zero as x approaches infinity. This solution is:

$$y_0(x) = e^{-\lambda x}, \qquad (\text{C.21})$$

where we have dropped the subscript on λ for convenience. We then insert y_0 into the left hand side of Eq. C.20 and solve the equation with homogeneous boundary conditions at zero and infinity. This solution is y_1. From then on we iterate, at each step using the previous solution in the right hand side. At each level we take care of all of the terms left over from the previous iteration. The full solution is the sum of the y_i, and $\mathcal{F}_{2n}$ is the derivative of the full solution at x equal to zero.

The solution, y_1, requires solving the inhomogeneous equation:

$$LL[y_1; \lambda] = 2h^2(\cosh(2x) - 1)e^{-\lambda x}. \qquad (\text{C.22})$$

This is readily accomplished using the relations:

$$\begin{aligned} LL[e^{-(\lambda+B)x}/B(2\lambda + B); \lambda] &= e^{-(\lambda+B)x} \\ LL[-xe^{-\lambda x}/2\lambda; \lambda] &= e^{-\lambda x}. \end{aligned} \qquad (\text{C.23})$$

These relations were found by manipulating the differential operator, LL, in the same way as in the previous section. Using these relations and the solution to the homogeneous equation, gives:

$$y_1(x) = h^2 \left(\frac{e^{-(\lambda-2)x}}{4(1-\lambda)} + \frac{e^{-(\lambda+2)x}}{4(1+\lambda)} - \frac{e^{-\lambda x}}{2(1 - \text{x2})} + \frac{xe^{-\lambda x}}{\lambda} \right). \qquad (\text{C.24})$$

The third solution, y_2, is found using Eq. C.24 in the right hand side of Eq. C.20. The solution of this equation requires more relations of the type in Eqs. C.23, which are again found by manipulating the operator, LL. The solution, y_2, consists of twelve terms and will not be shown here.

The fourth solution, y_3, is the solution to the equation:

$$\frac{\partial^2 y_3}{\partial x^2} - \lambda_{2n}^2 y_3 = 2h^2(\cosh(2x) - 1)y_2 . \tag{C.25}$$

Since we do not intend to go to higher iteration levels, we can find the derivative of y_3 at the origin through use of the Laplace transform. If we take the Laplace transform of Eq. C.25, using λ as the parameter in the transformation (i.e., multiply Eq. C.25 through by $\exp(-\lambda x)$ and integrate from zero to infinity), we find the desired derivative by means of a single integration. The Laplace transformation of Eq. C.25, taking into account the homogeneous boundary conditions at zero and infinity, is:

$$\left. \frac{dy_3(x)}{dx} \right|_{x=0} = -2h^2 \int_0^\infty (\cosh(2x) - 1)y_2 e^{-\lambda x} dx. \tag{C.26}$$

The final expression for $\mathcal{F}_{2n}$ is the sum the derivatives of yo, y_1 and y_2 at x equal to zero added to the result of integrating Eq. C.26:

$$\mathcal{F}_{2n} = -\lambda - \frac{h^2}{\lambda(\lambda^2 - 1)} - \frac{h^4(19\lambda^2 - 4)}{2\lambda^3(\lambda^2 - 4)(\lambda^2 - 1)^2}$$
$$- \frac{h^6(631\lambda^6 - 2159\lambda^4 + 736\lambda^2 - 144)}{2\lambda^5(\lambda^2 - 9)(\lambda^2 - 4)^2(\lambda^2 - 1)^3} + O(h^8/\lambda^{15}). \tag{C.27}$$

In this expression, λ is shorthand notation for λ_{2n}, which is equal to $\sqrt{a_{2n} + s/2}$, and h is $\sqrt{s}/2$.

C.4 Ranges of Applicability of Solutions

In the previous three sections, we gave solutions which were valid for different ranges of s and n. In this section we specify these regions.

The ratio of series in the first section, Eq. C.1, is computationally useful for low values of s. In this work we use this solution for $s \le 300 + 100n$ and for $n \le 10$.

The Γ and Ψ-function solution, Eq. C.18, is used for $s > 300 + 100n$ and for $n \leq 10$. Equation C.19 should give equal accuracy in this range, but in this work we use C.18. For n > 10, we use the exponential solution, **Eq.** C.27, for all values of s.

Using the three solutions in this way gives at least seven significant figures of accuracy. The weak link in the computation is $\mathcal{F}_0$. Neither the Fourier series representation, Eq. C.1, nor the Γ-function representation, Eq. C.18, is very accurate in the neighborhood of s equal to **300. As** the order increases, the accuracy of the representations of $\mathcal{F}_{2n}$ increases. For example, at $n = 10$ we obtain ten figures of accuracy for all s.

Appendix D

WELL PRESSURE TABLES

In this appendix we present tabular data computed from the solutions given in the main text. We cover three cases in five tables. The first two tables present p_{Dw} for the elliptical fracture case using the iterative solutions of Chapter 7. The next two tables compare the exact solution for an infinite conductivity fracture to two approximate formulae. The final table compares the exact solution with the infinitely long fracture solution for F_E equal to 0.1.

The data presented in these tables are (with the exception of the Gringarten et al. solution) computed using the algorithm of Stehfest (1970) to invert the Laplace space solutions. Since this is a numerical inversion technique, we cannot give explicit error bounds. In generating these tables, we have used eight terms of the inversion algorithm, i.e. $N = 8$. We believe that the tabulated pressures are accurate to at least three, and possibly four, significant figures.

D.1 Well Pressures for Elliptical Fracture

Tables D.1 and D.2 present well pressures for the elliptical.fracture. Data are presented for fracture conductivities from $\pi/10$ to 1000 for values of t_{Dx_f} from 10^{-4} to 10^{+3}. These data are computed using the exact solutions of Chapter 7. The low conductivity iterative solution, Eq. 7.19, was used for F_E equal to $\pi/10$, while the high conductivity iterative solution, Eq. 7.17, was used for all higher conductivities.

Note that the tabulation starts with $t_{Dx_f} = 10^{-4}$. In order to use the iterative solutions of Chapter **7** for this low range of t_{Dx_f}, we were forced to use a large number of terms in the fracture pressure series, Eq. 7.22 of Chapter 7.

In computing the data of Tables D.1 and D.2, we use the procedure outlined in Appendix B, Section **B.3** to compute the kernels. The difference is that the matrices were defined to contain 325 by 325 elements, rather than 125 by 125. We also sum the series, Eq. 7.22, to 290 terms rather than 100 terms.

D.2   The Infinite Conductivity Fracture

Tables D.3 and D.4 give tabulations of p_{Dw} for the infinite conductivity case. Also shown in this table are the approximate solutions of Gringarten et al. (1974) and Eq. 8.20 of Chapter 8. We include these tables because it was found that the tabulated data given by Kucuk and Brigham (1979) were inaccurate at early times.

The second columns of Tables D.3 and D.4 contain data obtained by evaluating the exact solution of Kucuk and Brigham (1979):

$$\bar{p}_{inf} = -\frac{1}{2s\mathcal{U}_0^0} \, . \tag{D.1}$$

These data were checked' against those given by an independent method described in Wilkinson (1989). The two methods agree to four significant figures, however both methods use the Stehfest (1970) algorithm to invert transformed solutions.

The third columns in Tables D.3 and D.4 contain data from the early time approximate solution of Chapter 8:

$$\bar{p}_{E.T.} = \frac{\pi}{s(2\sqrt{s} + 1)} \, . \tag{D.2}$$

The percentage difference between the two solutions, Eq. D.1 and Eq. D.2, are given in the fourth columns of Tables D.3 and D.4. These tables indicate that the error in using Eq. D.2 is essentially nil until a value of t_{Dx_f} of about 0.4. This means that Eq. D.2 is sufficiently accurate for use in the composite solutions of Chapter 8.

'personal communication: D.J. Wilkinson, Dowell Schlumberger, Ridgefield, Conn., Feb. **27,** 1991.

The fifth columns in Tables **D.3** and **D.4** present data from the equation:

$$p_{D,Grin} = \frac{\sqrt{\pi t_{Dx_f}}}{2} \left[erf \left(\frac{0.1299514}{\sqrt{t_{Dx_f}}} \right) + erf \left(\frac{0.87004857}{\sqrt{t_{Dx_f}}} \right) \right]$$
$$-0.0649757 \ Ei \left(\frac{-0.0168874}{t_{Dx_f}} \right) - 0.4350243 \ Ei \left(\frac{-0.7569845}{t_{Dx_f}} \right). \tag{D.3}$$

In this equation, "*erf*" is the error function and "*Ei*" is the exponential integral.

Equation **D.3** is the well known solution of Gringarten et al. **(1974).** The constants have been altered slightly to give greater accuracy during pseudoradial flow (see Kuchuk **(1987),** Appendix A). The reason that we tabulate this expression is that the data given by Kucuk and Brigham **(1979)** make Eq. **D.3** appear more accurate than it is. Tables **D.3** and **D.4** show that the errors in using Eq. **D.3** are as high as four percent. Also, the Gringarten et al. solution does not match the character of the exact solution—initially Eq. **D.3** overestimates the fracture pressure, then underestimates it and then asymptotes to the true pressure.

D.3 The Very Low Conductivity Fracture

The final table compares the exact solution of Chapter **7,** Eq. **7.19,** with that of the infinitely long fracture case. The infinitely long fracture solution is due to Wilkinson **(1989)** and is given by Eq. **8.1** of Chapter **8.**

Table **D.5** shows the comparison for $F_E = 0.1$: the exact solution for the elliptical case is in the second column and Wilkinson's solution is in the third column. The fourth column shows the percentage difference between the two solutions. This difference is less than one percent. So, $F_E = 0.1$ is a reasonable upper limit for use of Eq. **8.1.**

t_{Dx_f}	Elliptical Fracture Conductiv					y, F_E		
	1000	100π	100	10π	10	π	1.0	$\pi/10$
0.0001	0.01876	0.02113	0.02790	0.04483	0.07797	0.1383	0.2441	0.4317
0.0002	0.02603	0.02843	0.03547	0.05417	0.09297	0.1646	0.2899	0.5109
0.0003	0.03159	0.03401	0.04118	0.06081	0.1031	0.1821	0.3205	0.5635
0.0004	0.03627	0.03869	0.04595	0.06617	0.1110	0.1958	0.3441	0.6039
0.0005	0.04038	0.04281	0.05012	0.07079	0.1176	0.2070	0.3636	0.6370
0.0006	0.04408	0.04653	0.05388	0.07488	0.1234	0.2167	0.3802	0.6652
0.0004	0.04749	0.04993	0.05733	0.07860	0.1284	0.2252	0.3949	0.6900
0.0008	0.05065	0.05310	0.06053	0.08202	0.1330	0.2329	0.4081	0.7122
0.0009	0.05361	0.05607	0.06352	0.08521	0.1372	0.2399	0.4201	0.7323
0.001	0.05641	0.05888	0.06635	0.08820	0.1411	0.2464	0.4311	0.7507
0.002	0.07887	0.08137	0.08899	0.1118	0.1704	0.2933	0.5106	0.8822
0.003	0.09593	0.09845	0.1062	0.1295	0.1911	0.3250	0.5635	0.9682
0.004	0.1102	0.1127	0.1205	0.1442	0.2078	0.3496	0.6041	1.033
0.005	0.1227	0.1252	0.1331	0.1570	0.2221	0.3700	0.6376	1.086
0.006	0.1339	0.1364	0.1443	0.1685	0.2348	0.3877	0.6661	1.131
0.007	0.1441	0.1467	0.1546	0.1790	0.2462	0.4034	0.6912	1.171
0.008	0.1536	0.1562	0.1642	0.1887	0.2567	0.4 175	0.7137	1.205
0.009	0.1625	0.1651	0.1731	0.1977	0.2665	0.4305	0.7341	1.237
0.01	0.1709	0.1735	0.1815	0.2062	0.2756	0.4424	0.7527	1.266
0.02	0.2370	0.2396	0.2479	0.2735	0.3468	0.5314	0.8871	1.467
0.03	0.2861	0.2889	0.2973	0.3235	0.3991	0.5934	0.9757	1.595
0.04	0.3266	0.3293	0.3378	0.3645	0.4418	0.6426	1.043	1.691
0.05	0.3614	0.3642	0.3729	0.3999	0.4784	0.6843	1.099	1.767
0.06	0.3923	0.3952	0.4039	0.4313	0.5109	10.7207	1.147	1.832
0.07	0.4203	0.4232	0.4320	0.4596	0.5402	0.7533	1.188	1.888
0.08	0.4459	0.4488	0.4577	0.4856	0.5670	0.7830	1.226	1.937
0.09	0.4696	0.4725	0.4815	0.5096	0.5917	0.8102	1.260	1.981
0.1	0.4917	0.4947	0.5037	0.5320	0.6148	0.8355	1.291	2.021
0.2	0.6600	0.6630	0.6725	0.7023	0.7896	1.024	1.514	2.296
0.3	0.7776	0.7808	0.7905	0.8212	0.9111	1.153	1.660	2.467
0.4	0.8699	0.8731	0.8831	0.9143	1.006	1.253	1.771	2.592
0.5	0.9464	0.9497	0.9598	0.9914	1.084	1.335	1.861	2.692
0.6	1.012	1.015	1.026	1.058	1.152	1.405	1.936	2.774
0.7	1.070	1.073	1.083	1.116	1.210	1.466	2.002	2.845
0.8	1.121	1.124	1.135	1.167	1.263	1.520	2.059	2.907
0.9	1.167	1.171	1.181	1.214	1.310	1.569	2.111	2.962

Table D.l: Well Pressures for Elliptical Fracture, $t_{Dx_f} < 1.0$

t_{Dx_f}	Elliptical Fracture Conductivity, F_E							
	1000	100π	100	10π	10	π	1.0	$\pi/10$
1.0	1.210	1.213	1.224	1.256	1.353	1.613	2.157	3.012
2.0	1.505	1.509	1.519	1.553	1.652	1.919	2.475	3.343
3.0	1.689	1.693	1.703	1.737	1.837	2.107	2.668	3.541
4.0	1.823	1.827	1.838	1.872	1.972	2.243	2.807	3.682
5.0	1.929	1.932	1.943	1.978	2.078	2.350	2.915	3.792
6.0	2.016	2.019	2.030	2.065	2.166	2.438	3.004	3.883
7.0	2.090	2.094	2.104	2.139	2.240	2.513	3.080	3.959
8.0	2.155	2.158	2.169	2.204	2.305	2.578	3.145	4.025
9.0	2.212	2.215	2.226	2.261	2.362	2.635	3.203	4.084
10	2.263	2.267	2.278	2.312	2.414	2.687	3.255	4.136
20	2.603	2.607	2.618	2.653	2.755	3.029	3.599	4.481
30	2.804	2.808	2.819	2.853	2.955	3.230	3.800	4.683
40	2.947	2.950	2.961	2.996	3.098	3.373	3.944	4.827
50	3.058	3.061	3.072	3.107	3.209	3.484	4.055	4.938
60	3.148	3.152	3.163	3.198	3.300	3.575	4.146	5.029
70	3.225	3.229	3.240	3.275	3.377	3.652	4.223	5.106
80	3.292	3.295	3.306	3.341	3.443	3.718	4.289	5.173
90	3.351	3.354	3.365	3.400	3.502	3.777	4.348	5.232
100	3.403	3.407	3.418	3.453	3.555	3.830	4.401	5.284
200	3.749	3.753	3.764	3.799	3.901	4.176	4.747	5.631
300	3.952	3.955	3.966	4.001	4.103	4.378	4.950	5.834
400	4.095	4.099	4.110	4.145	4.247	4.522	5.093	5.977
500	4.207	4.210	4.221	4.256	4.359	4.634	5.205	6.089
600	4.298	4.301	4.313	4.347	4.450	4.725	5.296	6.180
700	4.375	4.379	4.390	4.424	4.527	4.802	5.373	6.257
800	4.442	4.445	4.456	4.491	4.594	4.869	5.440	6.324
900	4.501	4.504	4.515	4.550	4.652	4.927	5.499	6.383
1000	4.553	4.557	4.568	4.603	4.705	4.980	5.552	6.436

Table D.2   Well Pressures for Elliptical Fracture, $t_{Dx_f} \geq 1.0$

t_{Dx_f}	Exact p_{Dw}	Early Time $p_{D,E.T.}$	% diff	Gringarten $p_{D,Grin}$	% diff
).0001	0.01765	0.01765	-0-	3.01772	-0.44
1.0002	0.02491	0.02491	-0-	3.02507	-0.63
1.0003	0.03047	0.03047	-0-	3.03070	-0.77
1.0004	0.03514	0.03514	-0-	3.03545	-0.89
1.0005	0.03 924	0.03924	-0-	3.03963	-0.99
1.0006	0.04295	0.04295	-0-	3.04342	-1.09
1.0007	0.04635	0.04635	-0-	0.04689	-1.17
1.0008	0.04951	0.04951	-0-	D.05013	-1.25
1.0009	0.05248	0.05247	-0-	0.05317	-1.33
0.001	0.05527	0.05527	-0-	D.05605	-1.40
0.002	0.07772	0.07772	-0-	0.07927	-1.99
0.003	0.09477	0.09477	-0-	D.09708	-2.43
0.004	0.1090	0.1090	-0-	0.1121	-2.80
0.005	0.1215	0.1215	-0-	0.1253	-3.10
0.006	0.1327	0.1327	-0-	0.1372	-3.35
0.007	0.1430	0.1430	-0-	0.1480	-3.54
0.008	0.1525	0.1525	-0-	0.1581	-3.70
0.009	0.1613	0.1613	-0-	0.1675	-3.82
0.01	0.1697	0.1697	-0-	0.1763	-3.91
0.02	0.2358	0.2358	-0-	0.2450	-3.93
0.03	0.2849	0.2849	-0-	0.2945	-3.38
0.04	0.3253	0.3253	-0-	0.3343	-2.78
0.05	0.3601	0.3601	-0-	0.3681	-2.21
0.06	0.3911	0.3910	-0-	0.3978	-1.71
0.07	0.4190	0.4190	-0-	0.4244	-1.28
0.08	0.4446	0.4446	-0-	0.4486	-0.90
0.09	0.4683	0.4683	-0-	0.4710	-0.57
0.10	0.4904	0.4904	-0-	0.4918	-0.29
0.2	0.6586	0.6585	-0-	0.6510	1.15
0.3	0.7762	0.7762	-0-	0.7645	1.50
0.4	0.8684	0.8684	-0-	0.8552	1.52
0.5	0.9449	0.9449	0.01	0.9313	1.44
0.6	1.011	1.010	0.01	0.9970	1.33
0.7	1.068	1.068	0.02	1.055	1.22
0.8	1.119	1.119	0.03	1.107	1.12
0.9	1.166	1.165	0.05	1.154	1.03

Table **D.3:** Infinite Conductivity Fracture, $t_{Dx_f} < 1.0$

t_{Dx_f}	Exact p_{Dw}	Early Time $p_{D,E.T.}$	% diff	Gringarten $p_{D,Grin}$	% diff
1.0	1.208	1.207	0.07	1.197	0.95
2.0	1.504	1.498	0.37	1.496	0.48
3.0	1.687	1.674	0.80	1.682	0.30
4.0	1.822	1.798	1.28	1.818	0.21
5.0	1.927	1.893	1.76	1.924	0.16
6.0	2.014	1.969	2.23	2.012	0.13
7.0	2.088	2.032	2.69	2.086	0.11
8.0	2.153	2.085	3.13	2.151	0.09
9.0	2.210	2.131	3.57	2.208	0.08
10	2.261	2.171	3.98	2.260	0.07
20	2.602	2.412	7.30	2.601	0.03
30	2.802	2.531	9.69	2.802	0.02
40	2.945	2.606	11.53	2.945	0.01
50	3.056	2.658	13.02	3.056	0.01
60	3.147	2.698	14.27	3.147	0.01
70	3.224	2.729	15.34	3.224	-0-
80	3.290	2.755	16.28	3.290	-0-
90	3.349	2.776	17.11	3.349	-0-
100	3.401	2.794	17.86	3.401	-0-
200	3.747	2.893	22.79	3.747	-0-
300	3.950	2.938	25.61	3.950	-0-
400	4.094	2.965	27.57	4.094	-0-
500	4.205	2.984	29.05	4.205	-0-
600	4.296	2.997	30.23	4.296	-0-
700	4.373	3.008	31.22	4.373	-0-
800	4.440	3.017	32.06	4.440	-0-
900	4.499	3.024	32.79	4.499	-0-
1000	4.552	3.030	33.44	4.552	-0-

Table D.4: Infinite Conductivity Fracture, $t_{Dx_f} \geq 1.0$

t_{Dx_f}	$F_E = 0.1$			t_{Dx_f}	$F_E = 0.1$		
	Exact	Approx	% diff		Exact	Approx	% diff
3.0001	0.7480	0.7479	0.01	0.6	3.790	3.776	0.37
1.0002	0.8789	0.8788	0.01	0.7	3.865	3.850	0.39
1.0003	0.9644	0.9643	0.01	0.8	3.930	3.913	0.42
1.0004	1.029	1.029	0.01	0.9	3.987	3.970	0.44
1.0005	1.082	1.082	0.01	1.0	4.038	4.020	0.45
1.0006	1.127	1.127	0.01	2.0	4.379	4.354	0.56
1.0007	1.166	1.165	0.02	3.0	4.580	4.552	0.61
3.0008	1.200	1.200	0.02	4.0	4.723	4.692	0.64
3.0009	1.231	1.231	0.02	5.0	4.834	4.802	0.66
0.001	1.260	1.260	0.02	6.0	4.924	4.891	0.68
0.002	1.459	1.459	0.02	7.0	5.001	4.967	0.69
0.003	1.586	1.586	0.03	8.0	5.068	5.033	0.69
0.004	1.681	1.680	0.03	9.0	5.126	5.091	0.70
0.005	1.756	1.756	0.04	10	5.179	5.143	0.70
0.006	1.820	1.819	0.04	20	5.525	5.485	0.72
0.007	1.874	1.874	0.05	30	5.728	5.686	0.72
0.008	1.923	1.922	0.05	40	5.871	5.829	0.72
0.009	1.966	1.965	0.05	50	5.983	5.940	0.72
0.01	2.005	2.004	0.05	60	6.074	6.030	0.72
0.02	2.273	2.271	0.07	70	6.151	6.107	0.72
0.03	2.437	2.435	0.09	80	6.218	6.173	0.71
0.04	2.557	2.555	0.10	90	6.277	6.232	0.71
0.05	2.652	2.649	0.11	100	6.329	6.284	0.71
0.06	2.731	2.727	0.12	200	6.676	6.630	0.69
0.07	2.798	2.794	0.13	300	6.878	6.832	0.68
0.08	2.856	2.852	0.14	400	7.022	6.975	0.67
0.09	2.909	2.904	0.15	500	7.134	7.087	0.66
0.1	2.955	2.951	0.15	600	7.225	7.178	0.66
0.2	3.271	3.264	0.21	700	7.302	7.255	0.65
0.3	3.460	3.451	0.26	800	7.369	7.321	0.65
0.4	3.596	3.585	0.30	900	7.428	7.380	0.64
0.5	3.703	3.690	0.34	1000	7.480	7.433	0.64

Table D.5: Comparison with Infinitely Long Fracture, $F_E = 0.1$